Spring 1-1-2017

Modelling Transport and Deposition of Coarse Particles in Viscoplastic Tailings Beach Flows

John Matthew Treinen
University of Colorado at Boulder, jmtreinen@gmail.com

MODELLING TRANSPORT AND DEPOSITION OF COARSE PARTICLES IN VISCOPLASTIC TAILINGS BEACH FLOWS

by

J.M. TREINEN

B.S., University of Denver, 2006

M.S., University of Colorado, 2008

A thesis submitted to the

Faculty of the Graduate School of the

University of Colorado in partial fulfillment

of the requirement for the degree of

Doctor of Philosophy

Department of Civil, Environmental and Architectural Engineering

2017

This thesis entitled:
Modelling Transport and Deposition of Coarse Particles in Viscoplastic Tailings Beach Flows
written by John Matthew Treinen
has been approved for the Department of Civil, Environmental, and Architectural Engineering

_____
Professor Dobroslav Znidarcic, Committee Chair

_____
Professor Harihar Rajaram

*Date*_____

The final copy of this thesis has been examined by the signatories, and we
Find that both the content and the form meet acceptable presentation standards
Of scholarly work in the above mentioned discipline.

Treinen, JM (Ph.D., Civil, Environmental and Architectural Engineering)

Modelling Transport and Deposition of Coarse Particles in Viscoplastic Tailings Beach Flows

Thesis directed by Professor Dobroslav Znidarcic

Abstract

The flow of thickened mine tailings within a tailings storage facility is a complex interaction between unconstrained viscoplastic free surface flow and possible coarse particle settling within the flow depth. The broad focus of this work is developing a robust framework for modelling tailings beach flows. Modelling tailings flow evolution in three dimensions within a storage facility will ultimately provide greater understanding of beach slope formation, as well as the ability to optimize deposition sequencing.

This thesis focuses on the first step of developing a tailings model considering the transport and settling of mono-sized coarse particles within two dimensional (length and depth) laminar viscoplastic carrier fluid sheet flow. The 2D model consists of a semi-implicit finite difference shallow water sheet flow model for predicting the viscoplastic flow depth and discharge down the beach. The coarse particle transport and hindered settling within the flow are predicted using a scalar transport model. The scalar transport and shallow water flow model are coupled together using coarse particle rheology augmentation.

Two key novel advancements were made through the model development. The first is coupling the coarse particle rheology augmentation within the free surface flow to the coarse particle hindered settling behavior with depth. This coupling allows for the rheology augmentation due to the coarse solid fraction to be incorporated seamlessly into both the fluid flow solver and the particle settling model. The second advancement is expanding the rheology augmentation and hindered settling coupling to particle flows beyond the Stoke's flow regime.

Ultimately, the 2D model results are compared against Spelay's (2007) laminar settling experimental measurements for oil sand thickened tailings (TT) and composite tailings (CT) slurries, along with Spelay's 1D settling model. The 2D model provides improved prediction of the particle concentration

profiles within the fluid flow compared to the 1D model. The 2D model is also able to predict the increase in flow depth due to the particle accumulation on the bed, as well as the downslope particle transport and settling behavior.

ACKNOWLEDGEMENTS

Firstly, I am grateful for my advisor Professor Znidarcic's patience as I worked through this research as a part time student and practicing engineer. Progress often came slowly, but he was always quick to suggest a practical approach to move forward and maintain focus.

I am also thankful for Professor Rajaram's assistance in explaining and formulating the numerical implementation used in this work. Learning numerical methods through this research has been a truly valuable experience. I wish I would have discovered numerical methods much earlier in my professional career.

My committee members Professor Talmon, Dr. Spelay and Professor Crimaldi provided invaluable feedback through the study and ultimately made this thesis much stronger in many ways.

I am grateful for my family friends, and coworkers who provided encouragement and support through this process. My parents have been steadfast examples of hard work and lifelong learning, and I ever appreciative of their praise and support. My loving wife deserves special recognition for gentle encouragement and polite prodding over the years.

Finally, this work would not have been possible without the support of Dr. Robert Cooke. Rob has been a tremendous mentor and friend since we first met. He encouraged me to resume my graduate studies after I put them on pause to join Paterson & Cooke. I am truly grateful for his sacrifice to allow me to focus so much of my time on these studies while still being employed at P&C.

TABLE OF CONTENTS

TABLES

FIGURES

KEY NOMENCLATURE

Parameter		Unit
d	particle diameter	m
d_{50}	particle size at which 50% of the particles by mass are smaller than d_{50}	m
g	acceleration due to gravity	m/s^2
H,h	height	m
K	fluid consistency index	$Pa.s^n$
n	flow behavior index	-
Pe	Peclet number	-
Q	volumetric flow rate	m^3/s
q	discharge per unit width in sheet flow	m^2/s
r	radius	m
Re	Reynolds number	-
S	relative density	-
$U_{x,z}$	flow velocity in x, z direction	m/s
v_s	settling velocity	m/s
v_{HS}	hindered settling velocity	m/s
v_{ts}	terminal settling velocity	m/s
η	kinematic viscosity (μ/ρ)	m/s^2
$\dot{\gamma}$	shear rate	s^{-1}
φ	volumetric solids concentration of coarse particles	%
φ_m	maximum solids packing volumetric concentration of coarse particles	%
μ	dynamic viscosity	Pa.s
μ_P	Bingham plastic viscosity	Pa.s
ρ	density	kg/m^3
τ	shear stress	Pa
τ_y	yield stress	Pa
z_b	bed coordinate	m
z_s	flow surface corrdinate	m

Subscripts

a	apparent
b	Bingham Plastic
c	carrier fluid
l	liquid
m	mixture
p	particle
s	solids, settling
t	total

CHAPTER 1:
INTRODUCTION

1.1 Tailings Disposal Methods

Mine tailings are one of the most widely handled materials on the earth; approximately ten billion tons of tailings are produced each year and must be safely contained within tailings storage facilities into perpetuity (Boger, Hart 2008).

Historically, mine tailings have been deposited at fairly low solids concentrations (less than 30% by mass). The tailings are contained within embankments with sufficient freeboard below the embankment wall to prevent overtopping during deposition. Figure 1 presents a plan view of a typical[1] conventional tailings storage facility.

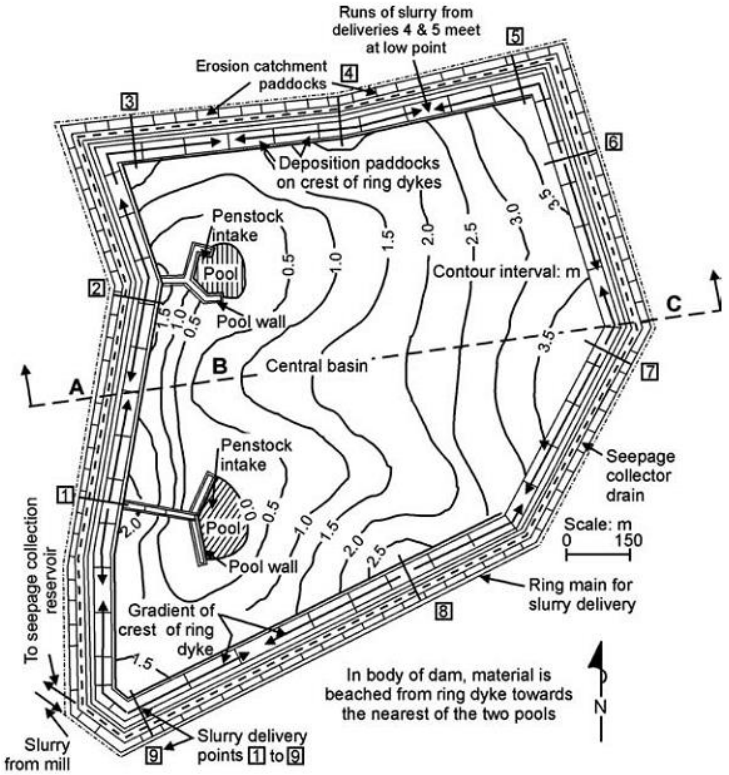

Figure 1: Plan View of Conventional Tailings Storage Facility (Blight 2009)

[1] The actual embankment shape and design is dependent on the underlying topography.

The tailings slurry is commonly deposited along the embankment via a ring main piping system. The solids are allowed to settle down the deposition beach and the decanted water is transported to the processing plant for recycle (Blight 2009). Conventional thickened tailings storage facilities are necessarily large as they must accommodate both the tailings solids and the significant water volume.

Advances in dewatering technology (thickeners) produce tailings at higher solids concentration within the processing plant, enabling significant water removal prior to deposition. For example, increasing solids mass concentration from 30% to 50% reduces water volume discharge into the facility by 60%. This reduction in discharged water results in:

- Reduced water loss due to evaporation and seepage within the storage facility.
- Reduced pump power consumption to deliver tailings to the facility as well as pump decant water back to the processing plant[2].
- Reduced storage facility volume and significant earthworks savings in containment structure construction.

Additionally, thickening of mine tailings can result in the ability to stack the tailings above the containment structure elevation, enabling enhanced storage capacity within a similar conventional storage facility footprint. Robinsky's original thickened tailings concept (1975) is provided in Figure 2. In some applications, such as a central thickened discharge (CTD) configuration, it may not be necessary to construct perimeter containment embankments, resulting in construction cost savings. Although, Fourie (2012) notes many of the perceived advantages of paste and thickened tailings discharge disposal methods have not been fully realized.

Of critical importance in the design of these thickened tailings containment structures is predicting the flow behavior of the discharged tailings and resulting slope of the deposition beach. If the beach slope

[2] This is not always the case since the high solids concentration tailings exhibit higher pipeline friction losses which may require higher pumping power.

is too shallow, the structure cannot store the required tailings volume for which it is designed. If the slope is too steep, the depositional area is not fully utilized, and erosion and runoff problems may occur.

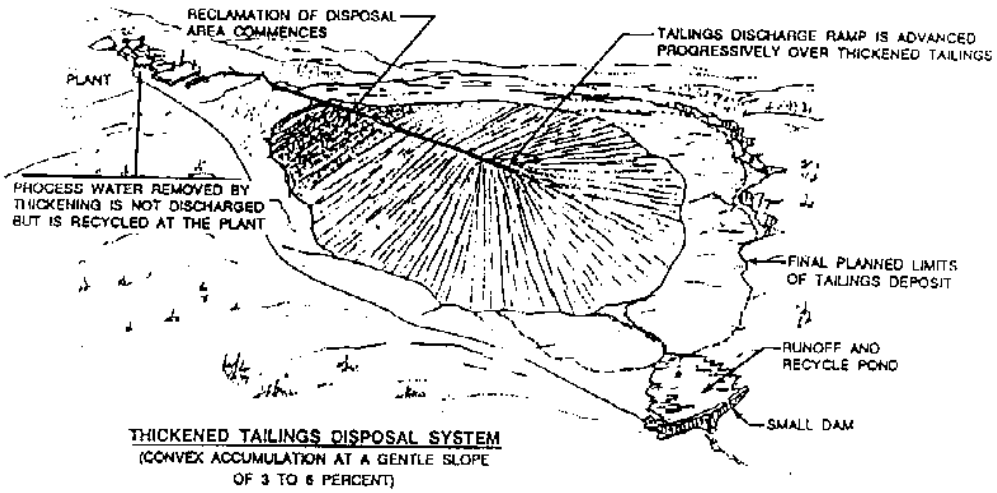

Figure 2: Robinsky's (1975) Original Thickened Tailings Deposition Concept

1.2 Overview of Beach Slope Prediction Models

1.2.1 Early Beach Slope Prediction – Dilute Conventional Systems

Predicting the beach slope of deposited tailings within the storage facilities has been a topic of research for several decades. For low density unthickened tailings deposited into conventional tailing storage facilities the primary foci of beach slope prediction have been characterizing the beach concavity and predicting the particle size sorting behavior along the beach.

Beach concavity is important in storage facility design and operation as it can have a significant impact on facility storage capacity. To quantify the concavity of conventional systems Melent'ev initially developed a Master Profile concept using the simple relationship (Kupper 1991):

$$\frac{y}{H} = \left(1 - \frac{x}{L}\right)^n , \tag{1}$$

where:

y/H = nondimensional relationship between height y and maximum height H

x/L = non-dimensional relationship between the length, x, and total beach length L, and

n = an exponent to quantify the beach concavity.

Additional work by Blight (1985), Kupper (1991), McPhail (1995), and Morris and Williams (1997) served to quantify the exponential parameter for the master profile model based on slurry classification, and explain the particle sorting behavior of dilute tailings.

Particle sorting behavior is important as it determines the hydraulic conductivity within the facility. For dilute tailings flows, the coarse fraction settles nearer the pipe discharge, while the fines typically settle further toward the center of the facility, as shown in Figure 3 (Blight 2009). The coarse particles result in a high-conductivity, fast-draining zone near the embankment walls, and a slower dewatering fines fraction in the center of the facility. Frequently the coarse fraction deposited near the embankment is used to for embankment wall construction. Understanding the particle sorting is critical in ensuring the stability and drainage characteristics of the facility.

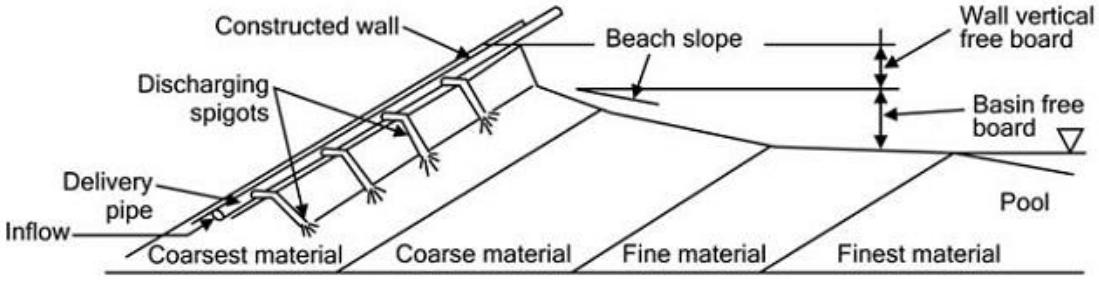

Figure 3: Particle Sorting in Conventional Unthickened Tailings Deposition (Blight 2009)

1.2.2 Recent Developments - Thickened Tailings Beach Slope Prediction

The higher concentration thickened and paste tailings typically results in non-Newtonian flow behavior. As a result, the beach slope is steeper than conventional dilute tailings disposal systems. The correct prediction of beach slope becomes critically important in these facilities, particularly when the tailings impoundment rise above the perimeter containment earthworks, if present.

Multiple researchers have developed models for predicting the beach slope for thickened tailings systems considering a variety of bases. They are summarized as follows:

- Stream power/entropy method, developed by McPhail (1995, 2008).
- Sedimentation slope method, developed by Fitton et al. (2006), Pirouz and Williams (2007), Fitton (2007), and Fitton and Slatter (2013).
- Lubrication theory method, developed by Simms (2007), Henriquez and Simms (2009), and Mizani et al.(2010).
- Slope stability method, developed by Li (2011).
- Slurry channel flow method, developed by Thomas and Fitton (2011).
- Debris flow method by Pinheiro et al., (2012).

Treinen et al (2014) provides a comparison of the three most common beach slope prediction models. From the discussion it is clear that further understanding of the beach flow behavior is needed in order to accurately predict the resulting beach slope.

The non-Newtonian flow behavior also results in less particle size sorting within the tailings flow down the beach compared to conventional tailings. Little work has been done to quantify the sorting susceptibility based on tailings properties.

1.3 Research Focus/Objectives

The broad focus of this work is to develop a robust framework for modelling tailings beach flows. The ultimate ability to model the evolution of tailings flows in three dimensions within a storage facility will provide greater understanding of the resulting beach slope formation, as well as the ability to optimize deposition sequencing.

The development of a three-dimensional tailings beach flow model must be completed in stages and validated at each step. This thesis focuses on the first step of developing a tailings model considering the transport and settling of a mono-sized coarse particle fraction within a two dimensional (length and depth) laminar sheet flow of viscoplastic carrier fluid. The specific objective of this work is to evaluate the ability

to model the coarse particle hindered settling and particle deposition along the beach using a rheology augmentation approach.

1.4 Thesis Structure

This work is divided into the following sections:

- Chapter 2 describes the fundamental aspects of tailings beach flow behavior to be included in the flow model
- Chapter 3 provides an overview of the pertinent previous numerical modelling research and discusses the numerical approach selected for this study
- Chapter 4 details the 2D numerical model implementation
- Chapter 5 provides validation and calibration of the individual 2D model components
- Chapter 6 presents results from the 2D modelling considering both viscoplastic carrier fluid flow and coarse particle transport and settling
- Chapter 7 summarizes the conclusions of the work
- Chapter 8 provides recommendations for future work.

CHAPTER 2:
FUNDAMENTAL ASPECTS OF TAILINGS BEACH FLOWS

2.1 Introduction

In developing a tailings beach flow model it is first necessary to discuss and understand the key fundamentals governing tailings beach flow behavior. The fundamentals are outlined in the following sections.

Ultimately, energy dissipation drives beach flow behavior. Energy dissipation during flow down a tailings beach is a complicated phenomenon as illustrated by the dissipation mechanisms presented in Table 1 for river sedimentation, debris flows, and hyper-concentrated river flows (Chanson 2004; Julien and León 2000).

Three key drivers are believed to have the most significant impact on energy dissipation down the beach and ultimately beach formation (Treinen et al. 2014; Treinen and Jewell 2015):

- Non-Newtonian flow behavior
- Particle settling behavior
- The flow path down the beach.

Table 1: Energy Dissipation Mechanisms

Flow related	**Particle related**
Viscous dissipation	Inter-particle collision of suspended particles
Turbulent eddy dissipation	Particle migration/diffusion
Bed/embankment interaction (wall shear stress)	Bed-layer collisions, saltation
	Bed erosion

2.2 Tailings Slurry Composition

Mine tailings vary significantly in composition from coarse sand particles in clear water that form a rapidly-settling, heterogeneous mixture (Gillies and Shook 2000), to fine clay viscoplastic slurries that are homogeneous and non-settling (Xu et al. 1993). Most typical mine slurries have a widely polydisperse particle size distribution and are treated as a mixed regime type slurry. The fine particle fraction comprises the pseudo-homogeneous rheologically active carrier fluid while the coarse particle fraction is prone to settling.

The cut point that separates the fine and coarse fractions is dependent on minerology, clay content, and surface chemistry of the tailings particles, but it is typically between 20 microns and 45 microns. For practical purposes the cut point is frequently selected as either 45 microns or -75 microns (Sanders et al. 2004). The minerology greatly influences the overall slurry behavior. A high clay content slurry is much more rheologically active than pulverized rock flour. Flocculants and other admixtures may create a shear history dependence on the rheological behavior.

As a simplification of the polydisperse nature of most mine tailings, this work considers a bimodal model slurry consisting of a monosize coarse particle fraction within a homogeneous, non-settling, viscoplastic carrier fluid. Although the model development considers a range of slurry properties, a typical oil sands thickened or "composite tailings" slurry is considered as the basis for the work. Typical reference properties are summarized in Table 2 (Spelay 2007).

Table 2: Model Tailings Properties

Carrier fluid		**Coarse Sand Fraction**	
Description	Clay slurry mostly containing kaolinites	Description	Fairly well-rounded, alluvial sand
Particle size	< 5μm	Particle size	100 to 500 μm
Slurry density, ρ_m	1050 to 1500 kg/m^3	Solids density, ρ_s	2650 kg/m^3
Bingham yield stress	1 Pa to 100 Pa	Coarse volume concentration, φ	15 to 30%v
Plastic viscosity, μ_P	0.001 to 0.1 Pa.s		

2.3 Fluid Flow Regime

As part of his beach slope prediction research, Fitton (2007) argued that beach flows must necessarily be turbulent. Pirouz et al. (2014) argues that the beach flow is necessarily within the transition region between laminar and turbulent flow. However, high density thickened tailings may exhibit considerable Bingham yield stress resulting in laminar flow down the beach (Fitton, 2013). In reality all three regimes are likely as the tailings flow transitions from pipeline discharge (turbulent) to fast moving channel flow (transition), to spreading delta flow (laminar).

For this investigation, only laminar flow is considered, as it provides a well-defined basis for the 2D model development. Correctly predicting turbulent flow in viscoplastic fluids is an active area of research (Rudman et al. 2004). While excluded from this initial work, a methodology to include turbulent flow in the beach flow model is discussed in Appendix A.

2.4 Carrier Fluid Fraction

The carrier fluid fraction is the rheologically active portion of the tailings slurry and is typically classified as a Bingham Plastic or Hershel-Bulkley viscoplastic fluid. Occasionally the carrier fluid does not exhibit a yield stress and the power law rheology model is used. Figure 4 presents a comparison of three rheology models at approximately equivalent high shear behavior. The Bingham plastic and power law models are ultimately simplifications of the Hershel-Bulkley model.

There is debate as to whether particle suspensions actually exhibit a true yield stress (Barnes 1999) or behave closer to power law fluids. Measuring the rheology at low shear rates can be challenging, and requires special attention (Stowe et al. 2014).

The impact the low shear rheology has on the overall flow and deposition behavior along the beach is unclear. McPhail's (2008) beach profile prediction method requires low shear rate rheology measurements using flume flows to calibrate the model. Understanding the sensitivity of the beach flow behavior to the low shear rheological behavior would provide further insight into this beach slope prediction approach.

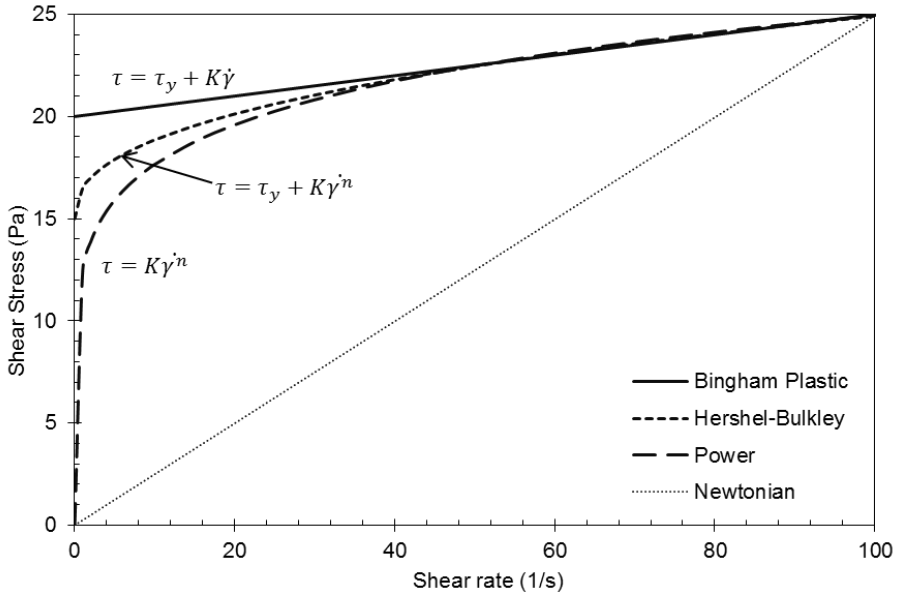

Figure 4: Comparison of Rheology Models with Similar High-Shear Behavior

2.5 Coarse Particle Fraction

The coarse particle fraction is suspended within the carrier fluid and transported with the fluid flow down the beach. A variety of forces can act on particles within the fluid flow, resulting in particle migration opposing the flow. Some of the forces include:

- Gravity
- Drag
- Inter-particle collision forces
- Lift force due to linear fluid shear (Saffman lift force)
- Lift force due to particle rotation (Magnus type force), generally negligible at high particle concentrations
- Virtual mass force, due to particle acceleration in a pressure gradient
- Basset force due to viscous effects in particle acceleration, often neglected
- Turbulent diffusion forces in turbulent flow
- Electrostatic forces (Brownian) due to varying particle charge
- Coulombic forces due to particle contact

- Additional external forces (electric fields, etc.).

The most influential forces are dependent on the particle size, concentration of interest, and flow regime. For the coarse particles considered within the laminar beach flow, only three forces are typically expected to dominate:

- Gravity
- Drag
- Lift forces due to fluid shear.

Gravity dominates the forces acting on the coarse particles within the flow; it is counteracted by the drag force as the particles settle. The hindered settling effect is discussed in detail in the following subsection.

The potential velocity slip and resulting particle drag due to the difference in down-slope carrier fluid velocity and coarse particle velocity is expected to be small in tailings flow and is not considered in this study. The influence shear lift has on the particles is further discussed in Section 2.5.3.

Additionally, it is likely Columbic forces become important once the particles settle into inter-particle contact on the beach. These Coulombic forces are not the primary interest in this study on understanding the beach flow behavior, but further discussion is provided in Section 4.7.

2.5.1 Particle Settling

Of particular interest in this beach flow modelling study is predicting the coarse particle migration and settling within the carrier fluid flow field. Much of the particle settling research has focused on settling within Newtonian fluids, discussed first below. Following the fundamental settling and sedimentation in Newtonian flow, the discussion advances to the impacts viscoplastic fluid behavior has on coarse particle settling.

Newtonian Fluids

Researchers have studied particle settling and sedimentation since the development of Stokes law for a single particle in 1851 (Chhabra 2006). Kynch's (1952) theory of sedimentation and Richardson & Zaki's (1954b) hindered settling work continue to be the foundation for many practical settling analyses considering particle settling in quasi-static fluid.

Kynch (1952) proposed a sedimentation theory based on the assumption that the particle settling velocity depends only on the local concentration. His sedimentation theory considers the flux continuity through a column depth and is solved using the method of characteristics. Of particular note is his observation from the possible range of characteristic lines in the theoretical model that discontinuities, or shocks, may form in the settling column depending on the shape of the flux curve. Kynch's initial model did not provide any method of determining the shape of flux curve, except to state that further experimental work was required to validate the sedimentation theory. Kynch (1959) later proposed a sedimentation model based on effective suspension viscosity, which is discussed in Section 5.4.2.

Richardson & Zaki (1954a) completed fairly extensive experimental fluidization and settling test work which considered a range of particle sizes, densities, and shapes and then aimed to further develop a theoretical framework to explain the results (1954b). Richardson & Zaki's resulting hindered settling model is of the form:

$$V_{HS} = V_{ts}(1-\varphi)^{n}, \tag{2}$$

where V_{ts} is the settling velocity of a single particle and n is a hindered settling coefficient. In the Stokes flow regime (Rep<0.1), the single particle terminal settling velocity is calculated as:

$$V_{ts} = \frac{2}{9}\frac{g r_p^2 \left(\rho_p - \rho_l\right)}{\mu_l}. \tag{3}$$

Outside of the Stokes regime the terminal settling velocity is determined based on the calculated drag coefficient. Cheng (2009), developed an explicit relationship for the drag coefficient and terminal settling velocity up to particle Reynolds numbers, Rep up to $2x10^5$. The drag coefficient is determined from the empirical relationship:

$$C_D = \frac{432}{d^{*3}}\left(1 + 0.022d^{*3}\right)^{0.54} + 0.47\left[1 - exp\left(-0.15d^{*0.45}\right)\right], \quad (4)$$

where :

$$d^* = d\left[\frac{\rho_l g(\rho_p - \rho_l)}{\mu_l^2}\right]^{1/3}, \; V_{ts}{}^* = V_{ts}\left[\frac{\mu_l g(\rho_p - \rho_l)}{\rho_l{}^2}\right]^{-1/3}, \text{ and } V_{ts}^* = \sqrt{\frac{4d^*}{3C_D}}. \quad (5)$$

Richardson & Zaki (1954a) found that an exponent of n = 4.65 best agreed with their experimental data under viscous flow conditions (Rep<0.2). At high Reynolds numbers (Rep ~ 500,) n decreases, and ultimately reaches a constant at Rep of n = 2.39. Additional researchers have further refined this exponential parameter. Garside and Al-Dibouni (1977) expanded it to up to particle Reynolds numbers of $3x10^4$ with the following relationship:

$$\frac{5.1 - n}{n - 2.7} = 0.1Re_p{}^{0.9}. \quad (6)$$

The Richardson & Zaki (1954b) and Kynch (1959) sedimentation models are only valid up to the "gel point" prior to particle consolidation. This limitation is suitable for relatively large rigid particles that become closely packed on settling. Clay-like particles and flocculated suspensions will experience further consolidation on settling. Various researchers (Bürger et al. 2013; Diehl et al. 2015; Kranenburg 1992; Pane 1985; Winterwerp and van Kesteren 2004) have developed expanded models that cover the full sedimentation and consolidation behavior.

Viscoplastic fluids

Settling of a single particle, let alone hindered settling, within viscoplastic fluids is much less understood. Most of the research to date has focused on single particle settling. Chhabra (2006) provides a summary of the research on both single particle and multi-particle settling within quiescent viscoplastic fluids. For example, Gumulya (2009; 2007) experimentally evaluated the settling of either vertically aligned or horizontally aligned spheres in viscoplastic fluid and found the local interaction between the two particles, as well as the fluid structure and shear history play a role in the settling behavior.

Chhabra notes that all of the sedimentation studies summarized indicate "a complex interplay between the rheology and initial configuration" (Chhabra 2006 p. 432). This interplay results in

inhomogeneities and structure formation (channelization, agglomeration) during the particle settling. For single particles settling in a viscoplastic fluid the proposed models are generally a modification of the Newtonian hindered settling formulation to account for the non-Newtonian effects and potential unsheared envelope surrounding the particle (Chhabra 2006).

It is important to first note that particles will only settle in a quiescent viscoplastic fluid provided the downward force due to a particle's mass can overcome the fluid yield stress. The criterion detailed in Chhabra (2006) and provided in equation (7) determines whether a particle will settle:

$$Y_G = \frac{\tau_y}{g d_p (\rho_s - \rho_l)}, \tag{7}$$

where τ_y is the yield stress, g is the gravitational constant, d_p is the particle diameter, and ρ_s and ρ_l are the respective densities of the solid particle and fluid.

The critical value of Y_G has been debated by various researchers and found to vary between 0.048 and 0.212 (Chhabra 2006). Tabuteau et al. (2007) determined a Y_G value of 0.145 from their careful experimental investigation of spherical particles falling within Carbopol gels. This is in good agreement with the 0.143 value predicted through modelling of a single particle settling in Bingham plastic fluids using finite element methods by Beris et al. (1985), confirmed by Blackery and Mitsoilis (1997), and expanded to Hershel Bulkley fluids by Beaulne and Mitsoilis (1997).

Figure 5 provides a plot of eq. (7) above considering the bounds of the critical values from the literature. The shaded region indicates the typical coarse particle sizes in most tailings. Even a relatively small yield stress of 1 Pascal will suspend the majority of typical mine tailings particles sizes.

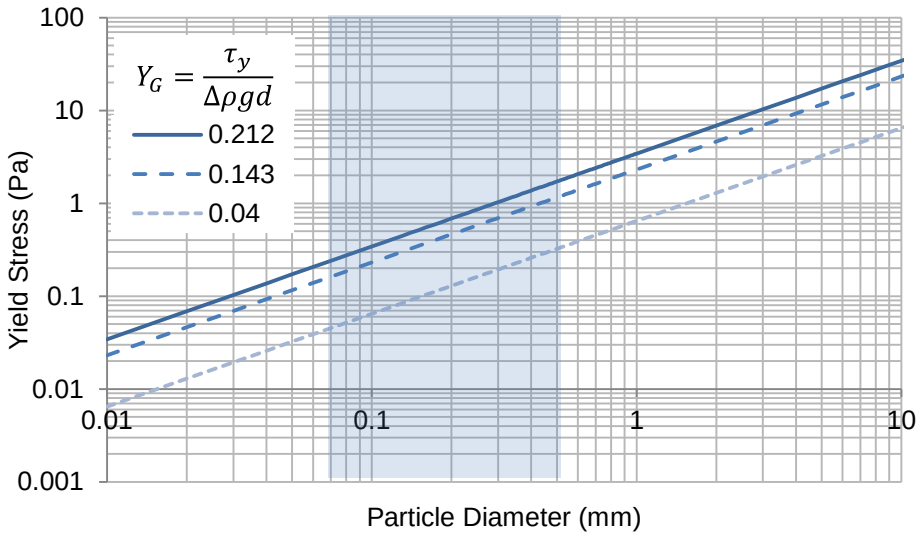

Figure 5: Particle Suspension Criteria in Viscoplastic Fluid (ρ_s = 2650, ρ_l = 1000)

The other means by which particles settle in a viscoplastic fluid is when the fluid is sheared, overcoming the yield stress. Work by Talmon and Huisman's (2005) as well as Ovarlez et al. (2012) aimed to measure and model the shear-settling of mono-sized particles in viscoplastic fluids.

Talmon and Huismann's (2005) settling velocity model, in equation (8), considers the shear stresses acting on a single particle as the particle rotates due to the applied fluid shear. Ultimately they obtained the standard Stokes formula with added empirical coefficient, α, as presented in equation (8). An alpha equal to 0.5 best matched their experimental results:

$$v_s = \frac{2\alpha}{9}\frac{g r_p^2(\rho_p - \rho_l)}{\mu_a(\dot{\gamma})}. \quad (8)$$

Talmon expanded this work (Talmon et al. 2014a; b) to concentrated suspension and incorporated the hindered settling effect using the Richardson & Zaki (1954a) formulation. Interestingly, they found an alpha of between 1 and 2 best matched the concentrated suspension results, indicating that concentrated suspensions in viscoplastic fluids settle faster than the Newtonian-based Richardson & Zaki model, while single particles settle slower than predicted by Stokes law. This may be due to the particle interaction and inhomogeneities discussed above.

Ovarlez et al (2012) work utilized MRI experimental techniques to measure the concentration gradient with depth in a Couette shear cell. They found that alpha in equation (8) above may vary from between 0.7 to 3 and appears dependent on the shear rate and material properties. They also found that the Couette geometry influenced the settling velocity of particles within both quiescent and sheared Newtonian fluid within the cell, further complicating the experimental results for the viscoplastic fluids. Another difficulty in determining the shear-induced sedimentation using a Couette apparatus is the fact that the shear rate is not constant across the gap. As a result, particles closest to the moving spindle[3] will settle faster than those against the stationary wall.

The result from Talmon et al. (2014b) and Ovarlez et al (2012) that the settling rate of a suspension of particles will between 0.5 and 3 times the hindered settling an equivalent Newtonian fluid at least confirms the relative impact the viscoplastic fluid may have on the particle settling rate. Due to the variability observed in the measured α, this additional adjustment factor is not considered in this study. Further refinement can be made in future work.

2.5.2 Suspension Viscosity/Rheology Augmentation

Newtonian Particle Suspensions

When particles are added to a carrier fluid they increase the overall mixture viscosity. Quantifying the total mixture viscosity of a particle[4] suspension dates back to Einstein's (1906) viscosity model for dilute suspensions with volumetric concentrations less than approximately 5%. Numerous researchers have aimed to expand the suspension viscosity-concentration relationship to higher concentrations. Several of the more well-known models are summarized in Table 3 and plotted for comparison in Figure 6.

The Krieger (1972) relationship is a simplification of the Krieger and Dougherty (1959) equation for monosized spheres with a close packed maximum concentration of 0.74 and the intrinsic viscosity

[3] Or cup, if cup rotates instead of spindle

[4] Typically mono-sized.

[μ] = 5/2. The Brouwers (2010) model is included in the table as Blazejewski (2012) notes that the Brouwers equation is an *original and exact, closed form expression based on geometrical considerations that predicts the viscosity of a concentrated suspension of monsized particles (p. 181).*

Table 3: Newtonian Viscosity Augmentation Models

Model	**Equation**
Einstein (1906)	$\frac{\mu_m}{\mu_f} = 1 + 2.5\varphi$ Valid only for very dilute suspensions
Eiler's (1941) equation cited in Leighton and Acrivos (1987a)	$\frac{\mu_m}{\mu_f} = \left(1 + \frac{1/2[\mu]\varphi}{1 - {\varphi}/{\varphi_m}}\right)^2$ The intrinsic viscosity $[\mu]$= 3
Krieger and Dougherty (1959)	$\frac{\mu_m}{\mu_f} = \left(1 - \frac{\varphi}{\varphi_m}\right)^{-[\mu]\varphi_m}$ $[\mu]$= 2.5 for spheres (intrinsic viscosity)
Landel Moser and Bauman (1963) cited in Paulsen (2007)	$\frac{\mu_m}{\mu_f} = \left(1 - \frac{\varphi}{\varphi_m}\right)^{-2.5}$
Thomas (1965)	$\frac{\mu_m}{\mu_f} = 1 + 2.5\varphi + 10.05\varphi^2 + 0.0027e^{16.6\varphi}$
Krieger (1972) used by Philips (1992)	$\frac{\mu_m}{\mu_f} = \left(1 - \frac{\varphi}{\varphi_m}\right)^{-1.82}$
Brouwers (2010)	$\frac{\mu_m}{\mu_f} = \left(\frac{1-\varphi}{1-\frac{\varphi}{\varphi_m}}\right)^{{B\varphi_m}/{1-\varphi_m}}$, where B= 2.5

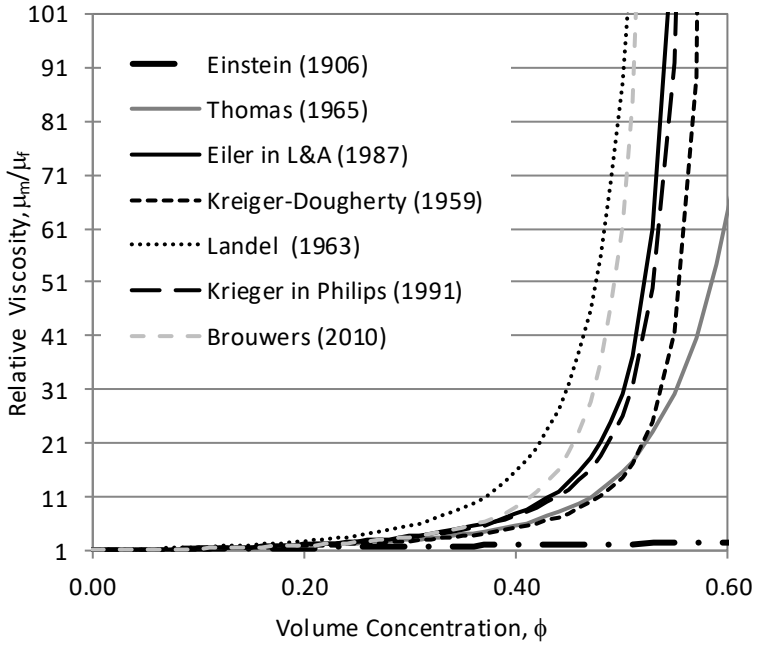

Figure 6: Comparison of Suspension Viscosity Relationships

Non-Newtonian Suspension Rheology Augmentation

Similar attempts have been made to quantify the rheology augmentation due to particles within non-Newtonian fluids. Early work of Highgate and Whorlow (1970) aimed to quantify the rheology augmentation in viscoplastic fluids. They suggest the effect on rheology can be determined independent of shear rate as long as one compares the suspension rheology to the carrier fluid at equivalent shear stress rather than shear rate. However, their testing was only completed up to 10%v.

Considering typical mineral slurries, Thomas (1999) extended the Landel, Moser and Bauman (1963) equation in Table 3 to apply to both the Bingham plastic yield stress and plastic viscosity parameters. Thomas (1999) then further expanded the correlations using the well-established exponential relationships correlating yield stress and plastic viscosity to volumetric concentration to develop a total yield stress model over a range of solids concentration.

Ancy and Jarrot (2001) aimed to develop a more mechanistic model to predict the increase in yield stress due to the coarse particles. They found the primary mechanisms resulting in an increase in yield stress

due to coarse particles were a depletion effect at low coarse fraction concentrations and inter-particle contact at high coarse fraction concentrations.

In addition to developing a model to predict the yield stress of monodisperse particles based on particle diameter, Zhou et al (1999) investigated the yield stress of polydisperse mixtures. Their polydisperse model, which considers a mean particle diameter, can also be used to predict the rheology augmentation of a bi-modal clay-sand mixture, as was done by Paulsen (2007).

Paulsen (2007) conducted a wide range of experimental test work with a well-behaved kaolin clay carrier fluid and a variety of sand and glass bead coarse fractions. He set out to evaluate earlier rheological augmentation models (e.g. Wildemuth and Williams (1985), Schaan et al. (2000), Thomas (1999), and Zhou et al (1999)) and aimed to develop a more mechanistic model for predicting rheology augmentation.

Paulsen (2007) discuses three regimes/contributors to viscosity/rheology augmentation:

- Volume exclusion region (<5% to 10%v), or depletion effect as discussed by Ancy and Jarrot (2001), where the augmentation is solely due to the decreased volume over which the rheologically active carrier fluid can be sheared
- Region of "Additional hydrodynamic effects" (~10% to below φ_m) where wake effects around particles, lubricated contact effects and other hydrodynamic effects result in a higher apparent viscosity
- Particle interaction zone (near $\varphi_{m)}$ where collisions and jamming may dominate.

Paulsen (2007) found that the quasi-empirical model of Thomas (1999) and the distance ratio model, with a similar form as proposed by Schaan et al.[5] (2000), agreed with the experimental measurements of both yield stress and plastic viscosity within approximately 15%. It is clear from Paulsen's comparison that the distance ratio model better predicts the rheology augmentation effect at high concentrations (<35%v)

[5] Note that Paulsen (2007) excluded the additional 2.5φ term proposed by Schaan et al (2000) with no explanation. As discussed by Spelay (2007), the term was to account for particle interaction, but is not valid in the dilute region.

compared to the Thomas (1999) correlation. Both models required adjustment of the empirical coefficients to best agree with the measured experimental data.

Paulsen (2007) also proposed a more mechanistic model, the residual clay concentration model, which considers the concentration difference of a carrier plus coarse fraction slurry to that of a carrier fluid-only slurry at equivalent yield stress or plastic viscosity. It provided slight improvement to the empirical models, requires further validation, and its actual implementation isn't clear.

Rahman (2011) repeated a similar test campaign to Paulsen (2007) with the key objective of developing more rigorous experimental procedures to help reduce the variability in the results. In particular, the work focused on deaerating the samples and maintaining consistent water chemistry; which was not done in the Paulsen test work. However, the variability in the data was not significantly decreased. Ultimately the experimental work resulted in updated coefficients for the Thomas (1999) empirical correlations. Rahman did not evaluate the distance ratio model in his work.

Also of interest in Rahman's (2011) work was evaluating the effect of particle size on the rheology augmentation models. In evaluating two particle sizes (90 and 190 micron) Rahman found no significant difference on the impact on the rheology augmentation between the two particles sizes. However, additional work by the Saskatchewan Research Council's (SRC) Pipe Flow Technology Centre[6] found that particle size appears to impact the rheology augmentation, depending on the sand size relative to the clay floc size (Spelay et al. 2014).

The SRC initially developed the rheology augmentation model presented in Gillies 2006's private communication, cited in Spelay (2007), and recently improved the correlations for the yield stress and plastic viscosity based on further experimental testing. The SRC used different diameters and shaped sands mixed with kaolin clay mixtures at various concentrations to improve the correlations. Its newer yield stress correlation is separated into two improved correlations, one for fine slurries with d_{50}<0.12 mm and one for

[6] The work of Paulsen, Spelay and Rahman was all completed in collaboration with the SRC.

coarse slurries with d_{50}>0.12 mm (Spelay et al. 2014). The results of this work are not yet public, and not presented in Table 4.

More recently Talmon et al. (2016) and Hanssen (2016) found good agreement between two additional rheology augmentation models and Thomas's (1999) correlation. The models were first calibrated to the experimental data measured by Thomas (1999) correlation prior to comparing their predictions over a range of sand concentrations. Because these two models showed similar results to Thomas 1999, and are calibrated based on Thomas's (1999) experimental data, they are not presented below.

The Thomas (1999) correlation, including updated coefficients from Paulsen (2007) and Rahman (2011) along with the distance ratio model with coefficients of Gillies (2006, cited in Spelay, 2007) and Paulsen (2007) are summarized in Table 4.

Figure 7 presents plots of the Bingham plastic viscosity models as a function of coarse volume concentration, while Figure 8 presents the Bingham plastic yield stress models. Note the distance ratio model has a much steeper power law form as compared to the Thomas correlation models.

All of the models presented in this section are based on empirical fits to experimental data. As is common in many slurry applications, the correlations may require further calibration against measured data prior to use in modelling. For this study, the most severe augmentation model with concentration, Gillies (2006, cited in Spelay, 2007), and the most moderate over the concentration range, Rahman (2011), are evaluated.

Table 4: Non-Newtonian Rheology Augmentation Models

<table>
<tr><th>Model</th><th>Equation[7]</th></tr>
<tr><td>Thomas (1999)</td><td>$$\frac{\mu_{Pt}}{\mu_{Pc}} = \left(1 - \frac{\varphi}{k_1 \varphi_m}\right)^{-2.5}$$
$$\frac{\tau_{yt}}{\tau_{yc}} = \left(1 - \frac{\varphi}{k_2 \varphi_m}\right)^{-2.5}$$
where k_1 and k_2 is a fitting parameter and the term $k\varphi_m$ varies between 0.6 and 0.9 based on particle size distribution spread and selected value for φ_m
<table><tr><th>Model</th><th>$\mathbf{k_1}$</th><th>$\mathbf{k_2}$</th></tr><tr><td>Thomas (1999)</td><td>1.5</td><td>1.5</td></tr><tr><td>Paulsen (2007)</td><td>1.943</td><td>1.943</td></tr><tr><td>Rahman (2011)</td><td>1.841</td><td>2.869</td></tr></table></td></tr>
<tr><td>Distance ratio model
Gillies (2006, in Spelay, 2007)</td><td>$$\frac{\mu_{Pt}}{\mu_{Pc}} = 1 + \mathrm{A}(\lambda)^{\mathrm{B}}$$
$$\frac{\tau_{yt}}{\tau_{yc}} = 1 + \mathrm{C}(\lambda)^{D}$$
where λ is the linear concentration:
$$\lambda = \left[\left(\frac{\varphi_{max}}{\varphi}\right)^{1/3} - 1\right]^{-1}$$
<table><tr><th>Model</th><th>A</th><th>B</th><th>C</th><th>D</th></tr><tr><td>Paulsen (2007)</td><td>0.113</td><td>2.13</td><td>0.113</td><td>2.13</td></tr><tr><td>Gillies (2006) in Spelay (2007)</td><td>0.21</td><td>2</td><td>0.016</td><td>2.5</td></tr></table></td></tr>
</table>

[7] Where the viscosity augmentation models in Table 3 were relative to a Newtonian fluid viscosity, the rheology augmentation models here are relative to the carrier fluid (water plus fines). The *c* (carrier fluid) and *t* (total) subscripts indicate this difference.

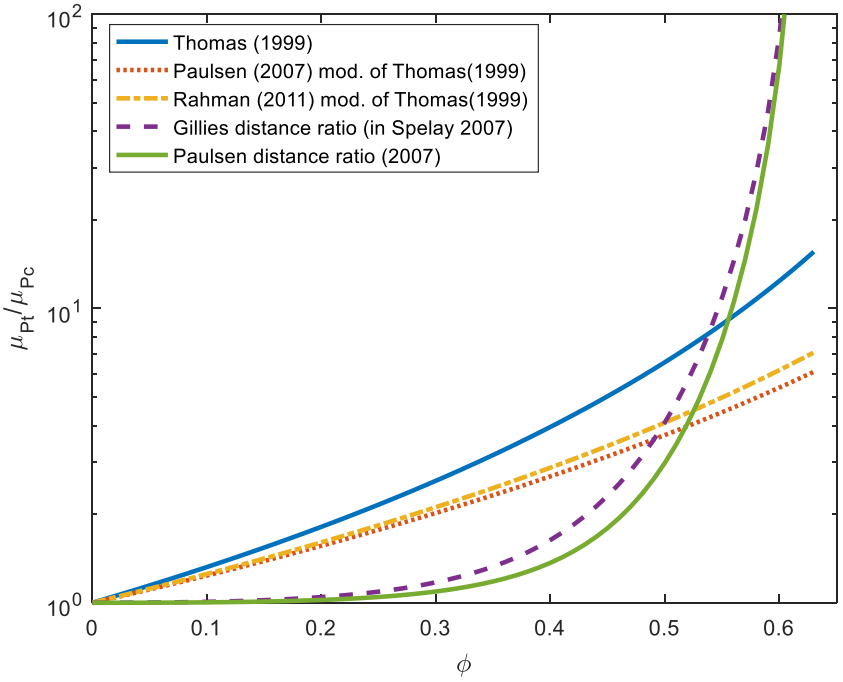

Figure 7: Bingham Plastic Viscosity Augmentation Models

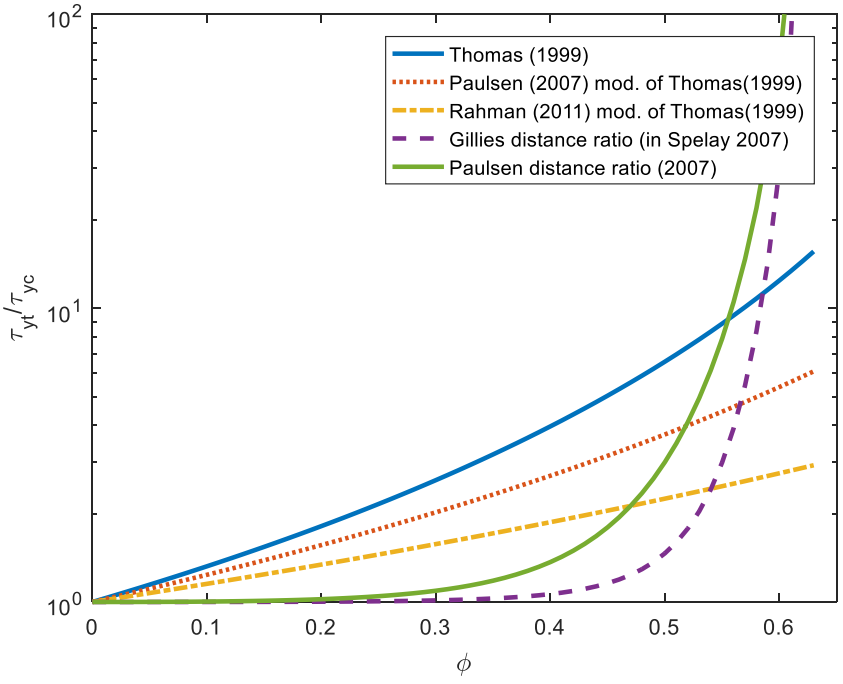

Figure 8: Bingham Yield Stress Augmentation Models

2.5.3 Particle Shear Migration

One key particle migration mechanism of concern in this study, in addition to the settling discussed above, is laminar shear-induced particle migration (Acrivos et al. 1993; Leighton and Acrivos 1985, 1987a; Phillips et al. 1992). Significant research has been completed, generally using neutrally buoyant particles subjected to simple shear flows:

- Rotational Couette flows (Leighton and Acrivos 1987a)
- Simple pressure driven Poiseuille flows and gravity driven inclined film flow (Schaflinger et al. 1990)
- Laminar pipe flows (Zhang and Acrivos 1994)
- Free surface flows (Singh et al. 2006).

A result of shear-induced particle migration is the possibility of viscous resuspension of particles. Once resuspension occurs, equilibrium is reached and the particle settling flux and shear migration flux balance each other. Leighton and Arcrivos (1986) advanced the earlier work of Gadala-Maria F. A. (1979, as cited in Leighton and Acrivos, 1986) and investigated the viscous resuspension phenomenon for mono-sized particles using an annular Couette shear suspension test apparatus. Using a similar experimental setup, Leighton and Acrivos (1987b) aimed to quantify the coefficient of self-diffusion in concentrated suspensions for the shear migration model developed in their prior work.

Shear-induced particle migration is of interest in laminar beach flows because it may result in a viscous resuspension of particles as they settle near the bed. In his work on non-Newtonian coarse-particle laden channel flows, Spelay (2007) modelled the shear-induced migration using the Philips et al. (1992) constitutive shear migration model. Spelay found that the shear migration and resulting resuspension is present, but that the sedimentation flux is generally dominant (2007).

A parametric comparison between the expected settling flux range and shear migration flux is presented in Appendix B. As similarly concluded by Spelay (2007), for the negatively buoyant coarse particles and rheological behavior considered in this study, hindered settling dominates the flow behavior. Consequently, the shear migration effect is excluded from the model development. It is important to note

that for studies considering high yield stress carrier fluids or solids concentrations near the maximum packing concentration, shear particle migration may play a role in the concentration profile development.

As discussed in Section 4.4 a false diffusivity is included in the numerical model development to assist in convergence. This diffusivity is essentially similar to including the diffusive resuspension effect. However, it is several orders of magnitude greater than what would be expected based on Leighton & Acrivos's (1987b) work. Section 5.4.5 provides a justification that the false diffusivitiy in the numerical model work does not significantly impact the results. This evaluation further reinforces that the viscous resuspension effect is dominated by the particle settling in these flow scenarios.

2.6 Beach Flow Path

As discussed in Simms et al (2011) and presented in Figure 9, the flow path down a tailings beach typically has three regions:

- A plunge pool, where energy is dissipated as the flow transitions from pipe flow to channel flow
- A relatively long channel flow region where little or no deposition is expected
- A delta-type flow profile where the flow spreads.

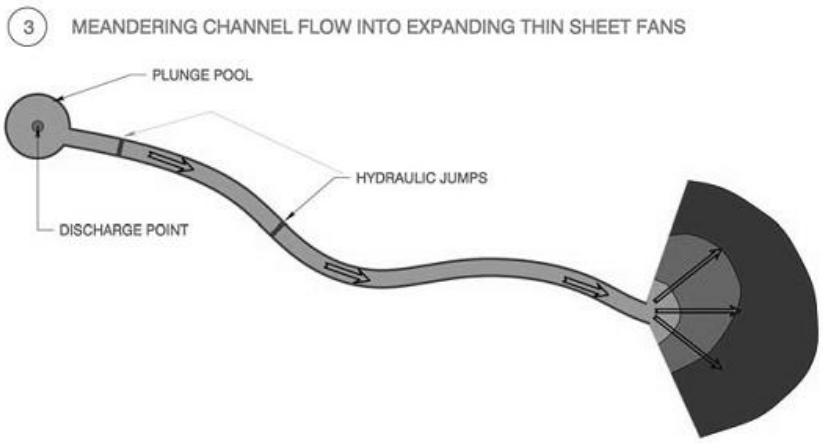

Figure 9: Tailings beach flow path (Williams 2010 written comm., in Simms et al.2011)

However, the concept does not fully explain the deposition of tailings in regions between the discharge point and the fan. Treinen & Jewell (2015) provide the following explanation along with the expanded flow profile in Figure 10:

> *The fan beaches at an angle that is steeper than the channel because the slurry in the fan is settling while the slurry in the channel is settling to a lesser extent (or not at all, as in the equilibrium slope models) and is transferring slurry over previously deposited fans to the developing fan. The beach extends when the settled tailings in the end fan build up sufficiently to block the channel and the slurry cuts through to establish a new equilibrium position, whereupon and the development of a new fan commences. The above process takes place in conjunction with meandering of the flow stream so that multiple fans form as the stream pauses along a particular flow route. The meander direction changes in concert accordance with variations in slurry characteristics, which occurs due to mineralogical variations, thickener fluctuations, and surging in the pipeline etc. This almost certainly contributes to the development of a slightly concave profile that is characteristic of thickened tailings beaches in practice (page 223).*

The ultimate objective in modelling tailings beach flows is to be able to model the full time-dependent 2D spreading and channelizing flow behavior and coarse particle deposition within the deposition area. However, simpler models need to first be developed to validate the flow behavior in:

1) Planer sheet flow down an incline with coarse particle settling
2) Confined channelized flow with coarse particle settling.

This work focuses on correctly modeling the planer sheet flow with coarse particle settling with the intent of establishing a foundation on which to expand the model in future work. Neither the complex plunge pool flow behavior and mixing, nor the potential delta formation is considered in this work.

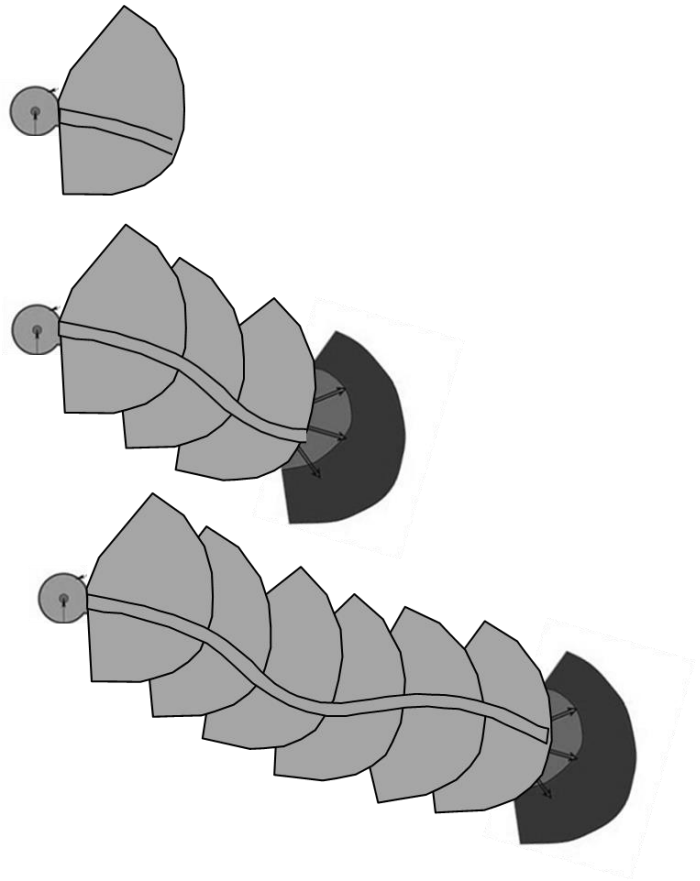

Figure 10: Anticipated Tailings Beach Flow Path (Treinen and Jewell 2015)

2.7 Chapter Summary

Tailings beach flow behavior is a complex interplay of meandering viscoplastic free surface carrier fluid flow down a beach coupled with coarse particle transport and settling within the fluid flow. The coarse particle rheology augmentation impacts both the settling behavior of the coarse particles and the flow behavior of the overall tailings mixture.

Additional complications such as turbulent flow and particle suspension along with more typical polydisperse particle size distribution further complicate the flow behavior of many tailings flows. The model development in this work focuses on a simplified bi-modal tailings flow.

CHAPTER 3:
PERTINENT PREVIOUS WORK

3.1 Overview

Of particular importance in modelling tailings beach flow behavior is the ability to model reasonably large overland distances (up to several kilometers) while maintaining accurate depth-wise resolution of the concentration and flow profiles. The shallow water formulation is a common approach to modelling overland flood and flow routing and serves the starting point to discuss the numerical modelling approach for this work.

A natural progression, as detailed in Figure 11, is found in the literature advancing basic water flood modelling to consider sediment transport, viscoplastic debris flows, and ultimately particle laden viscoplastic flows. The discussion in this chapter first focuses on some of the primary research in these overland flows, along with several other key relevant tailings flow investigations, before focusing on the specific shallow water model formulation in the model development for this work.

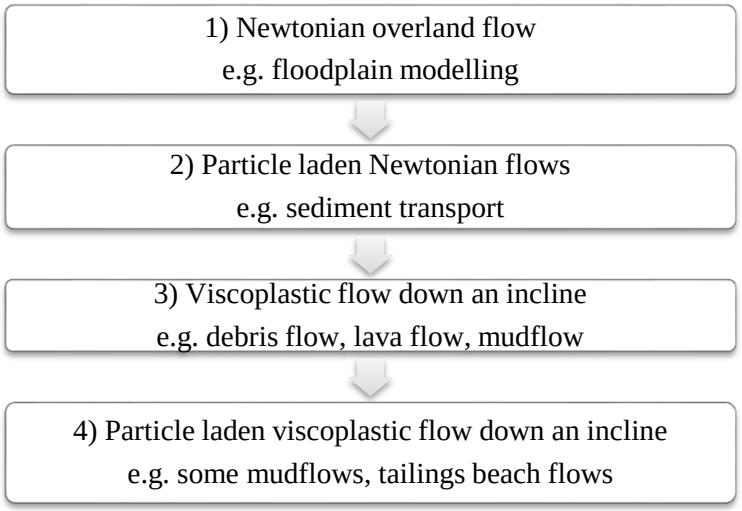

Figure 11: Research Areas in Overland Flows

3.2 Overland Flood Modelling

Surface hydrologists have developed numerous modelling tools (e.g. HEC-RAS (U.S. Army Corp. of Engineers 2016), Mike (DHI 2016), Delft-3D (Deltares 2016), and numerous others) to predict the flow of surface runoff and tidal surges during storm events. They are typically based on a shallow water or kinematic wave fluid flow approximations. The assumption of Newtonian fluid early on in the model development generally makes these models unsuitable for use in analyzing viscoplastic beach flows without significant adaption.

The one exception is Delft-3D, an open source overland flow modelling package developed by Deltares. Modifications to Delft-3D to model tailings flow were initiated by Sittoni et al. (2015) and advanced by Deltares at the same time as this study. Currently, the Delf-3D model appears able to to predict coarse particle settling and transport within 2D viscoplastic sheet flow (Sittoni et al. 2016; Talmon et al. 2016). A comparison between the approach developed in this study and the current 2D viscoplastic sheet flow Deltares model would help provide validation for both modelling approachs.

Current work is underway to expand the model to full 3D tailings flow modelling. Given the development, it may be most efficient to utilize the Delft-3D model for future tailings flow investigations. While Delft-3D is available as an open source software package, the current 2D tailings flow model is currently still under development and not publicly available.

3.2.1 Sediment Transport

Many of the surface hydrology models incorporate sediment transport models, including the Newtonian viscosity augmentation considerations discussed in Section 2.5.2. However, most sediment transport occurs at low solids concentration (<5%v) in turbulent water flow. Sediment transport models are not directly applicable to viscoplastic tailings flows without modification.

3.3 Debris/ Mud/Lava/Avalanche Flow Modelling

As the solids concentration of the sediment increases in overland flows, the resulting hyper-concentrated mud floods and mudflow suspensions may begin to exhibit non-Newtonian behavior (Julien

and Lan 1991). Models with the inclusion of a non-Newtonian fluid behavior can typically be lumped into a generic class of models termed debris flow models. In Figure 12, Takahashi (2007) provides a debris flow taxonomy depending on composition. This discussion focuses only viscous debris flow.

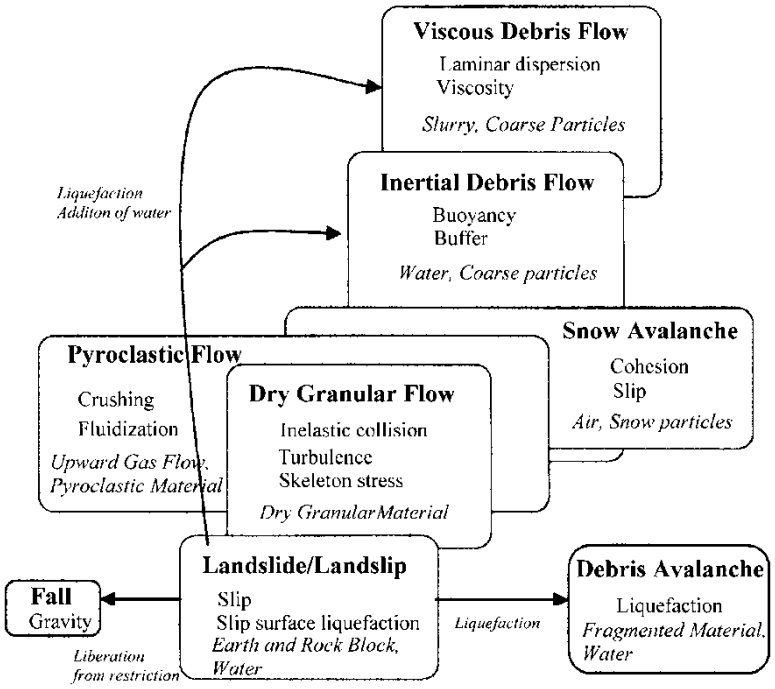

Figure 12: Types of Debris Flow (Takahashi 2007)

The debris flow models of interest in this investigation are either homogeneous debris flows where only the viscoplastic behavior is considered or bi-modal debris flows that also incorporate a second rigid phase.

Homogenous flows

Considerable attention has been given to developing analytical shallow water models for homogeneous debris flows and viscoplastic fluids in general. Johnson (1970) developed an analytical expression for the velocity profiles of Bingham plastic debris flow confined in a semi-circular channel as well as infinite sheet flow. Coussot and Proust (1996) developed an analytical model to predict the unconfined two dimensional flow down an incline based on the long wave simplification of the fluid.

Other general research in viscoplastic fluid behavior considering the shallow water or lubrication approximation is also applicable to homogeneous debris flows. Liu and Mei (1990) investigated the one-dimensional sheet flow of Bingham plastic fluid down an inclined plane. Of particular interest in their study were the ultimate static profiles once the fluid came to a rest after deposition on the inclined plane. They also developed a finite difference method for predicting the transient discharge onto a plane. Balmforth et al (2002, 2006) expanded on the work of Liu and Mei (1990) to investigate the two-dimensional slow spreading of viscoplastic fluid domes on an inclined plane. Yuhi and Mei (2004) investigated the slow spreading of fluid over conical hills and in conical basins.

These analytical models are the basis of the lubrication theory tailings beach slope prediction methods proposed by Simms (2007) and tailings deposition modelling of Henriquez et al. (2009) and Swenson et al (2014). These methods are able to accurately predict the resulting concave down stationary profiles of small-scale (<100 m) quasi-homogeneous tailings during a relatively short deposition of a finite volume. However, they do not represent typical concave up large-scale tailings deposition profiles after long-term continual deposition, which likely results from flow channelization and the natural resulting energy dissipation within the channel (McPhail 2008) or the potentially variability in tailings properties (Fitton et al. 2007).

Several software packages and models are available for predicting the flow of homogenous viscoplastic debris and mudflow. The Bing “Subaqueous and Subaerial Finite-Source Debris Flow Model” developed by Imran et al. (2001) provides a freely available 2D (length and height) model for modelling a homogeneous Hershel Bulkley fluid down an inclined slope. The primary limitations of this model are that it is a compiled executable and cannot be modified, and it only considered a fixed initial volume of fluid at the top of the slope. Many debris flow models only consider a finite volume release of material (i.e. landslides) rather than a continuous discharge common to tailings flows. Pinheiro et al. (2012) was successful in utilizing Bing for modelling beach flow behavior of MFT oil sands tailings by artificially adjusting the initial volume to correspond to a downslope flow rate.

A more advanced mudflow model is the two-dimensional Flo-2D mudflow model ("Flo-2D Pro" 2016) developed based on the thesis work of O'Brien (O'Brien 1986; O'Brien et al. 1993). Given the commercial nature of the software it is not possible to alter the implementation to include the coarse particle settling of interest in this work.

Two-Phase Debris flows

The rigid phase in debris flows typically consists of large scale rocks and boulders common in landslide events. In these flows, the kinetic and frictional interaction between these large boulders is more important than the particle settling and deposition phenomenon on which this study is focused.

Within the debris flow classification, the field of hyperconcentrated flow research is the most applicable to tailings beach flows. Hyperconcentrated flows are typically classified as flows with a stable, fine silt fraction with appreciable viscosity or yield stress and a sand size fraction that is transported within the carrier fluid silt (Pierson 2005). However, there are two key differences in these flows compared to beach flows: the sand fraction concentration in hyperconcentrated flows generally exceeds the carrier fluid concentration, and the sand will ultimately settle out as the flow stops. Pierson also argues that hyperconcentrated flows are always turbulent, or contain a turbulent layer near the bed, but the flows also can exhibit a laminar plug region at the surface (2005). This is similar to the argument of Pirouz et al. (2014) that beach flows are typically transitional flows that exhibit some degree of turbulence with depth.

3.4 Additional Pertinent Tailings Flow Research

3.4.1 CFD Methods

Yang's (2009) work on modelling coarse sand flow into large-scale tailings embankments in both 2D and 3D configurations confirms that commercial CFD codes such as ANSYS Fluent are able to model large scale tailings deposition scenarios.

Treinen and Jacobs (2015) investigated the hindered settling and shear particle migration in simple geometries (static cylinder and Couette flow) using the ANSYS Fluent CFD package using the built-in Granular Kinetic Theory (GKT) Eulerian-Eulerian particle model. Although the GKT model was able to

fairly accurately model the hindered settling, the model could not model neutrally buoyant particle migration in simple shear. To minimize numerical diffusion in the concentration profiles within the solution due to Eulerian-Eulerian framework, relatively small elements were required, which significantly increased the computation time.

From this work, it was apparent that significant adaptation was required to the CFD code to efficiently model the tailings free surface flow. No additional investigation into CFD methods was pursued for this study.

3.4.2 Spelay (2007) 1D Finite Volume Model

Considering the flow and particle behaviors included in the approach, Spelay's (2007) numerical modelling of coarse particle transport in laminar flow is the most directly applicable to the model development in this work. Spelay utilizes a finite volume approach to model the coarse sand particle movement within a viscoplastic kaolin clay carrier fluid. The fluid fraction is solved from the Navier-Stokes equations. A scalar transport approach is used to model the coarse particle hindered settling and shear particle migration. However, Spelay's model has the following limitations:

- The flow and particle concentration predictions are limited to a single vertical dimension.
- The flow height is fixed and does not increase as solids deposit on the bottom of the channel.
- The model only considers the plastic viscosity augmentation; no Bingham yield stress augmentation is included.

3.4.3 Deltares/Barr Engineering Collaboration on Oil Sands Tailings Modelling

Sisson et al (2012) developed an analytical tailings deposition model to evaluate the segregation potential of oil sands NST slurry as it flowed down the beach. The main objective in this deposition scheme is to capture as many fines within the sand matrix upon deposition as possible.

Sisson's et al (2012) analytical model considered the transport and hindered settling of coarse sand in a carrier fluid with power law rheological behavior. The shear rate, and resulting apparent viscosity, is incorporated into the hindered settling calculations. However, there is no coupling of the coarse particles to

the flow behavior; the coarse particle fraction does not influence the flow velocity profile through a rheology augmentation effect. Additionally, while their model can predict the coarse particle sedimentation rate with distance down the beach, they only compare the predicted average bulk sedimentation over the entire length to experimental flume tests; localized comparisons are not made.

Sheets et al. (2014) focused on modelling oil sand CT-type tailings flows, treating them as Newtonian river delta flows using the Delft-3D software package. They utilized standard sediment transport models to predict both the fine (44 micron size) silt fraction and coarse sand fraction (100 micron size) within the 3D deposit basins. As they acknowledged the concentrations of both were above the typical natural sediment concentrations by at least an order of magnitude, however, the resulting delta profiles produced physically realistic bed slopes and fines distribution. They do acknowledge that the limitation to Newtonian flow behavior limits the modelling approach for higher concentration viscoplastic tailings flows.

3.5 Novelty of Proposed Model Compared to Previous Work

To date, no tailings model research has coupled a viscoplastic shallow water flow model to the scalar transport model for predicting the advection and hindered settling of coarser particles within the flow through a rheology augmentation approach. This model development includes the following novel advances:

- Coupling the flow behavior, including local flow velocities profiles and overall discharge, to the coarse sand fraction concentration through rheology augmentation
- Solving the hindered settling of the coarser particle fraction through both the apparent viscosity due to the flow velocity profile and the hindrance effect due to the sand concentration
- Determining the local coarse sand concentration profile evolution with both beach length and time
- Evaluating the influence of coarse deposition has on flow height along the beach length.

3.6 Chapter Summary

This chapter first presented an overview of numerical modelling approaches for overland flow modelling. The most applicable model formulations for this work come from debris and hyperconcentrated flow research. The homogeneous flow models, and in particular the analytical equations for viscoplastic flows down inclines, serve as validation cases for developing the tailings model.

At the start of this work, no model development work focused on modeling tailings beach flows by coupling the coarse particle hindered settling and rheology augmentation to the overall tailings flow behavior. Developing a standalone model, rather than adapting existing available approaches. was key to ensuring the key drivers within the flow, as discussed in Chapter 2, were correctly incorporated.

From the review, the shallow water formulation is most appropriate for modeling the tailings flows since it serves as the basis of many of the overland flow modelling approaches. The fundamentals, and key assumptions, of the simplified one dimensional shallow water model are highlighted in the next chapter.

The recent advances in the Delft 3D slurry model completed by Deltares concurrently with this study incorporate the coarse particle settling and rheology augmentation into a well-established overland flow modelling software. Following evaluation of their recent developments and modelling approach, migrating this study into the Delft 3D model may efficiently expand the tailings model to consider 3D flow behavior.

CHAPTER 4:
NUMERICAL MODEL IMPLEMENTATION

4.1 Chapter Overview

This chapter details the model formulation and specific implementation steps including the finite difference shallow water solution method and scalar transport model used to predict the particle advection and hindered settling within the flow. Table 5 summarizes the steps in the beach flow model solution.

Table 5: Solution Flow Chart

	Solution Steps		*Key outputs*	*Numerical Solution Method*
Carrier Fluid solver	1	Velocity profile calculation and depth averaged discharge	$q_x(x)$, $\dot{\gamma}(x,z)$	Trapezoidal integration
	2	Shallow water equation solver	H(x)	Semi-implicit finite difference method
	3	Vertical advective velocity determination	$u_z(x,z)$	-
Coarse particle scalar transport solver	4	X-wise coarse particle advection	$\varphi(x,z)$	Method of Characteristics
	5	Z-wise coarse particle advection and particle settling	$\varphi(x,z)$, $v_{HS}(x,z)$	Implicit upwind finite difference with Picard Iteration

Figure 13 provides the model coordinates and parameter definition in both continuous and discrete form. The underlying bed profile elevation along the beach is $z_b(x)$, while the resulting flow surface elevation at each point is $z_s(x)$. The height difference between the free surface and bed is the flow height, H(x). The depth-varying velocity in the x direction is denoted as $U_{xz}(x,z)$ and the depth varying coarse concentration profile is defined by $\varphi(x,z)$. In discrete form, each x coordinate point is defined by the increment i, while the depth coordinate is defined by j.

Commonly in 1D sheet flow models, the x direction is aligned with the bed slope (Liu and Mei 1990) . This was not done in this study to simplify the model formulation to depend only on the free surface slope, as ultimately presented in equation (14) below.

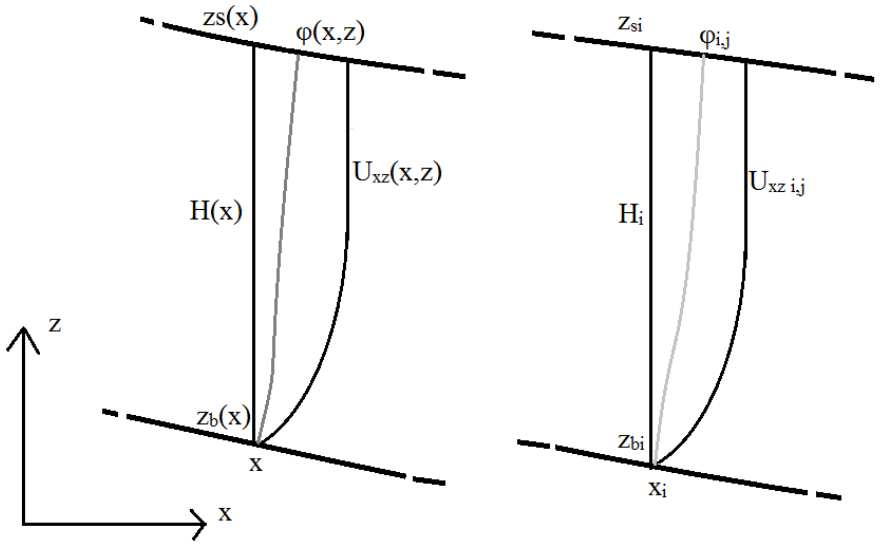

Figure 13: Model Coordinates

As detailed above, the majority of debris flow and thin film flow models utilize the depth averaged shallow water or lubrication theory approximation to model the flow behavior. The approximation simplifies the governing mass and momentum equations for flows where the depth is significantly smaller than the length or width, without impacting the accuracy of results (Vreugdenhil 1994). In addition to overland flow models, the shallow water equations are used to model a wide variety of environmental flows including tsunamis, atmospheric weather patterns, and glacier flows.

Because of the potential coarse particle concentration variation with depth and its impact on both the fluid flow profile through the rheology augmentation, and hindered settling behavior, it is necessary to develop a standalone numerical model rather than attempt to adapt existing commercial or open source overland flood or debris flow models.

4.2 Major Assumptions in Model Development

The following assumptions are made in the model development:

- The particle size distribution of the tailings is considered bimodal:
    - The fine fraction (-45 micron) is homogeneous and non-settling

    - The coarse fraction is monodisperse.
- The mixture flow obeys the shallow water requirements discussed below.
- The flow remains laminar.
- The coarse particle settling obeys the well-established hindered settling behavior in Newtonian fluids.
- Shear particle migration is excluded.
- Only 1D x-wise flow is considered but particle transport includes both x-wise advection and z-wise settling.

4.3 Carrier Fluid Component

4.3.1 Assumptions and Limitation of the Shallow Fluid Approach

In addition to the overarching assumptions summarized in Section 4.2above, the assumptions in the shallow water formulation are provided below to emphasize the limitations of the shallow water flow model:

- The fluid thickness, or height, is small compared to the length (Vreugdenhil 1994).
- The formulation also assumes constant (or near constant) density with depth. In the tailings model the density will actually change slightly with depth, but can be handled through numerical integration through the depth.
- Fluid acceleration is negligible.
- Fluid inertia is negligible.
- The flow is incompressible flow.

4.3.2 Shallow Water Continuity and Momentum Conservation

The continuity equation used in the shallow water models is derived from depth integrating the conservation of mass equation for incompressible fluids, yielding:

$$\frac{\partial H}{\partial t}+\frac{\partial q_x}{\partial x}+\frac{\partial q_y}{\partial y}=0, \tag{9}$$

where the depth integrated discharges q_x and q_y are commonly written in terms of the depth averaged velocities hu, and hv (Vreugdenhil 1994). More simplistically, the change in volume of an incompressible fluid element of fixed length dx, and width dy is dependent only on the change in height, dH/dt. This volume change must balance any change in flow into or out of the element (Miller, 1984). For a 1D infinite sheet flow this reduces to:

$$\frac{\partial \mathrm{H}}{\partial \mathrm{t}} + \frac{\partial q_x}{\partial x} = 0. \tag{10}$$

The standard conservative form of the shallow water linear momentum conservation equations is derived by depth averaging the Navier-Stokes equations and applying appropriate boundary conditions. Ignoring lateral stresses and assuming simple bottom stresses, the "standard" 2D shallow water form is (Vreugdenhil 1994).

$$\begin{aligned} &\frac{\partial}{\partial t}(au) + \frac{\partial}{\partial x}(au^2) + \frac{\partial}{\partial y}(auv) - fav + ga\frac{\partial h}{\partial x} + c_f u\sqrt{u^2+v^2} = 0, \\ &\frac{\partial}{\partial t}(av) + \frac{\partial}{\partial x}(auv) + \frac{\partial}{\partial y}(av^2) - fau + ga\frac{\partial h}{\partial y} + c_f v\sqrt{u^2+v^2} = 0, \end{aligned} \tag{11}$$

where a is h-z_b, h is the elevation of the free surface and z_b is the elevation of the bed surface.

For one-dimensional flow and neglecting the acceleration terms, the balance of linear momentum through the flow depth in the downslope x-direction[8] can be greatly simplified to (Liu and Mei, 1990):

$$\rho g sin(\theta) - \frac{\partial p}{\partial x} + \frac{\partial \tau}{\partial z} = 0. \tag{12}$$

Considering the shallow water assumption that the flow length is significantly greater than the flow depth and ignoring the inertia terms, the hydrostatic pressure distribution through the fluid, assuming no external atmospheric pressure on the free surface, $P(z_s) = 0$, is written as:

$$p = \rho g(z_s - z)cos(\theta). \tag{13}$$

Combining equations (12) and (13) Liu and Mehi (1990) developed analytical expressions for the velocity profile and depth averaged discharge for Bingham plastic flows on a constant inclined slope. Incorporating

[8] Here the x-direction is aligned with the inclined slope.

the mass conversation equation (10) they also developed a transient flow solution using finite difference methods.

For this modelling approach, the above equations are further simplified considering for small angles $\sin(\theta) \approx \tan(\theta) \approx 0$, and $\cos(\theta) \approx 1$. This approximation is generally valid for slopes less than 1/10. Considering this approximation, the pressure distribution equation in equation (13) is differentiated and combined with equation (12) to yield the overall momentum balance through the flow depth:

$$\frac{\partial \tau}{\partial z} = \rho g \frac{\partial z_s}{\partial x}. \tag{14}$$

Integrating with depth yields the familiar linear shear stress distribution:

$$\tau(z) = \rho g \frac{\partial z_s}{\partial x}(z_s - z). \tag{15}$$

Relating this shear stress distribution to the rheological constitutive relationships, discussed in Section 2.3, yields the necessary equations to model the tailings flow.

4.3.3 Vertical Velocity Profile and Depth Averaged Discharge

The 2D tailings flow model in this study considers both non-Newtonian flow behavior, and coarse particle rheology augmentation. As a result, an expression for the velocity depth profile, and resulting depth integrated discharge, cannot be developed analytically.

The velocity profile is calculated at each point and numerically integrated to obtain the resulting depth averaged discharge. Because the velocity profile and flow depth are tracked with depth at each x coordinate point, the 1D shallow water model effectively becomes a 2D model, although only the x-wise shallow water equations are required.

For an incompressible fluid with constant density, the linear shear stress profile with depth is defined as:

$$\tau_{xz}(\mathrm{z}) = \rho g sin(\alpha)(H - z), \tag{16}$$

where H is the local free surface height ($z_s = z_b + H$) and sin(α) is the bed slope. Through the appropriate fluid constitutive model, the shear stress is related to the strain rate, du/dz. The basic constitutive model for a Newtonian fluid is:

$$\frac{\partial u}{\partial z} = \frac{\tau_{xz}}{\mu}. \tag{17}$$

Combining equations (16)and (17) and integrating yields the velocity profile with depth:

$$u(z) = \frac{\rho g sin(\alpha)}{\mu} \int (H - z) dz = \frac{\rho g sin(\alpha)}{\mu} \left(Hz - \frac{1}{2} z^2 \right). \tag{18}$$

Integrating again results in the depth averaged discharge q:

$$q = \frac{\rho g sin(\alpha)}{\mu} \int_0^H \left(Hz - \frac{1}{2} z^2 \right) dz = \frac{H^3}{3} \frac{\rho g sin(\alpha)}{\mu}. \tag{19}$$

Viscoplastic fluids are complicated by the potential inclusion of an unsheared plug within the fluid cross section due to the fluid yield stress. The Hershel Bulkley constitutive model is:

$$\frac{\partial u}{\partial z} = \left(\frac{\tau_{xz-} \tau_y}{K} \right)^{1/n}. \tag{20}$$

Because the strain rate is zero within the plug region, it is necessary to determine the plug velocity and size separately, and then integrate the above equation only within the sheared zone. Chen et al. (2007) provides an analytical expression for the Herschel Bulkley velocity profile:

$$u(z) = \int \left(\frac{\tau_{xz-} \tau_y}{K} \right)^{\frac{1}{n}} dz = \frac{n}{n+1} \left(\frac{\rho g sin(\alpha) H s^{n+1}}{K} \right)^{\frac{1}{n}} \left[1 - \left(1 - \frac{z}{Hs} \right)^{\frac{n+1}{n}} \right], \tag{21}$$

$$0 \le z \le Hs.$$

The plug velocity is

$$up = \frac{n}{n+1} \left(\frac{\rho g sin(\alpha) H s^{n+1}}{K} \right)^{1/n}, \qquad Hs \le z \le H, \tag{22}$$

where Hs is determined by:

$$Hs = H - Hp, \qquad where\ Hp = \frac{\tau_y}{\rho g sin(\alpha)}. \tag{23}$$

If $\tau_y > \rho g sin(\alpha)$, no flow can occur. Integrating the velocity profile results in the depth averaged discharge:

$$q = \int_0^{Hs} u(z)\, dz + \int_{Hs}^H up\, dz = \frac{n}{n+1} \left(\frac{\rho g sin(\alpha) H s^{n+1}}{K} \right)^{1/n} \left[H - \frac{n}{2n+1} Hs \right]. \tag{24}$$

Note that when n = 1 and $\tau_y = 0$, the v(s) equation above reduces to the Newtonian analytical expression above.

Once the coarse particle fraction is included in this implementation, the rheology augmentation due to coarse solids concentration variation with depth must also be taken into consideration. The constitutive equation for a Bingham plastic fluid, with the inclusion of coarse particles becomes:

$$\frac{\partial u}{\partial z} = \left(\frac{\tau_{xz-}\tau_y(\varphi)}{\mu_P(\varphi)}\right), \tag{25}$$

where the yield stress, τ_y, and plastic viscosity, μ_P, are no longer constant, but dependent on the coarse particle volume fraction. The Gillies (2006, cited in Spelay, 2007) relationships, presented in Table 4 are used to augment the total fluid rheology. The correlation for the Bingham yield stress is:

$$\frac{\tau_{yt}}{\tau_{yc}} = 1 + 0.016\lambda^{2.5}. \tag{26}$$

The plastic viscosity relationship is:

$$\frac{\mu_{Pt}}{\mu_{Pc}} = 1 + 0.21\lambda^2, \tag{27}$$

where λ is the linear concentration, defined in Section 2.5.2 as:

$$\lambda = \left[\left(\frac{\varphi_{max}}{\varphi}\right)^{1/3} - 1\right]^{-1}. \tag{28}$$

Additionally, the model also incorporates the nonlinear shear stress profile due to the resulting density variation with depth:

$$\tau_{xz}(\mathrm{z}) = \rho(z)gsin(\alpha)(H - z), \tag{29}$$

where

$$\rho(\mathrm{z}) = \rho_l + \varphi(z)(\rho_s - \rho_l). \tag{30}$$

Given the potential variation in both coarse particle concentration and strain rate within the fluid depth, an analytical solution for the depth averaged discharge is not practical. A trapezoidal integration scheme is used to integrate equation (25) to obtain the velocity profile and ultimately the depth averaged discharge. The steps in determining the velocity profiles at each x-coordinate point are:

(i) Calculate rheology profiles based on current coarse particle concentration

(ii) Calculate the shear stress profile with depth considering the variation in particle volume concentration

(iii) Determine strain rate profile, du/dz, using constitutive rheology model and shear stress profile

(iv) Numerically integrate strain rate profile to obtain velocity profile

(v) Numerically integrate velocity profile to obtain depth averaged discharge.

4.3.4 Discretized Shallow Water Solution

A semi-implicit finite difference approach is used for the shallow water flow model implementation. In a semi-implicit scheme, the depth average discharges are calculated on the half nodes and lagged by one time step. The discharge is first written in terms of a diffusivity. D, as (Rajaram 2015):

$$q=-D\frac{\partial(z_s)}{\partial x}=-D\frac{\partial(z_b+H)}{\partial x}=-D\frac{\partial H}{\partial x}-D\frac{\partial z_b}{\partial x}, \tag{31}$$

where q is determined by evaluating the flow profile in the z direction, as discussed in the preceding Section 4.3.3. With q known, the equation is rearranged to find D:

$$D=\frac{-q}{\frac{\partial(z_s)}{\partial x}}, \tag{32}$$

and the governing equation, in 1-D, becomes:

$$\frac{\partial H}{\partial t}+\frac{\partial}{\partial x}\left(-D\frac{\partial H}{\partial x}-D\frac{\partial z_b}{\partial x}\right)=0. \tag{33}$$

The governing equation in finite difference form is:

$$\frac{H_j^{n+1}-H_j^n}{\Delta t}+\left[\frac{\left(q_{j+1/2}-q_{j-1/2}\right)}{\Delta x_j}\right]=0. \tag{34}$$

Knowing:

$$q_{j+1/2}=-D_{j+1/2}\left[\frac{\left(z_{s,j+1}-z_{s,j-1}\right)}{x_{j+1}-x_j}\right], \tag{35}$$

one can rearrange to determine the diffusivities:

$$D_{j+1/2}=-q_{j+1/2}\left[\frac{x_{j+1}-x_j}{\left(z_{s,j+1}-z_{s,j-1}\right)}\right]. \tag{36}$$

Substituting (36) back into the governing equation (33) yields:

$$\frac{\mathrm{H}_j^{n+1} - \mathrm{H}_j^n}{\Delta t} + \frac{1}{\left(\Delta x_{j,1/2}\right)}\left[-\mathrm{D}_{j+\frac{1}{2}}\frac{\left(z_{b,j+1} - z_{b,j}\right) + \left(\mathrm{H}_{j+1}^{n+1} - \mathrm{H}_j^{n+1}\right)}{\Delta x_j} - -\mathrm{D}_{j-\frac{1}{2}}\frac{\left(z_{b,j} - z_{b,j-1}\right) + \left(\mathrm{H}_j^{n+1} - \mathrm{H}_{j-1}^{n+1}\right)}{\Delta x_{j-1}}\right] = 0. \quad (37)$$

From this point, the equation can be rearranged to a more standard form:

$$[A]\left(\mathrm{H}_{j-1}^{n+1}\right) + [B]\left(\mathrm{H}_j^{n+1}\right) + [C]\left(\mathrm{H}_{j+1}^{n+1}\right) = [\mathrm{f}], \quad (38)$$

so

$$\left[\frac{-\mathrm{D}_{j-\frac{1}{2}}\Delta t}{\Delta x_{j-1}\Delta x_{j,1/2}}\right]\left(\mathrm{H}_{j-1}^{n+1}\right) + \left[1 + \frac{\mathrm{D}_{j+\frac{1}{2}}\Delta t}{\Delta x_j \Delta x_{j,1/2}} + \frac{\mathrm{D}_{j-\frac{1}{2}}\Delta t}{\Delta x_{j-1}\Delta x_{j,1/2}}\right]\left(\mathrm{H}_j^{n+1}\right) + \left[\frac{-\mathrm{D}_{j+\frac{1}{2}}\Delta t}{\Delta x_j \Delta x_{j,1/2}}\right]\left(\mathrm{H}_{j+1}^{n+1}\right) = \mathrm{H}_j^n + \frac{\mathrm{D}_{j+\frac{1}{2}}\left(z_{b,j+1} - z_{b,j}\right)\Delta t}{\Delta x_j \Delta x_{j,1/2}} - \frac{\mathrm{D}_{j-\frac{1}{2}}\left(z_{b,j} - z_{b,j-1}\right)\Delta t}{\Delta x_{j-1}\Delta x_{j,\frac{1}{2}}}. \quad (39)$$

Or, more concisely:

$$-A_1\left(\mathrm{H}_{j-1}^{n+1}\right) + [1 + A_1 + A_2]\left(\mathrm{H}_j^{n+1}\right) - A_2\left(\mathrm{H}_{j+1}^{n+1}\right) = \mathrm{H}_j^n + A_2\left(z_{b,j+1} - z_{b,j}\right) - A_1\left(z_{b,j} - z_{b,j-1}\right), \quad (40)$$

where:

$$A_1 = \mathrm{D}_{j-\frac{1}{2}}\frac{\Delta t}{\Delta x_{j-1}\Delta \mathrm{x}_{\mathrm{j},1/2}},\ A_2 = \mathrm{D}_{j+\frac{1}{2}}\frac{\Delta t}{\Delta x_j \Delta \mathrm{x}_{\mathrm{j},1/2}}.$$

In matrix form the set of equations becomes:

$$\begin{bmatrix} (b_1) & (c_1) & 0 & \cdot & \cdot & \cdot & \cdot \\ \cdots & \cdots & \cdots & 0 & \cdot & \cdot & \cdot \\ 0 & -A_1 & [1 + A_1 + A_2] & -A_2 & 0 & \cdot & \cdot \\ \cdot & 0 & -A_1 & [1 + A_1 + A_2] & -A_2 & 0 & \cdot \\ \cdot & \cdot & 0 & -A_1 & [1 + A_1 + A_2] & -A_2 & 0 \\ \cdot & \cdot & \cdot & 0 & \cdots & \cdots & \cdots \\ \cdot & \cdot & \cdot & \cdot & 0 & (a_J) & (b_J) \end{bmatrix} \begin{bmatrix} \mathrm{H}_1^{n+1} \\ \cdots \\ \mathrm{H}_{j-1}^{n+1} \\ \mathrm{H}_j^{n+1} \\ \mathrm{H}_{j+1}^{n+1} \\ \cdots \\ \mathrm{H}_J^{n+1} \end{bmatrix} = \begin{bmatrix} \mathrm{f}_1^{n+1} \\ \cdots \\ \mathrm{f}_{j-1}^{n+1} \\ \mathrm{f}_j^{n+1} \\ \mathrm{f}_{j+1}^{n+1} \\ \cdots \\ \mathrm{f}_J^{n+1} \end{bmatrix}. \quad (41)$$

The tridiagonal matrix is then solved using the Thomas algorithm (Chapra and Canale 2002).

4.3.5 Boundary Conditions

In the 1D model a known flow rate, q, is applied at the start of the model, as shown in Figure 14. To define the boundary condition, the known q is applied at a fictitious -1/2 node. So that the shallow water equation for point 1 is:

$$\frac{H_1^{n+1} - H_1^n}{\Delta t} + \left[\frac{\left(q_{1/2} - q_{-1/2}\right)}{\Delta x_j}\right] = 0, \tag{42}$$

where:

$$q_{j+1/2} = -D_{j+1/2}\left[\frac{\left(z_{s,j+1} - z_{s,j-1}\right)}{x_{j+1} - x_j}\right]. \tag{43}$$

Since $q_{-1/2}$ is a known value, substituting $D_{1/2}$ into the equation yields:

$$\frac{H_1^{n+1} - H_1^n}{\Delta t} + \frac{1}{\left(\Delta x_{2,1/2}\right)}\left[-D_{\frac{1}{2}}\frac{\left(z_{b,2} - z_{b,1}\right) + \left(H_2^{n+1} - H_1^{n+1}\right)}{\Delta x_{2-1}} - q_{-1/2}\right] = 0, \tag{44}$$

and combining like terms results in:

$$[1 + A_2]\left(H_1^{n+1}\right) - A_2\left(H_2^{n+1}\right) = H_1^n + A_2\left(z_{b,2} - z_{b,1}\right) + q_{-\frac{1}{2}}\frac{\Delta t}{\left(\Delta x_{\frac{1,1}{2}}\right)}. \tag{45}$$

The coefficients for substitution into equation (41) at point 1 become:

- $a_1 = 0$ (not used)
- $b_1 = (1+A_2)$
- $c_1 = -A_2$, and
- $f_1 = H_1^n + A_2\left(z_{b,2} - z_{b,1}\right) + q_{-1/2}\frac{\Delta t}{\left(\Delta x_{1,1/2}\right)}$.

Note that $\left(\Delta x_{1,1/2}\right)$ is not known since $(x_{j+1/2}-x_{j-1/2})$ is not defined ($x_{j-1/2}$ does not exist). For simplicity it is taken that $x_{j-1/2} = -x_{j+1/2}$.

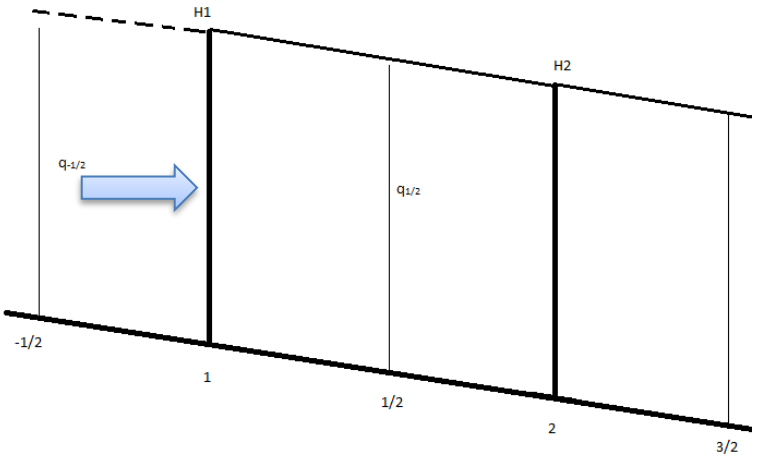

Figure 14: Input Boundary Condition

The other alternative for defining the source boundary condition is to fix H at point 1; q is then determined based on the fixed height value. In this case the tridiagonal coefficients become:

- $a_1 = 0$ (not used)
- $b_1 = 1$
- $c_1 = 0$, and
- $f_1 = H_{known}$.

For simplicity, the end point of the model is defined as having a fixed height of 0 and the model length is large enough so that the flow never reaches the endpoint.

For evaluating the flow through a short beach length segment over a long duration, it is possible to set the height and q flux equal to the upstream values, essentially creating an output boundary condition. This scenario is not evaluated in this work.

4.4 Coarse Particle Component

4.4.1 Governing equations

A scalar transport model is used to predict the coarse particle motion with the flow and hindered settling behavior. The 2D (1D x-wise flow and z-wise vertical settling) particle transport equation follows the general form of the advection-diffusion equation:

$$\frac{\partial \varphi}{\partial t} + \frac{\partial}{\partial x}(\varphi u_x) + \frac{\partial}{\partial z}(\varphi u_z) - \frac{\partial}{\partial z}\left(D\frac{\partial \varphi}{\partial z}\right) = 0. \quad (46)$$

The diffusion term is included in the scalar transport model to provide better solution convergence of the non-linear settling equation. The vertical velocity, u_z, consists of both the advective velocity due to the flow geometry and coordinate definition, and the hindered settling velocity.

4.4.2 Coordinate Transformation

It is advantageous to transform Equation (46) into a relative z-wise ζ coordinate system where

$$\zeta = \frac{z - z_b}{z_s - z_b} = \frac{z - z_b}{H}. \quad (47)$$

This transformation results in ζ varying between 0 and 1 for a given flow depth H. The transformation of the partial derivatives from z to ζ is provided in Appendix C. From the transformation, the particle transport equation becomes:

$$\frac{\partial \varphi}{\partial t} + u_x(\zeta)\frac{\partial \varphi}{\partial x} + u'_z(\zeta)\frac{\partial \varphi}{\partial \zeta} - \frac{1}{H^2}\frac{\partial}{\partial \zeta}\left(D\frac{\partial \varphi}{\partial \zeta}\right) = 0, \tag{48}$$

where the resulting relative vertical advective velocity is:

$$u'_z(\zeta) = \frac{u_z(\zeta)}{H} - \frac{\zeta}{H}\frac{\partial \mathrm{H}}{\partial \mathrm{t}} + \left(-\frac{\zeta}{H}\frac{\partial \mathrm{H}}{\partial \mathrm{x}} - \frac{1}{H}\frac{\partial z_b}{\partial \mathrm{x}}\right)u_x(\zeta). \tag{49}$$

4.4.3 Vertical Velocity Component

Since the flow is incompressible the vertical flow velocity component $u_z(x,z)$ can be obtained from the requirement that (Hooke 2005):

$$\frac{\partial u_x}{\partial \mathrm{x}} + \frac{\partial u_z}{\partial \mathrm{z}} = 0. \tag{50}$$

Again using the ζ coordinate transformation detailed in Appendix C, equation (79) is rearranged to yield:

$$\frac{\partial \mathrm{u_z}}{\partial \zeta} = -\frac{\partial}{\partial \mathrm{x}}(\mathrm{Hu_x}) + \frac{\partial \mathrm{z_b}}{\partial \mathrm{x}}\frac{\partial \mathrm{u_x}}{\partial \zeta} + \frac{\partial \mathrm{H}}{\partial \mathrm{x}}\frac{\partial}{\partial \zeta}(\mathrm{u_x}\zeta). \tag{51}$$

Integrating from ζ to 1 results in an expression for the vertical velocity component:

$$\mathrm{u_z}(1) - \mathrm{u_z}(\zeta) = -\int_{\zeta}^{1}\frac{\partial}{\partial \mathrm{x}}(\mathrm{Hu_x})\partial\zeta + \frac{\partial \mathrm{z_b}}{\partial \mathrm{x}}[\mathrm{u_x}(1) - \mathrm{u_x}(\zeta)] + \frac{\partial \mathrm{H}}{\partial \mathrm{x}}[\mathrm{u_x}(1) - \zeta \mathrm{u_x}(\zeta)]. \tag{52}$$

Knowing zs = zb+H and $\mathrm{u_z}(1) = u_x(1)\frac{\partial z_s}{\partial x}$ yields:

$$\mathrm{u_z}(\mathrm{x},\zeta) = \int_{\zeta}^{1}\frac{\partial}{\partial \mathrm{x}}(\mathrm{Hu_x})\partial\zeta + \mathrm{u_x}(\zeta)\left[\frac{\partial \mathrm{z_b}}{\partial \mathrm{x}} + \zeta\frac{\partial \mathrm{H}}{\partial \mathrm{x}}\right]. \tag{53}$$

To solve for the vertical velocity, the integral must be evaluated numerically using trapezoidal integration. Substituting $u_z(x, \zeta)$ into equation (49) above yields a simplified expression for $u'_z(x, \zeta)$

$$\mathrm{u'_z}(\zeta) = \frac{1}{\mathrm{H}}\int_{\zeta}^{1}\frac{\partial}{\partial \mathrm{x}}(\mathrm{Hu_x})\partial\zeta - \frac{\zeta}{\mathrm{H}}\frac{\partial \mathrm{H}}{\partial \mathrm{t}}. \tag{54}$$

4.4.4 Numerical Implementation

Following Holly and Usseglio-Polatera (1984), a fractional time step split operator method is used to solve the transport equation. The x-wise advection component is solved using the method of

characteristics. The ζ -wise hindered settling, vertical advection, and diffusion components are then solved using an upwind finite difference scheme.

X-direction Advection

The x-direction advection is first solved:

$$\frac{\partial \varphi}{\partial t} + u_x \frac{\partial \varphi}{\partial t} = 0. \tag{55}$$

Following Holly (1984) equation (55) is written as the total derivative:

$$\frac{D\varphi}{Dt} = 0. \tag{56}$$

The concentration remains constant along the trajectory defined by the differentials (in x-z plane):

$$\frac{dx}{dt} = u_x, \text{ and } \frac{d\zeta}{dt} = u_\zeta. \tag{57}$$

To find the point-to-point-trajectory, the differentials are integrated:

$$\int_{x_a}^{x_i} dx = \int_{t_n}^{t_{n+1}} u_x(x,\zeta,t)dt$$

and

$$\int_{\zeta_a}^{\zeta_i} d\zeta = \int_{t_n}^{t_{n+1}} u_\zeta(x,\zeta,t)dt. \tag{58}$$

Using a trapezoidal integration approximation for the right hand side yields for the x-direction advection (Urroz 2004):

$$x_a = x_i - \frac{(t_{n+1} - t_n)}{2}[u_x(x_i,\zeta,t_{n+1}) - u_x(x_a,\zeta,t_n)]. \tag{59}$$

The unknown velocity $u_x(x_a,\zeta,t_n)$ at the point x_a, which likely lies between x-grid points, can be found by linear interpolation between x-grid points. Linear interpolation is appropriate for the velocity since the velocity data at the grid points is determined from the 1st order accurate semi-implicit SWE formulation. Using linear interpolation, the velocity at point a is:

$$u_x(x_a,\zeta,t_n) = u_x(x_{i-1},\zeta,t_n) + \frac{x_a - x_{i-1}}{x_i - x_{i-1}}[u_x(x_i,\zeta,t_n) - u_x(x_{i-1},\zeta,t_n)]. \tag{60}$$

Substituting the velocity back into the equation for x_a yields:

$$x_a = \frac{x_i + \frac{(t_{n+1}-t_n)}{2(x_i-x_{i-1})}[u_x(x_i,\zeta,t_n) - u_x(x_{i-1},\zeta,t_n)]x_{i-1} + \frac{(t_{n+1}-t_n)}{2}[u_x(x_i,\zeta,t_{n+1}) - u_x(x_{i-1},\zeta,t_n)]}{\left[1 + \frac{(t_{n+1}-t_n)}{2(x_i-x_{i-1})}(u_x(x_i,\zeta,t_n) - u_x(x_{i-1},\zeta,t_n))\right]}. \quad (61)$$

If x_a does not fall between x(i-1) and x(i) the above linear interpolation of the velocity profile may cause gross extrapolation. To ensure that x_a falls between x(i-1) and x(i), the Courant number should be less than or equal to 1:

$$Cr = \frac{u\Delta t}{\Delta x} \leq 1. \quad (62)$$

In the numerical implementation the Courant number at the free surface, where the velocity is the maximum, is calculated and verified to be less than or equal to 1.

Once x_a known, the concentration at that point is found by interpolating the concentration data at point x_a within $[x_{i-1}, x_i]$ using a cubic hermite interpolation scheme. The cubic hermit interpolation is advantageous as it minimizes the numerical diffusion inherent in linear interpolation (Fritsch and Carlson 1980; Holly and Preissmann 1977). Other researches have utilized cubic spline interpolation since it does not require the calculation of derivatives at the endpoints. However, cubic splines can be more prone to diffusion and oscillation than the cubic hermite (Tsai et al. 2004). A comparison of the three approaches is presented in Section 5.4.1.

ζ -direction Advection and Settling

The second step of the operator splitting approach is to solve the ζ-wise scalar transport equation:

$$\frac{\partial \varphi}{\partial t} + u'_{zT}(\zeta)\frac{\partial \varphi}{\partial \zeta} - \frac{1}{H^2}\frac{\partial}{\partial \zeta}\left(D\frac{\partial \varphi}{\partial \zeta}\right) = 0. \quad (63)$$

The vertical velocity in the equation consists of both the relative advective velocity and the hindered settling velocity[9]:

$$u'_{zT}(\zeta) = u'_z(\zeta) + \frac{1}{H}v_{hs}(\zeta). \quad (64)$$

The hindered settling model velocity is calculated from Stokes settling with the inclusion of the concentration effect and Brouwers (2010) suspension viscosity model. The suspension viscosity is

[9] Note, the inclusion of the 1/H in the hindered settling term is due to the z to ζ coordinate transformation.

determined with flow depth considering the apparent shear rate of the rheology-augmented mixture as will be discussed in Section 5.4.3:

$$v_{s,H} = \frac{2\alpha}{9}\frac{g r_p^2 (\rho_p - \rho_l)(1-\varphi)^2}{\mu_m}. \tag{65}$$

Discretized Upwind Hindered Settling Model

Considering an implicit, upwind finite difference discretization with the starting node at the free surface, the discretized form of the ζ-wise hindered settling model becomes:

$$\frac{(\varphi_j^{n+1} - \varphi_j^n)}{\Delta t} + \frac{(u'_{zT,j}\,\varphi_j^{n+1} - u'_{zT,j-1}\,\varphi_{j-1}^{n+1})}{\Delta\zeta} - \frac{D}{H^2}\frac{(\varphi_{j+1}^{n+1} - 2\varphi_j^{n+1} + \varphi_{j-1}^{n+1})}{\Delta\zeta^2} = 0. \tag{66}$$

Rearranging yields the standard tridiagonal form which can be solved using the Thomas algorithm (Chapra and Canale 2002; Rajaram 2015):

$$a_j\varphi_{j-1}^{n+1} + b_j\varphi_j^{n+1} + c_j\varphi_{j+1}^{n+1} = f_j^n. \tag{67}$$

Due to the highly nonlinear form of the equation, utilizing a Picard iteration scheme (Rajaram 2015) helps ensure convergence of solution at each time step. In this form, equation (67) is written in terms of an incremental change in φ:

$$a_j(\varphi_{j-1}^{n+1,m} + \delta\varphi_{j-1}^{n+1,m}) + b_j(\varphi_j^{n+1,m} + \delta\varphi_j^{n+1,m}) + c_j(\varphi_{j+1}^{n+1,m} + \delta\varphi_{j+1}^{n+1,m}) - \varphi_j^n = 0. \tag{68}$$

Rearranging yields:

$$a_j^{n+1,m}(\delta\varphi_{j-1}^{n+1,m}) + b_j^{n+1,m}(\delta\varphi_j^{n+1,m}) + c_j^{n+1,m}(\delta\varphi_{j+1}^{n+1,m}) = f_j^{n+1,m}. \tag{69}$$

where

$a_j^{n+1,m} = \frac{-u'_{zT,j-1}}{\Delta\zeta} - \frac{D}{H^2\Delta\zeta^2}$,

$b_j^{n+1,m} = \frac{1}{\Delta t} + \frac{u'_{zT,j}}{\Delta\zeta} + \frac{2D}{H^2\Delta\zeta^2}$,

$c_j^{n+1,m} = \frac{-D}{H^2\Delta\zeta^2}$, and

$f_j^{n+1,m} = \left[\frac{\varphi_j^{n+1,m} - \varphi_j^n}{\Delta t} + \frac{(u'_{zT,j}\,\varphi_j^{n+1,m} - u'_{zT,j-1}\,\varphi_{j-1}^{n+1,m})}{\Delta\zeta} - \frac{D}{H^2}\frac{(\varphi_{j+1}^{n+1,m} - 2\varphi_j^{n+1,m} + \varphi_{j-1}^{n+1,m})}{\Delta\zeta^2}\right]$.

To obtain the solution, the equations are solved using the Thomas algorithm[10], and the increment is added to the previous increment's solution:

$$\varphi_j^{n+1,m+1} = \varphi_j^{n+1,m} + \delta\varphi_{j-1}^{n+1,m}. \tag{70}$$

Iteration continues until the maximum value of $f_j^{n+1,m}$ falls below the specified error tolerance.

Boundary Conditions

Both the free surface and bottom have zero total flux boundary conditions:

$$\left(u'_{zT,1}\,\varphi_1^{n+1}\right) + \frac{D}{H^2}\frac{(\varphi_1^{n+1} - \varphi_2^{n+1})}{\Delta\zeta} = 0, \tag{71}$$

and

$$\left(u'_{zT,J}\,\varphi_J^{n+1}\right) + \frac{D}{H^2}\frac{\left(\varphi_{J-1}^{n+1} - \varphi_J^{n+1}\right)}{\Delta\zeta} = 0. \tag{72}$$

Rearranging yields the additional coefficients required to solve the settling equations:

$$a_1^{n+1,m} = 0,$$

$$b_1^{n+1,m} = u'_{zT,1} + \frac{D}{H^2\Delta\zeta},$$

$$c_1^{n+1,m} = \frac{-D}{H^2\Delta\zeta},$$

$$f_1^{n+1,m} = \left[u'_{zT,1}\varphi_1^{n+1,m} - \frac{D}{H^2\Delta\zeta}\left(\varphi_2^{n+1,m} - \varphi_1^{n+1,m}\right)\right],$$

and

$$a_J^{n+1,m} = \frac{D}{H^2\Delta\zeta},$$

$$b_J^{n+1,m} = u'_{zT,J} - \frac{D}{H^2\Delta\zeta},$$

$$c_J^{n+1,m} = 0,$$

$$f_J^{n+1,m} = \left[u'_{zT,J}\,\varphi_J^{n+1,m} - \frac{D}{H^2\Delta\zeta}\left(\varphi_J^{n+1,m} - \varphi_{J-1}^{n+1,m}\right)\right].$$

[10]Note that the negative of f (-f) is input into the Thomas algorithm in this scenario.

The sharp increase in viscosity, and ultimately the discontinuity at the maximum solids packing concentration, φ_m, in the rheology augmentation (or viscosity augmentation model for Newtonian fluids, see Section 2.5.2) naturally limits the maximum concentration at the settled bed to the maximum solids packing concentration. A cut-off in the numerical implementation to specify the maximum allowable solids concentration is not necessary. Similarly, the solids flux function goes to zero at zero concentration, resulting in a minimum allowable concentration of zero at the boundaries.

4.5 Time Incrementation

To maintain a stable solution, the time step for the ζ-wise settling and advection typically needs to be smaller than the time step for the flow solution solver step and the x-wise particle advection. Rather than limiting the two preceding solution steps to the slower ζ-settling time step, the model uses a fractional time step approach. For each flow time step, the settling solver time step is subdivided into smaller time steps and solved up to the total flow time step before moving onto the next flow time step increment. The number of subdivisions for the settling solver is a manual input to the model.

4.6 Numerical Efficiency

A traditional implementation of the upwind settling model requires iteration through the ζ coordinates at each x coordinate to populate the Thomas algorithm coefficient vectors (a, b, c, and f) in the settling model. To reduce the computation time, the Thomas coefficients are vectorized across the x-coordinate direction. This enables the coefficient matrices to be determined, and concentration profiles solved simultaneously for all x coordinates.

Additionally, the model incorporates threshold flow height requirements to limit calculations only to x coordinates where the fluid height is greater than a specified threshold. For the particle advection, the threshold is heights greater than zero. For the settling calculation the threshold is typically 0.01 m fluid height.

4.7 Deposition and Flow Stoppage Considerations

Two phenomena may result in flow stoppage due to coarse particle settling. The first is inter-particle contact resulting in soil-type strength due to Coulombic friction or cohesion. This has not been incorporated into the model as any appreciable shear strength gain will require long term slurry consolidation.

The second is the gelled type bed phenomenon reported by Talmon (2004), where the fluid stops moving once yield stress due to coarse particle rheology augmentation overcomes the driving fluid shear stress due to gravity. This phenomenon is directly incorporated into the model by linking the coarse particle hindered settling to the resulting rheology augmentation within the flow solver.

Recently Chen et al. (2015) incorporated bed erosion and deposition mechanisms into their EDDA (Erosion Deposition Debris flow Analysis) flow model software using a limit equilibrium Mohr-Coulomb approach. The model also considers the empirical exponential yield stress increase with increasing volumetric mixture concentration proposed by O'Brien and Julien (1988).

In essence their work combines the friction and gelled bed concepts, arguing that the frictional particle effect on yield stress is present at low solids concentrations, and the rheology augmentation effect takes over at higher concentrations. Note however, that they only consider the yield stress increase of the total mixture with concentration and not a true rheology augmentation due to only the presence of coarse particles, as discussed in Section 2.5.2.

4.8 Chapter Summary

The tailings flow model uses finite difference forms for both the shallow water fluid model and scalar concentration transport model. The shallow water model uses a semi-implicit half-node approach and is solved using the tridiagonal Thomas algorithm. Due to the varying coarse solid concentration with depth, numerical integration is required to determine the local velocity profiles and depth averaged discharge.

The scalar x-wise advection utilizes the method of characteristics while the particle settling uses an upwind finite difference with Picard iteration. A fractional time step maintains stability of the settling

calculations while allowing larger time steps for the flow and advection steps. To decrease computation time, a vectorized Thomas algorithm approach solves the settling model at each x coordinate simultaneously.

CHAPTER 5:
MODEL COMPONENT VALIDATION AND CALIBRATION

5.1 Introduction

The model validation discussed in this chapter evaluates the individual components in the model formulation against established analytical and experimental work supplied in the literature. The following component validations are presented:

- The vertical velocity integration scheme is evaluated against:
    - Homogeneous Newtonian and Bingham plastic analytical velocity profiles
    - Spelay's (2007) vertically varied concentration profiles and resulting flow velocity profiles.
- The 1D shallow water flow model is validated against homogenous viscoplastic lubrication theory equations.
- The x-wise 1D coarse particle advection model is compared against the expected transport of a concentration pulse in a steady flow field using three interpolation schemes.
- The hindered settling model is evaluated against Treinen and Jacob's (2015) hindered settling predictions using a granular kinetic theory CFD approach.

In addition to validating the individual model components, numerical parameters are also calibrated as part of the validation. The results of this validation step ensure that each of the model components is implemented correctly prior to combining them into full tailings flow model.

5.2 Vertical Velocity Component Validation

5.2.1 Homogeneous fluids

The numerical integration scheme used to determine the velocity profile with depth and discharge are validated against the Newtonian and Bingham plastic analytical solutions discussed in Section 4.4.1 above. Figure 15 presents a comparison of the numerical and analytical velocity profiles for a Newtonian

case, while Figure 16 presents the comparison for a Bingham Plastic case. The flow depth and rheology parameters are listed in Table 6 along with a comparison of the depth-average discharge values.

The numerical scheme agrees well with the analytical solution for the two cases. Utilizing a greater number of points within the depth would decrease the error in the numerical scheme. Also note in the implementation that the exact plug depth for viscoplastic Bingham Plastic or Hershel Buckley fluids does not necessarily fall exactly on one of the numerical calculation points. Specifically setting one of the depth coordinates to this point would increase the accuracy of the depth averaged discharge calculation[11].

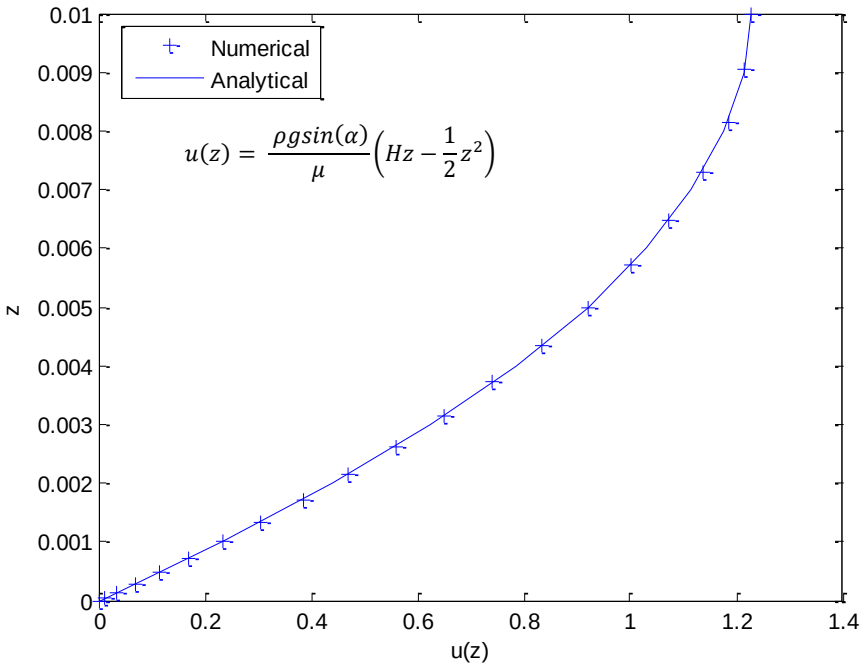

Figure 15: Newtonian Velocity Profile Comparison

[11] Provided a sufficient number of depth coordinates are used, the improvement will be minimal.

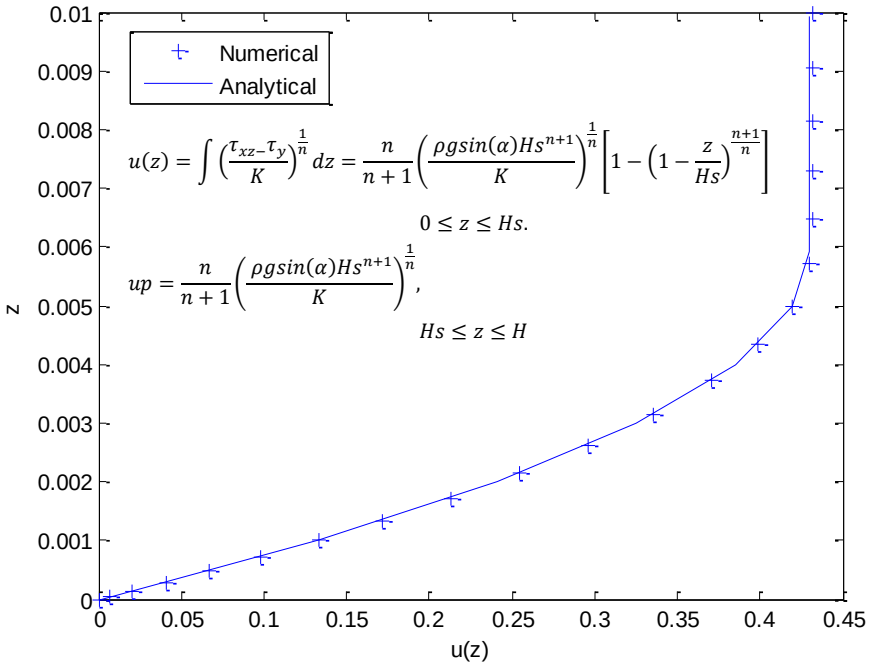

Figure 16: Non-Newtonian Velocity Profile Comparison

Table 6: Comparison of Numerical and Analytical Discharge Results

Case	*Numerical Depth-averaged Discharge, q*	*Analytical Depth-averaged Discharge, q*	*Error*
Newtonian H = 0.01 m μ = 0.01 Pa.s	8.1653x10^{-3} m^3/s	8.175x10^{-3} m^3/s	-0.12%
Bingham Plastic H= 0.01 m τ_y = 1 Pa K = μ_p = 0.01 Pa.s n = 1	3.4543x10^{-3} m^3/s	3.4521x10^{-3} m^3/s	0.064%

5.2.2 Viscoplastic Fluid with Coarse Particle Validation

The above comparison between the numerical scheme and analytical expressions for the Newtonian and Bingham plastic fluids confirms that the vertical integration scheme behaves as intended for homogeneous fluids. The purpose of including the numerical integration scheme is to account for the influence of the coarse particles, and resulting rheology augmentation on the flow behavior with depth. No direct validation to analytical expressions can be made once the coarse particle concentration gradient is included within the flow depth.

The most directly applicable comparison for this validation case is to compare the predicted velocity profile using the numerical integration scheme of equation (25) discussed in Section 4.3.3 (referred to as the numerical Z-model for this discussion) to the velocity profiles predicted by Spelay's (2007) 1D model considering depth varying concentration profiles. Spelay's predicted coarse particle concentration profile is input into the numerical Z-model profile, and the resulting velocity profile is compared to the velocity profile prediction of Spelay (2007). The material properties used for comparisons are summarized in Table 7. Spelay's predicted concentration profiles plots determined from the flow scenarios given the Table 7 parameters are presented in Figure 17.

As a baseline, Figure 18 presents the comparison between Spelay's (2007) concentration profile and the numerical integration Z-model assuming constant concentration and rheology with depth. With the exception of case E4, the predictions are in relatively good agreement indicating that for these particular cases. The rheology augmentation doesn't have a significant influence on the velocity profile. Chen's (2007) analytical velocity profiles for homogenous Bingham plastic flow are included for reference and are coincident with the Z model predictions. It is important to note that with constant concentration profiles, the Z-model agrees with Chen's (2007) analytical solution, while Spelay's model differs somewhat. This agreement with Chen (2007) holds true for Case E4 even though both disagree with Spelay's prediction. The cause of the discrepancy between them isn't immediately clear, other than that Spelay uses a bi-viscosity model to avoid numerical instabilities, and this may result in some deviation from the Z-model and Chen's (2007) solution.

Spelay notes that he excludes the yield stress rheology augmentation effect in his model implementation; only the plastic viscosity augmentation effect with depth is considered. The yield stress augmentation effect is included based on initial concentration, but not varied with depth. Figure 19 compares the numerical integration Z-model used in this work with Spelay's results, now considering this concentration and viscosity variation with depth. The analytical homogeneous velocity profile from Chen (2007) is included for reference.

The Z-model and Spelay's results are in fairly good agreement for the CT Gypsum cases. Compared to Spelay's predictions, the numerical integration model slightly under predicts the velocity profiles for the Thickened tailings cases E2 and E5. The cause of this under-prediction isn't immediately clear other than possible differences in numerical implementation schemes. The main advantage of including the concentration and viscosity variation with depth is seen in the prediction for Case E10 where the influence of the settled solids on the velocity profile is captured.

For final comparison, the influence including the yield stress augmentation has on the flow velocity profiles is presented in Figure 20. Little difference is seen in the thickened tailings comparison cases (E2, E4, and E5) because the augmentation effect is small at the low coarse particle concentration, 11%v to 13%v, for these cases. The yield stress augmentation is more significant at the higher coarse solids concentration, ~28%, for the CT cases E7 and E9. Including the yield stress augmentation has a significant impact on the flow velocity for these cases.

Table 7: Z-wise Velocity Calculation Spelay (2006) Comparison – Model Parameters

Case	**Thickened Tailings**			**CT-Tailings with Gypsum**		
Spelay numerical model reference	E2	E4	E5	E7	E9	E10
Spelay Test reference	15	16	17	12	13	14
Slope	4.0°	4.5°	5.4°	2.0°	2.5°	3°
Flow rate	5 L/s	5 L/s	5 L/s	5 L/s	5 L/s	2.5 L/s
H (Rh of exp.)	0.0455 m	0.0441 m	0.0415 m	0.0256 m	0.0231 m	0.0281 m
$\tau_{y,\ carrier}$	33.6 Pa	45.5 Pa	47.3 Pa	7.3 Pa	10.3 Pa	10.3 Pa
$K_{b,carrier}$	0.0245 Pa.s	0.0232 Pa.s	0.0214 Pa.s	0.0028 Pa.s	0.0028 Pa.s	0.0028 Pa.s
$d_{particle}$	0.188 mm					
ρ_s	2650 kg/m^3					
$\rho_{carrier}$	1303 kg/m^3			1188 kg/m^3		
$\varphi_{initial}$	13.1%	11.3%	11.5%	27.5%	22.7%	28%
φ_{max}	58.2%					

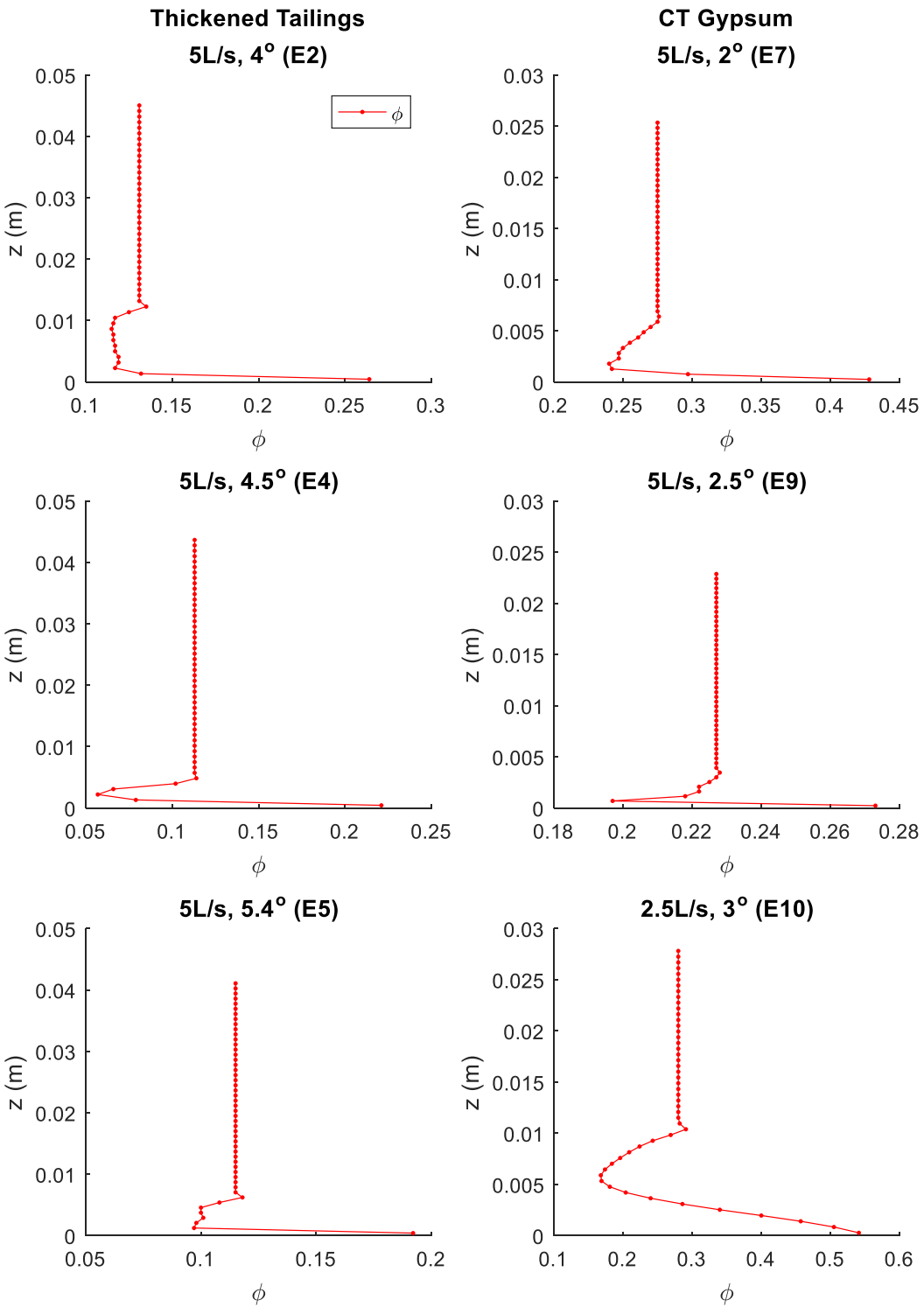

Figure 17: Spelay Concentration Profiles for Input into Z-wise Velocity Model

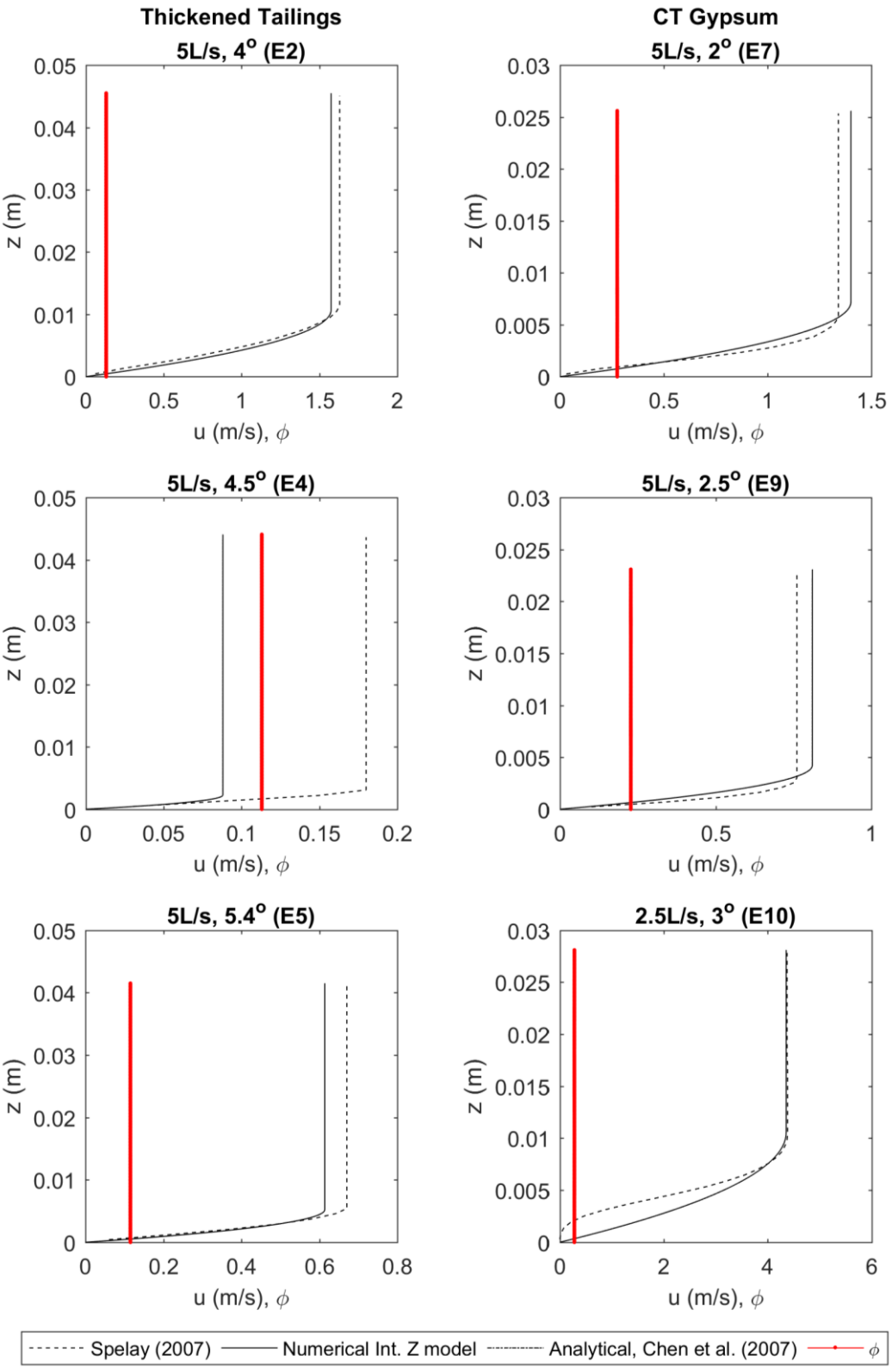

Figure 18: Spelay Comparison, Constant Concentration

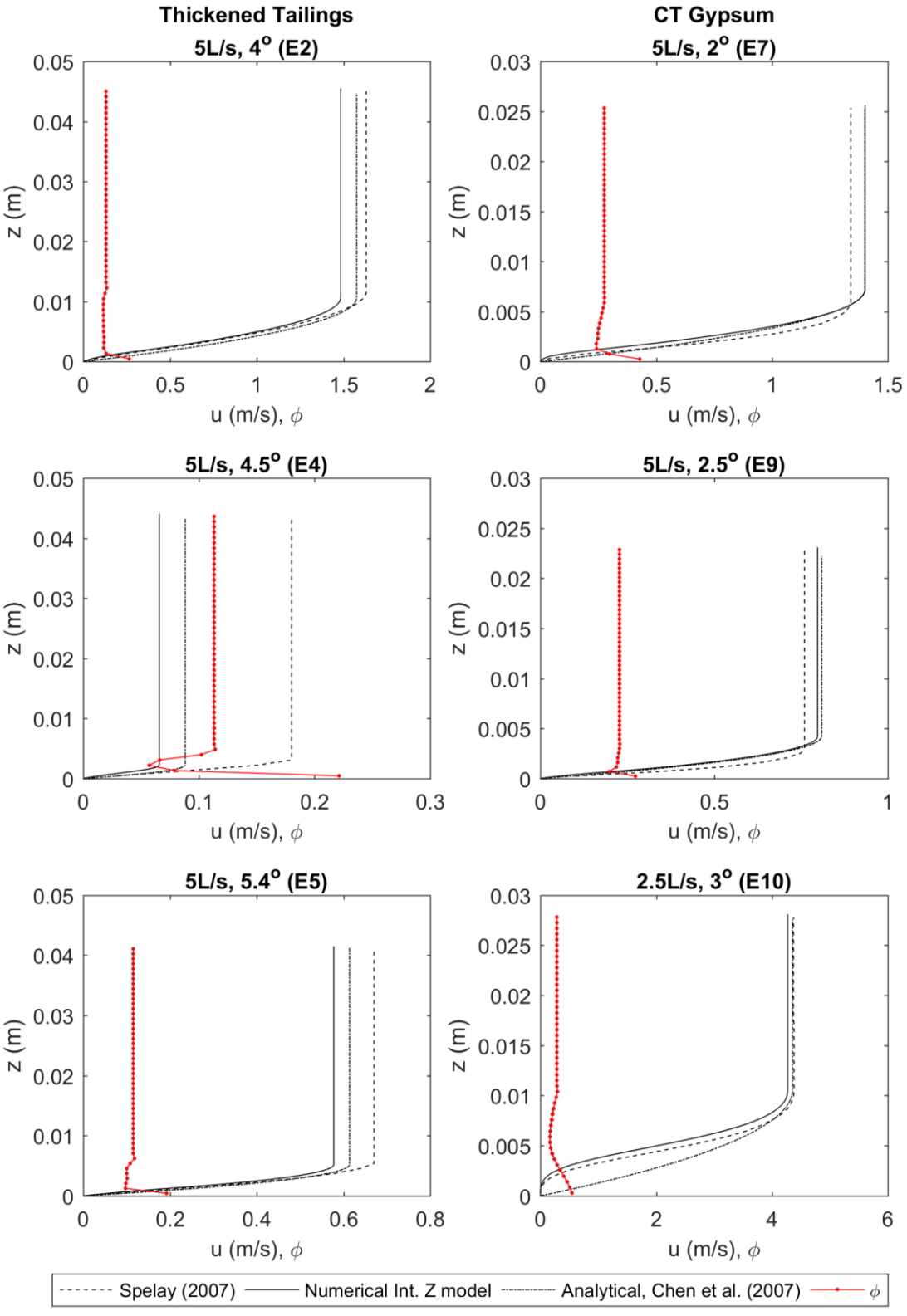

Figure 19: Comparison to Spelay's Model Predictions, No Yield Stress Augmentation

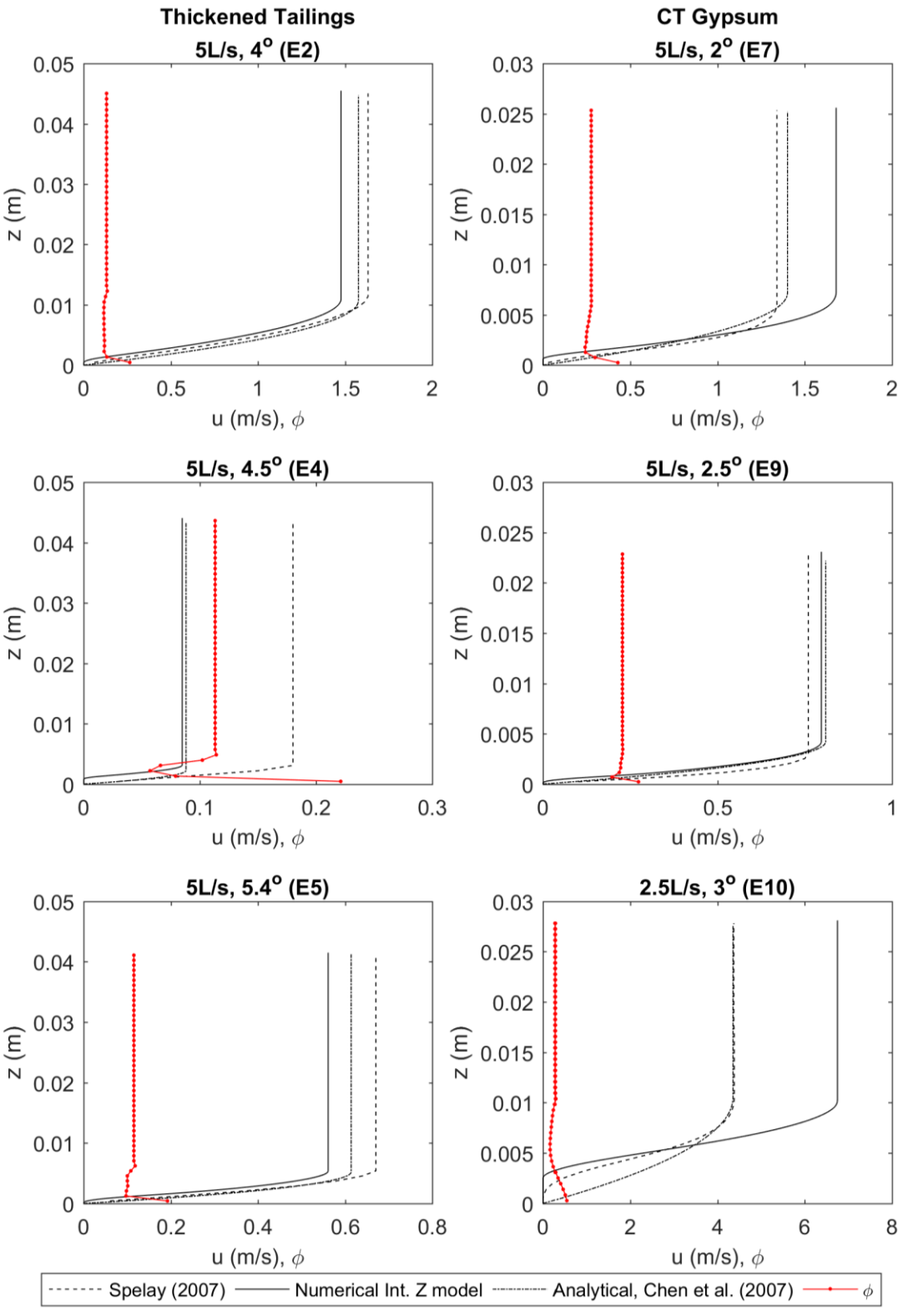

Figure 20: Comparison to Spelay's Model Predictions, with Yield Stress Augmentation

This comparison verifies that the numerical integration approach developed for the z-wise flow velocity and discharge determination can adequately predict both the expected homogenous flow profiles of Newtonian and Bingham Plastic fluids. The model also sufficiently captures the impact the coarse particle concentration gradient with depth may have on the flow velocity profile.

5.3 One Dimensional Shallow Water Model for Homogeneous Flow

Due to the yield stress, depositing a Bingham plastic fluid should result in a concave down fluid profile when the fluid ultimately comes to rest. Various configurations (i.e. deposition on a flat slope, 1D inclined slope, conical slopes) have been studied (Balmforth et al. 2002; Coussot and Proust 1996; Yuhi and Mei 2004), as discussed in Section 3.3.

To evaluate whether the 1D model correctly predicts this concave down stagnant profile once input flow is stopped and the discharged fluid is allowed to come to rest, the final shape of the stagnant fluid is compared to two well-known analytical solutions detailed in Simms (2007). First, a fixed volume of fluid steadily discharged onto several inclined slopes (0.5%, 0.75%, 1.0%) and then allowed to come to a rest. Once the fluid is stagnant, the fluid depth should reach the expected critical fluid depth at which the fluid yield stress balances the gravity potential due to the slope:

$$h_c = \frac{\tau_y}{\rho g sin(\alpha)}. \tag{73}$$

The overall deposit profile (h,x) should result in a convex profile. For validation along the entire length, the resulting flow depth and surface slope (dH/dx) are input into the analytical expression relating the bed shear stress to the fluid height and slope as detailed in Simms (2007):

$$\tau(x) = h(x)\rho g cos(\alpha)\left[tan(\alpha) - \frac{\partial h}{\partial x}\right]. \tag{74}$$

Once the fluid is static on the incline, the calculated bed shear stress $\tau(x)$ should equal τ_y (1 Pa for these cases) along the slope, except at the toe of the deposit where the flow depth has not reached the critical depth. Figure 21 presents the resulting flow depth profiles, flow rate q indicating the flow has reached nearly stagnant conditions, and the calculated shear stress acting at the bed surface using the Simms (2007) relationship.

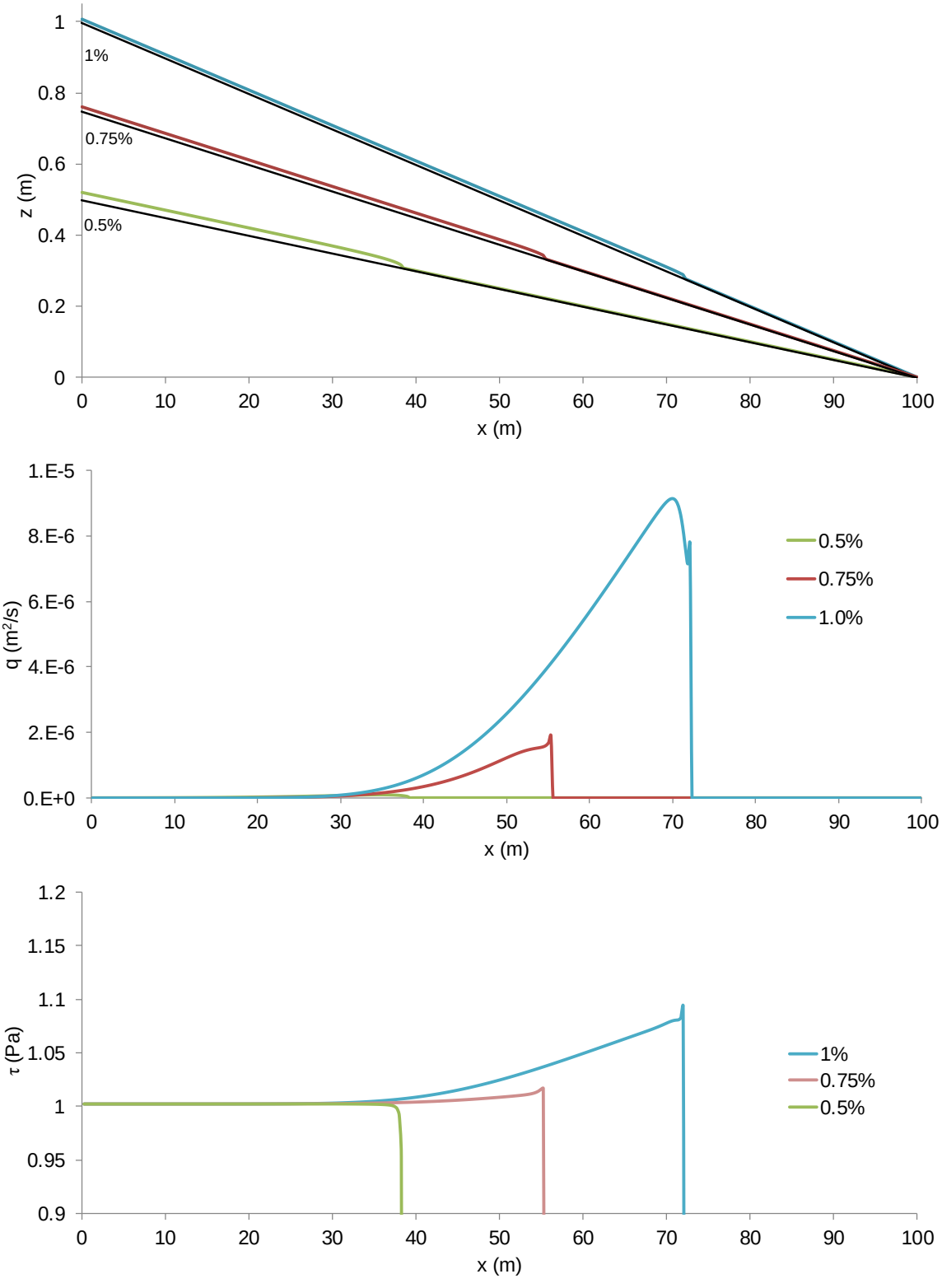

Figure 21: Homogeneous 1D Bingham Plastic (τ_y = 1 Pa) Flow Down Incline

As a second validation, a fixed volume of fluid is steadily discharged onto an essentially flat[12] slope. The intent of this comparison is to verify that the 1D model is numerically stable and can accurately capture the buildup of fluid under little gravity potential. The results of the simulation are compared to simplified analytical expression for a flat slope provided in Simms (2007):

$$h(x)^2 - h_0^2 = \frac{2\tau_y}{\rho g}(x - x_0), \tag{75}$$

where

x = horizontal distance

h = the height along x

x_0 = the total flow distance the fluid has covered

h_0 = the height at the start of the profile.

Figure 22 presents the comparison between the resulting deposit profiles and the analytical model for two Bingham Plastic yield stress values. The resulting profiles agree well with the analytical solution.

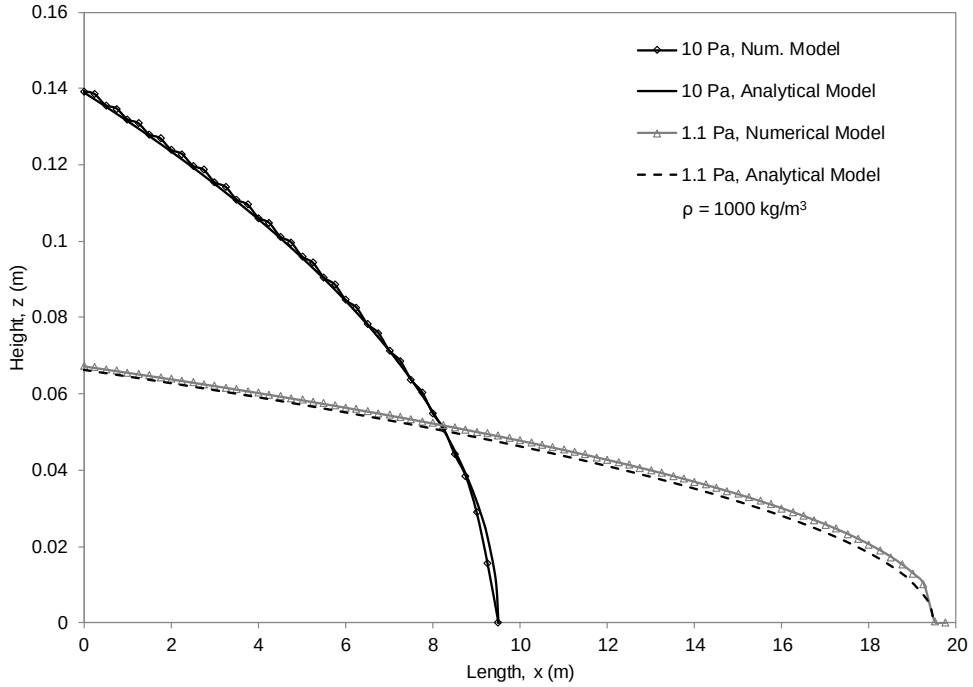

Figure 22: Comparison between Numerical and Analytical Deposition of Bingham Plastic Fluid on Flat Slope

[12] A completely flat slope results in unstable model behavior.

5.4 Scalar Transport Model Validation

The scalar transport model consists of the x-wise particle advection component, z-wise advection component, and the z-wise hindered settling component. The components are solved using an operator splitting approach, and validating them independently is appropriate.

5.4.1 Coarse Particle 1D x-wise Advection

The 1D x-wise advection component of the model (equations (55) through (61)) solved using the method of characteristics (MOC) is verified to maintain mass conservation and concentration profile considering a constant u_x velocity profile and initial square concentration profile within the flow field.

Figure 23 presents a comparison between the selected cubic hermite interpolation scheme discussed in Section 4.4.4 and alternate linear and cubic spline interpolation schemes built into Matlab[13]. Both the linear and cubic hermite schemes are mass conserving; the spline is not due to the oscillatory nature of the spline interpolation. The oscillations may occasionally predict negative concentrations near the leading and trailing fronts of the concentration wave.

The cubic interpolation scheme maintains a much sharper concentration profile compared to the linear scheme. While the spline maintains relatively sharp fronts, the oscillations in the spline scheme do not make it suitable for use in the x-direction advection model.

The primary limitation of the cubic hermite interpolation scheme is that it is not time step[14] independent. Figure 24 presents a comparison of the concentration profiles after 30 seconds for three time steps. All three time steps are below the Courant number criteria. As seen in the figure, as the Courant number decreases, the cubic hermit scheme lags the expected concentration profile velocity. This time scale dependence must be monitored in the full model implementation to ensure that the particle advection matches the underlying fluid flow profile. To maintain suitable Courant conditions for the x-wise advection, a fractional time step approach is used to solve the carrier fluid flow solution and hindered settling

[13] Matlab functions interp1() and spline(), respectively.

[14] Or conversely element size

components. This allows the overall time step to remain relatively high for the coarse particle advection component so that the Courant number is close to 0.5 to limit any potential advection lag.

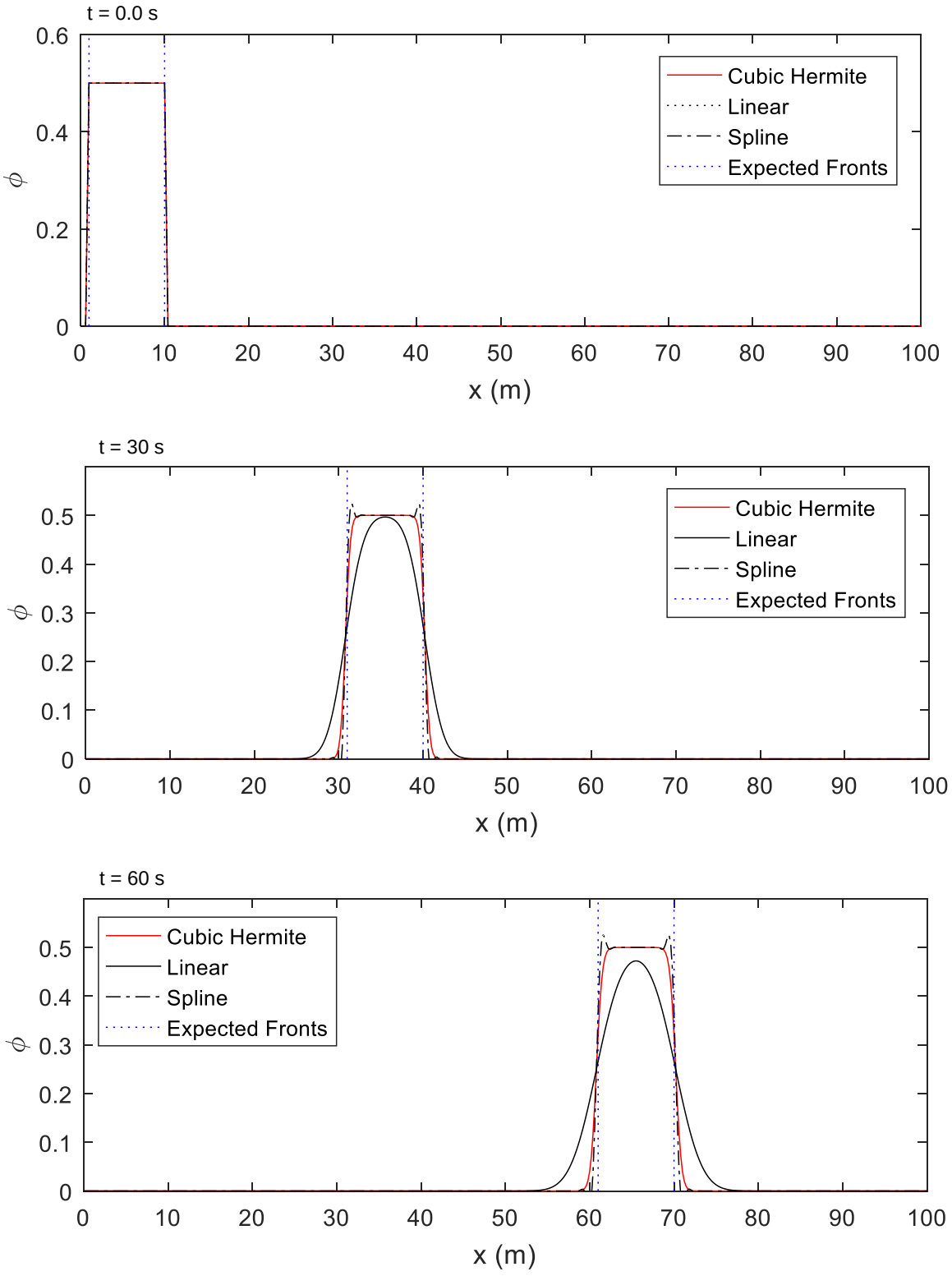

Figure 23: Comparison of Cubic Hermite, Linear and Spline Interpolation Schemes for MOC Advection Model ($U_x = 1$, $\Delta t = 0.1$, $\Delta x = 0.2$)

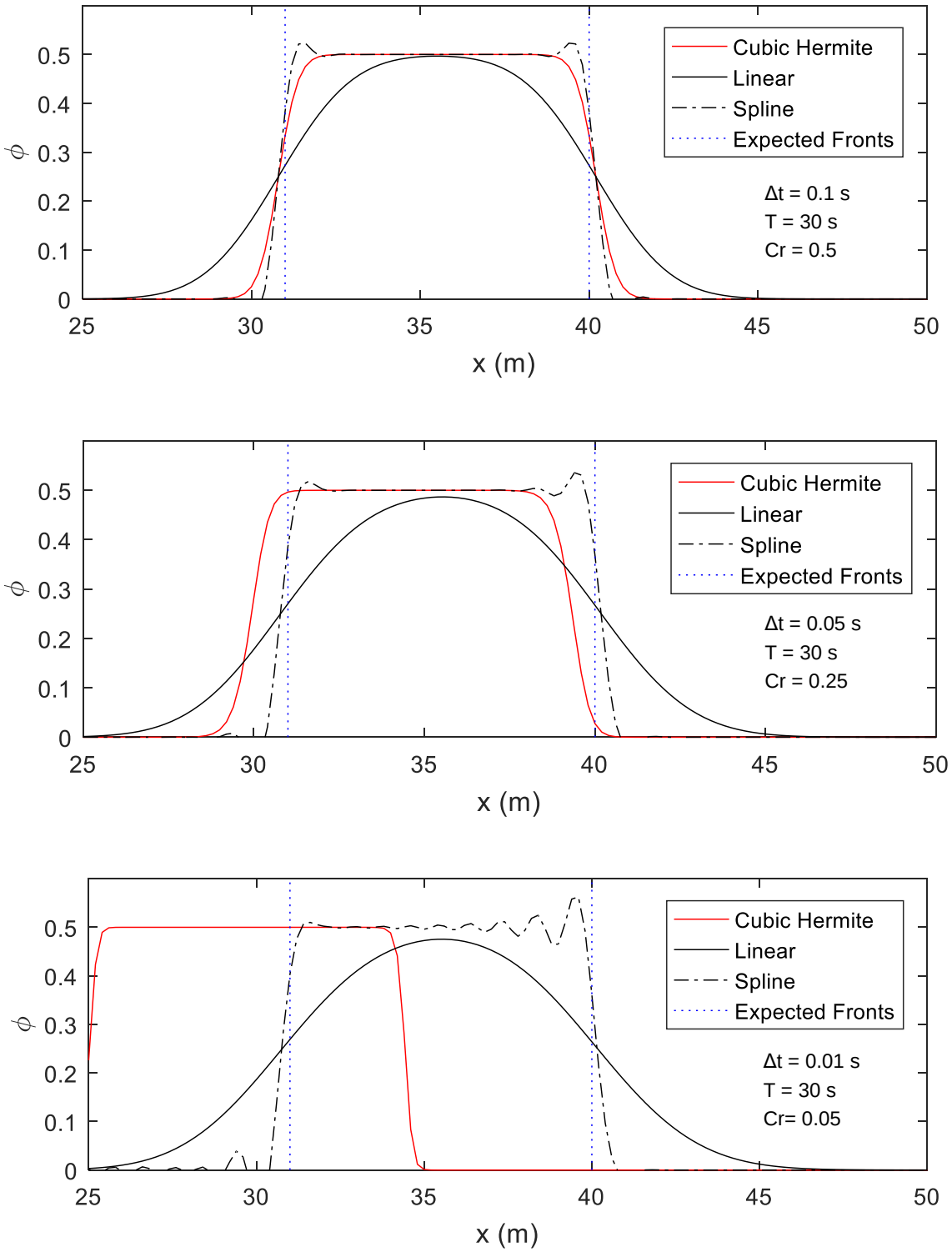

Figure 24: 1D MOC Advection Time Step Comparison ($U_x = 1$, $\Delta x = 0.2$)

5.4.2 Vertical Particle Advection Evaluation

For completeness, the scalar transport model in Section 4.4 included both the particle advection and settling components in the vertical direction. In evaluating the particle advection component relative to the hindered settling and x-wise particle advection, it was found that the vertical advection component is negligible, except at the flow front. At the flow front, the relative vertical advective velocity is substantial, and causes numerical convergence problems. However, the localized behavior at the flow front is ignored in this study since the focus is on the temporal deposition of coarse particles in steady flow region upstream of the flow front.

Figure 25 presents a contour plot of the ratio of the relative hindered settling velocity, $\frac{1}{H}v_{hs}(\zeta)$, to the relative vertical advective velocity, $u_z^{'}(\zeta)$ for Spelay's E10[15] flow scenario. Figure 26 presents the same plot, excluding the unsheared plug (white) where the settling velocity is zero, and limiting the velocity ratio to ±1. Figure 27 presents the same figure with relaxed limits of ±10. Under typical steady flow conditions in this study, the relative hindered settling velocity in equation (64), is typically at least an order of magnitude larger than the relative vertical advective velocity. As a result, the vertical advective component is excluded for the remainder of the modelling work in this study. Doing so alleviates significant convergence problems at the flow front.

[15] Case E10 is selected for this comparison since it has a large degree of settling, resulting in greater vertical advective velocities than some of the other cases.

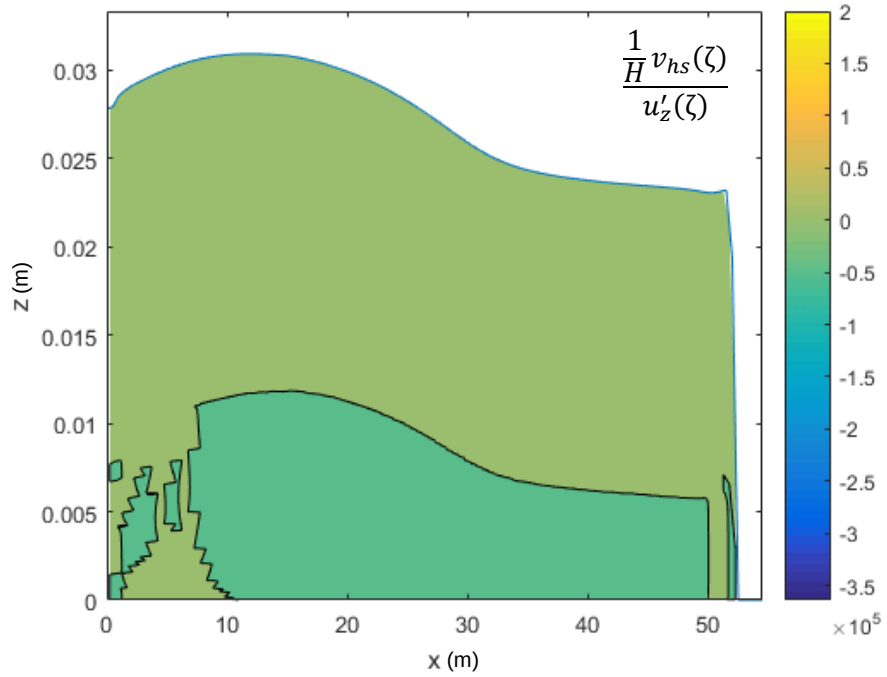

Figure 25: Contour Plot of Vertical Velocity Ratio, no Limits

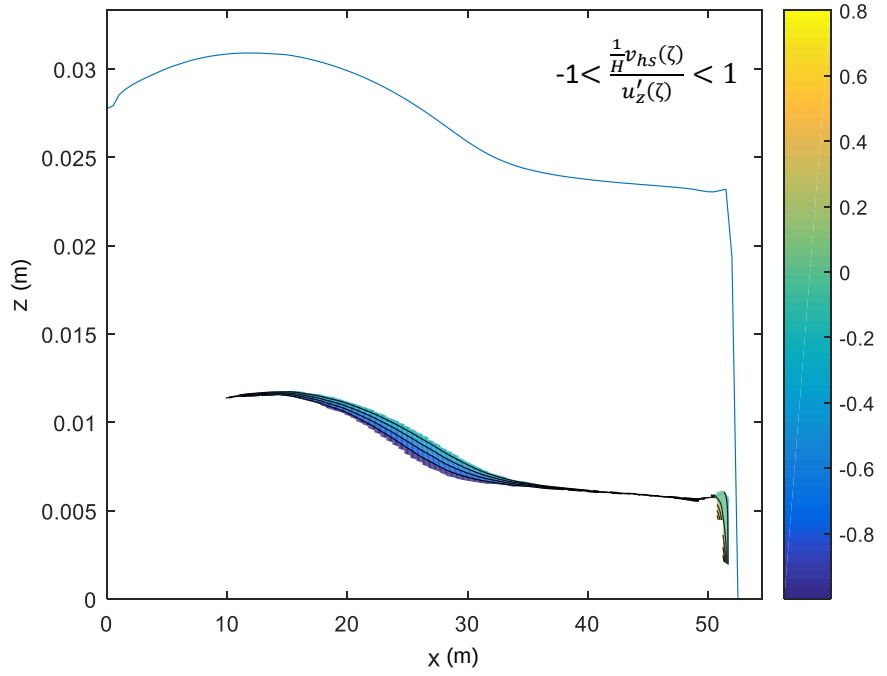

Figure 26: Contour Plot of Vertical Velocity Ratio, Limited to ±1

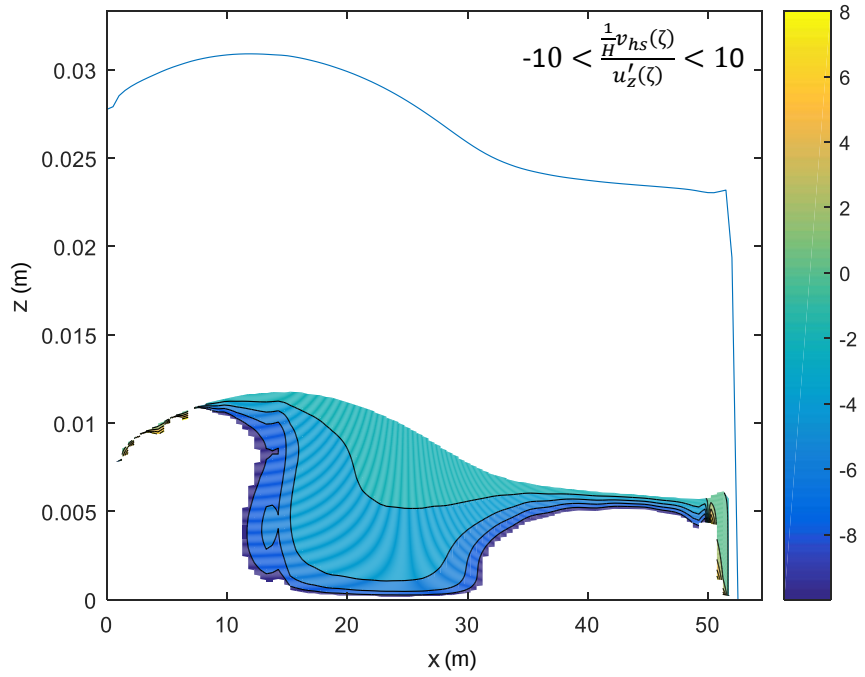

Figure 27: Contour Plot of Vertical Velocity Ratio, Limited to ±10

5.4.3 The Relationship between Hindered Settling and Viscosity Augmentation

Of particular interest in this study is the relationship between hindered settling behavior and viscosity augmentation phenomenon discussed above. This comparison is particularly important when aiming to model both the impact rheology augmentation has on the bulk flow behavior, and hindered settling within the flow field.

Newtonian Flow

The Richardson and Zaki (1954b) hindered settling model discussed in Section 2.5.1 above, is a widely used simplified empirical relationship to predict the hindered settling velocity of a particulate suspension. Although the exponential form was developed based on mostly theoretical foundations, the exponential n value was ultimately determined by empirical fit to experimental data (Blazejewski 2012).

Robinson (1926) appears the first to propose modelling particle sedimentation by replacing the fluid density and viscosity with the suspension viscosity and density in the Stoke's settling formulation (as discussed in Richardson and Zaki (1954a) and Blazejewski (2012)). This approach is referred to as the

pseudo-fluid method and a variety of hindered settling models have been developed from it, as discussed below. The basic Robinson form is as follows (1926)[16],:

$$V_{HS} = \mathrm{k}\frac{\mathrm{g}r_p^2(\rho_\mathrm{s} - \rho_\mathrm{m})}{\mu_m}. \tag{76}$$

Considering the slip velocity between the particle phase and fluid phase yields a more appropriate representation of the hindered settling velocity (Blazejewski 2012; Kynch 1959). As water is displaced by the solids, continuity requires that the solids flux equals the water displacement flux:

$$v_s\varphi = -(1-\varphi)v_w. \tag{77}$$

This inclusion results in a hindered settling formulation with an additional (1-φ) term, often referred to as the "return flow" effect (Oliver 1960):

$$V_{HS} = v_s - v_w = \frac{2}{9}\frac{\mathrm{g}r_p^2(\rho_\mathrm{s} - \rho_\mathrm{l})(1-\varphi)}{\mu_m}. \tag{78}$$

Both Steinour (1944) and Hawksley (1954, cited in Oliver, 1960, and Blazekewski, 2012) argued that there should be an additional (1-φ) term to account for the suspension mixture density, as described by Olivier (1960), or the "mean pressure gradient in the suspension", as described by Blazejewski (2012), This yields a hindered settling equation of the form:

$$V_{HS} = \frac{2}{9}\frac{\mathrm{g}r_p^2(\rho_\mathrm{p} - \rho_\mathrm{l})(1-\varphi)^2}{\mu_m}. \tag{79}$$

There is disagreement about the most appropriate form of the equation and which viscosity and density (suspension or liquid) to use. Kynch (1959) argued that a single (1-φ) term was appropriate, but that the viscosity, $\mu_{RE,}$ of a representative, non-settling fluid of similar viscosity and density to the suspension be used:

$$\frac{\mathrm{V}_{HS}}{\mathrm{V}_{ts}} = \frac{(1-\varphi)}{\mu_{Re}}. \tag{80}$$

Oliver argued that the Gurel (1951) formulation (as cited in Oliver, 1960), which utilizes a similar concept but second order concentration effect, better fit the data:

[16] The standard constant 2/9 is replaced with a constant k to account for particle shape effects.

$$\frac{V_{HS}}{V_{ts}} = \frac{(1-\varphi)^2}{\mu_R}, \tag{81}$$

where μ_{Re} is the measured relative viscosity ($\mu_{Re} = \mu_m/\mu_f$).

Blazejewski (2012) set out to determine which equation (78) or (79) better fit a range of existing and new experimental settling data, and how the results agreed with a variety of hindered settling models, including the Richardson & Zaki model. Ultimately he found the pseudo-fluid approach produces reasonable hindered settling predictions, and that the 2nd order equation (79) better agreed with the experimental results. The same conclusion was argued by Oliver (1960).

Blazejewski ultimately proposed a new model based on the maximum backflow velocity, discussed by Oliver (1960), and suspension viscosity, but ignoring the 2nd order suspension density effect:

$$\frac{V_{HS}}{V_{ts}} = \frac{(1-\varphi)}{\mu_R(1+\varphi)}. \tag{82}$$

The empirical Thomas (1965) viscosity model provided the best fit when the resulting hinder settling velocities were compared to the experimental dataset (Blazejewski 2012). Blazejewski did not, other than the Einstein (1906) and Thomas (1965) equations, consider any of the well know suspension viscosity models summarized in Table 3 in his comparison.

When the settling flux is plotted as a function of concentration, as seen in Figure 28, the differences between the viscosity models become clearer. The Krieger (1972), Eiler (1941) and Brouwers (2010) models are in closest agreement. These models also have the advantage of terminating at the maximum packing concentration, φ_m unlike the Thomas (1965) or Richardson & Zaki (1954b) equations. Additionally, the Richardson & Zaki model over-predicts the hindered settling velocity above φ>0.33 (Blazejewski 2012). The closest three above have the advantage of predicting much smaller hindered velocities at these higher concentrations. Blazejewski (2012) found the Brouwers (2010) viscosity model along with equation (79) above produced very good[17] agreement to the experimental results he considered in his analysis.

[17] The model had the 3rd lowest sum of weighed squared residuals at 0.644, compared to the best comparison at 0.618.

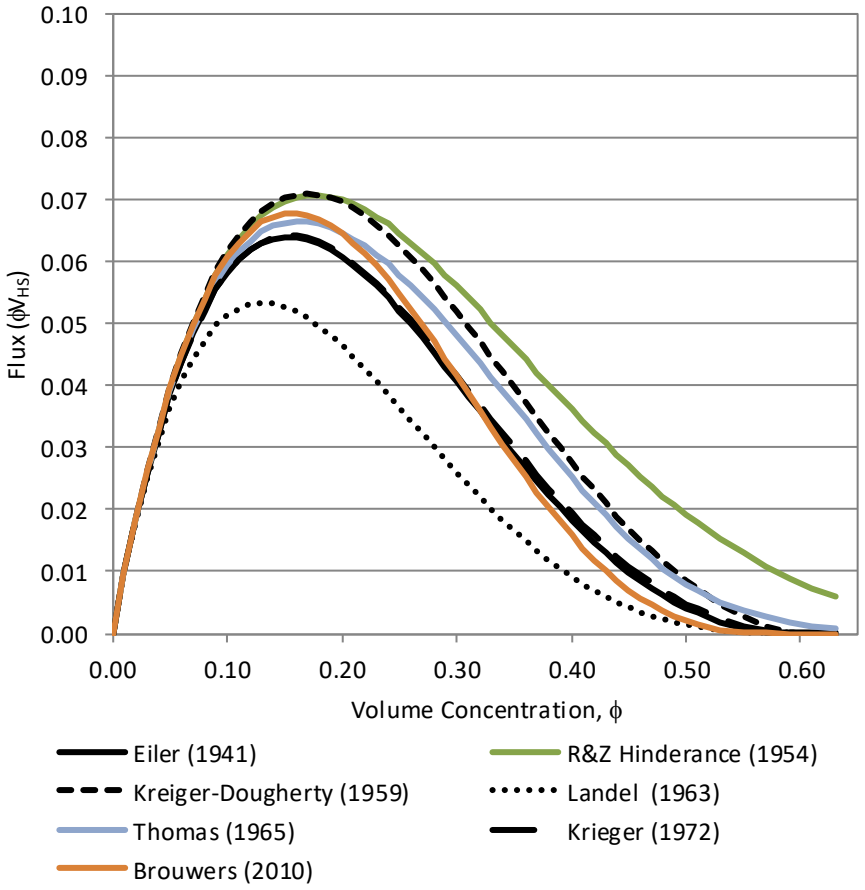

Figure 28: Hindered Settling Flux Function Plotted for the Various Viscosity Models[18]

Non-Newtonian flow

Non-Newtonian viscoplastic flow adds the further complication of the fluid viscosity shear-rate dependency to the rheology augmentation and settling effects. Figure 29 presents the suitability of the rheology augmentation models to predict the hindered settling effect over a range of shear rates. To determine the flux function for a Bingham plastic fluid, the apparent viscosity at given shear rate and concentration is determined and used in the hindered settling model in Equation (79). These are plotted in comparison to the flux function for the Newtonian Richardson and Zaki (1959) and Brouwer (2010) viscosity models presented above. Figure 29a presents the flux calculated using the Gillies (2006, in Spelay,

[18] A fluid viscosity of 1 Pa.s and maximum packing factor, φ_m =0.6 is considered in the calculations.

2007) rheology augmentation model, while Figure 29b presents the calculated flux using the Thomas (1999) correlation.

As seen in Figure 29, the flux function approaches the hindered settling function utilizing the Brouwer (2010) viscosity model as shear rates increase. The Gillies (2006, cited in Spelay, 2007) distance ratio rheology augmentation model agrees fairly well with the Brouwers (2010) model for shear rates of 10 1/s and 100 1/s. Based on this analysis, using the Gillies rheology augmentation model to determine the mixture apparent viscosity at a given shear rate, along with the hindered settling formulation in Equation (79) is more appropriate than the Thomas (1999) equation to predict the hindered settling behavior within the flow field.

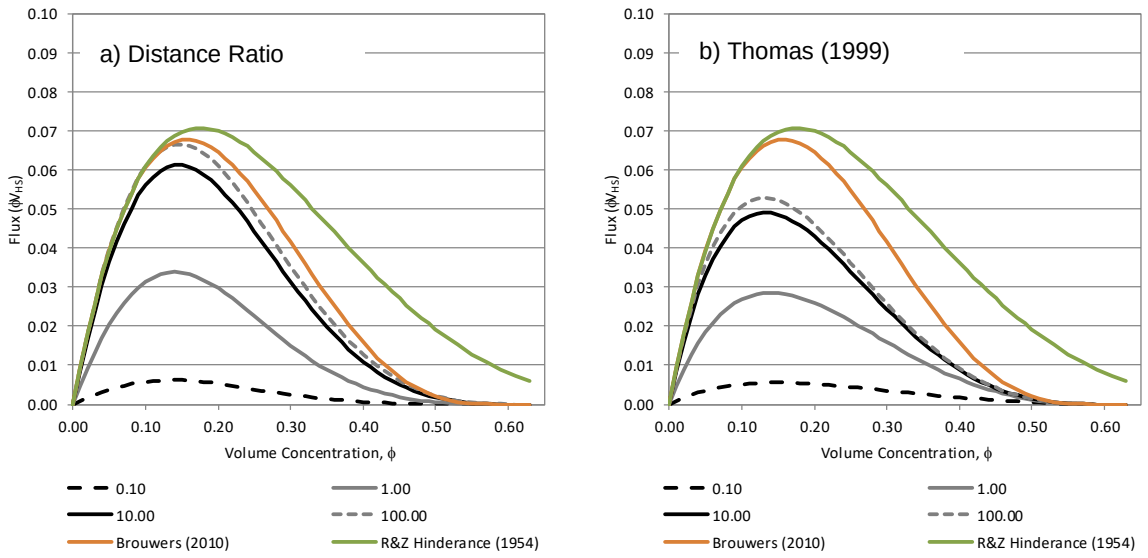

Figure 29: Hindered Settling Flux at Different Shear Rates using Gillies Distance Ratio (Spelay, 2007) (a), and Thomas (1999) Rheology Augmentation Models (b)

5.4.4 Upwind Coarse Particle Hindered Settling Model

Prior to incorporating the hindered settling model into the full scalar transport formulation, the model was first validated against concentration profiles obtained from Treinen and Jacob's (2015) CFD predictions of hindered settling behavior in static cylinder settling columns. While significant hindered settling velocity data is available in the literature, only Hernando et al. (2014), who used Laser Induced

Fluorescence to measure the concentration of settling monosized particles, has been found to provide contours of the particle concentration evolution with time during static cylinder tests. Unfortunately, the contour plot available in the literature was not amenable to extract the measured data. Hernando et al (2010) did find that their test results did agree well with the Richardson & Zaki (1954b) flux function with n = 4.65 truncated at a maximum particle packing that dependent on particle size.

The intent of this validation isn't to exactly replicate experimental data, but to confirm that the predicted settling velocity and concentration profiles are reasonable. As a result, Treinen and Jacob's (2015) CFD predictions are considered an appropriate comparison.

Treinen and Jacob's (2015) work investigated the suitability of a Eulerian-Eulerian granular kinetic theory CFD approach to model the hindered settling of coarse particles in water. They found the predicted hindered settling velocity of the particles agreed well with the expected Richard & Zaki (1954b) hindered settling model, utilizing Garside and Al-Dibouni's (1977) improved relationship for the n exponent. The model setup and settling velocity comparison is discussed in Treinen and Jacobs (2015). One output of that work was the temporal predictions of concentration with depth within the settling cylinders.

For this validation step three hindered settling velocity models are compared to the GTK CFD results:

- The Richardson & Zaki (1954b) model, discussed in Section 2.5.1:

$$V_{HS} = V_{ts}(1-\varphi)^{4.7}, \tag{83}$$

- A modified Richardson and Zaki model, which was developed as part of this investigation to limit the settled concentration to the maximum particle packing concentration, φ_m, by adjusting empirical coefficients:

$$V_{HS} = V_{ts}0.85\left(1-\frac{\varphi}{\varphi_m}\right)^{2.25}, \tag{84}$$

- And the viscosity augmentation approach discussed in Section 5.4.3 using the Brouwers (2010) suspension viscosity model:

$$v_{HS} = \frac{V_{ts}(1-\varphi)^2}{\left[\left(\frac{1-\varphi}{1-\varphi/\varphi_m}\right)^{2.5\varphi_m/1-\varphi_m}\right]}. \quad (85)$$

The three hindrance functions are plotted in Figure 30 for comparison. Table 8 summarizes the parameters used in the study.

Figure 31 presents a comparison of the upwind finite difference hindered settling model developed for this investigation to the predicted concentration profiles determined from the CFD investigation. As seen in the figure, all three initially predict a faster settling front at the top of the column than the CFD prediction does, but overall predict the concentration profiles fairly well. As expected, the Richardson & Zaki (1954) model over predicts the settled bed concentration since it is not limited to the maximum bed packing concentration. The Brouwers (2010) model tracks the CFD predictions closer than the other two initially; it is slower to settle to the final maximum concentration once the solids have settled into a bed mass at the bottom of the cylinder.

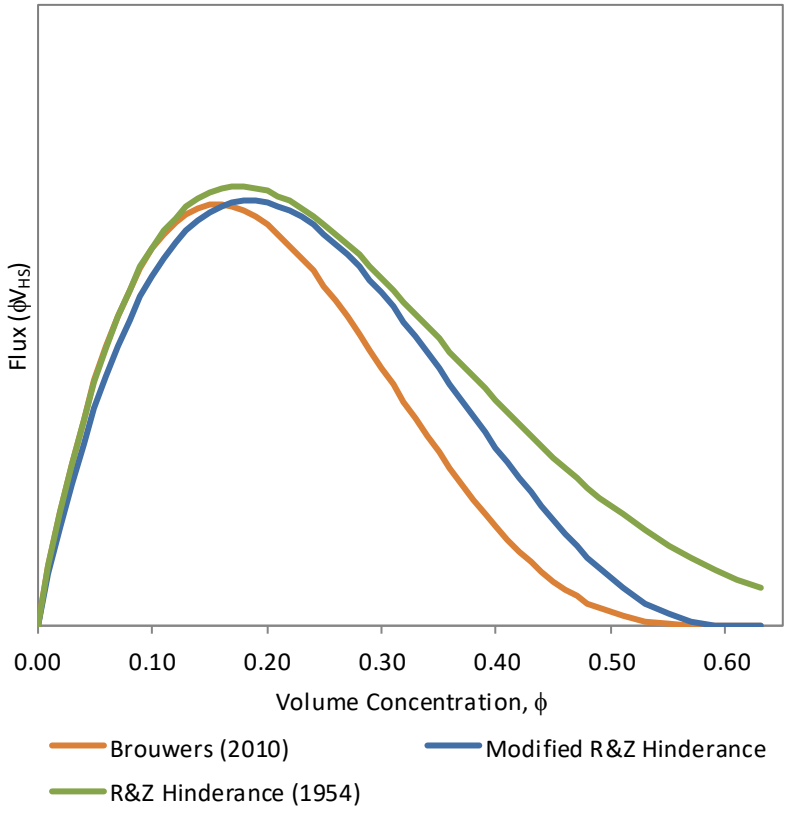

Figure 30: Hindered Settling Flux Functions

Table 8: Hindered Settling CFD Comparison Parameters

Parameter	Value
H	0.3 m
ρ_s	2650 kg/m^3,
ρ_w	1000 kg/m^3
φ_0	0.25
φ_m	0.6
μ_w	0.001 Pa.s
D	1.0×10^{-5} m^2/s
Δz	0.0001 m
Δt	0.0001 s

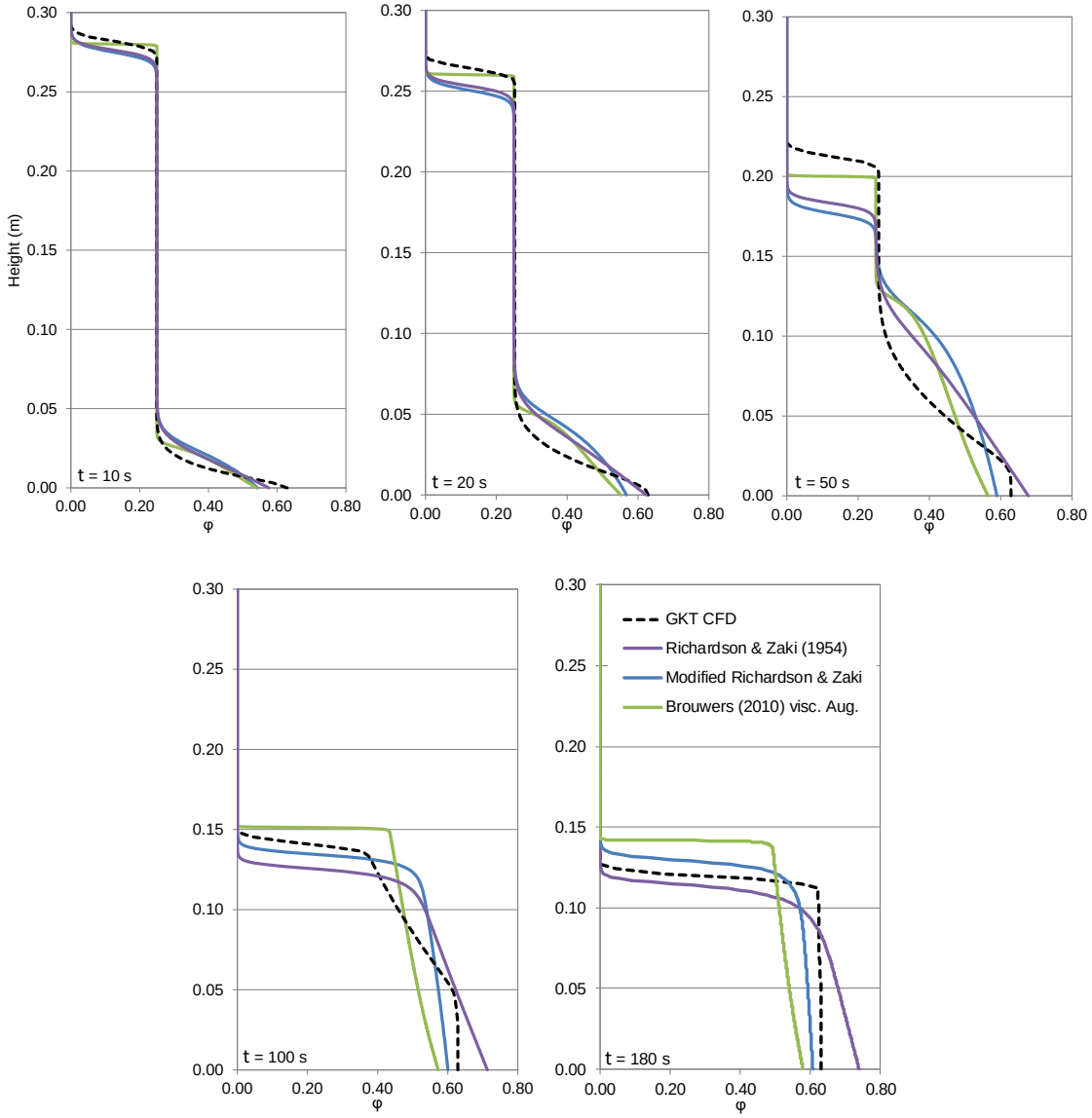

Figure 31: Comparison of 100 μm Static Cylinder Settling Concentration Profiles with CFD Results

5.4.5 Evaluation of Diffusivity Impact on Settling

The upwind numerical hindered settling model includes an artificial diffusivity to assist with convergence. Using the same model test case and 100 micron diameter particles as in the preceding Section 5.4.2, the influence this diffusivity has on the hindered settling is investigated in Figure 32. A diffusivity of at least $D = 1x10^{-5}$ m^2/s is required to minimize the amount of artificial diffusion in the settling results.

Higher diffusivities result in settled bed concentrations much lower than the expected maximum packing concentration.

To predict a stable convergent solution at low diffusivities, the Δz element size must be small, resulting in potentially long computation times. A comparison of the element size for a fixed diffusivity value of $D = 1x10^{-5}$ m^2/s is presented in Figure 33. The resulting concentration profiles are independent of the element size up to $\Delta z = 1x10^{-3}$ m. The solution would not converge above this size.

The particle size also impacts the required diffusivity to maintain sharp settling concentration profiles. A comparison of the concentration profiles considering different diffusivities for 1000 μm diameter particles is presented in Figure 34. From these results a diffusivity of $D=1x10^{-4}$ m^2/s conservatively maintains a sharp concentration profile for a particle size of 1000 μm. However, an element size of $\Delta z = 1x10^{-4}$ m is required to obtain a convergent solution. Figure 35 presents a comparison of the concentration profiles for element sizes between $\Delta z = 1x10^{-4}$ m and $\Delta z = 1x10^{-6}$ m and verifies the resulting concentration profiles are independent of element size. Comparing the results of the 100 μm and 1000 μm particles suggests that as the particle size increases a lower diffusivity is required to maintain acceptably sharp concentration profiles. Although not investigated directly, a similar augment can be made for viscosity. Lower viscosities result in higher settling rates, and therefore would require a higher diffusivity to maintain sharp concentration profiles than higher viscosity fluids.

It is important to recognize that the particle Reynolds number, Rep, is approximately 150 in the 1000 μm particle size case, which is well above the typical limit of 1.0 for which Equation (3) provides appropriate results. The predicted freely settled velocity is 5.8 times greater than expected and the presented concentration profiles are not realistic. However, this analysis does serve the function of calibrating the required diffusivity parameter.

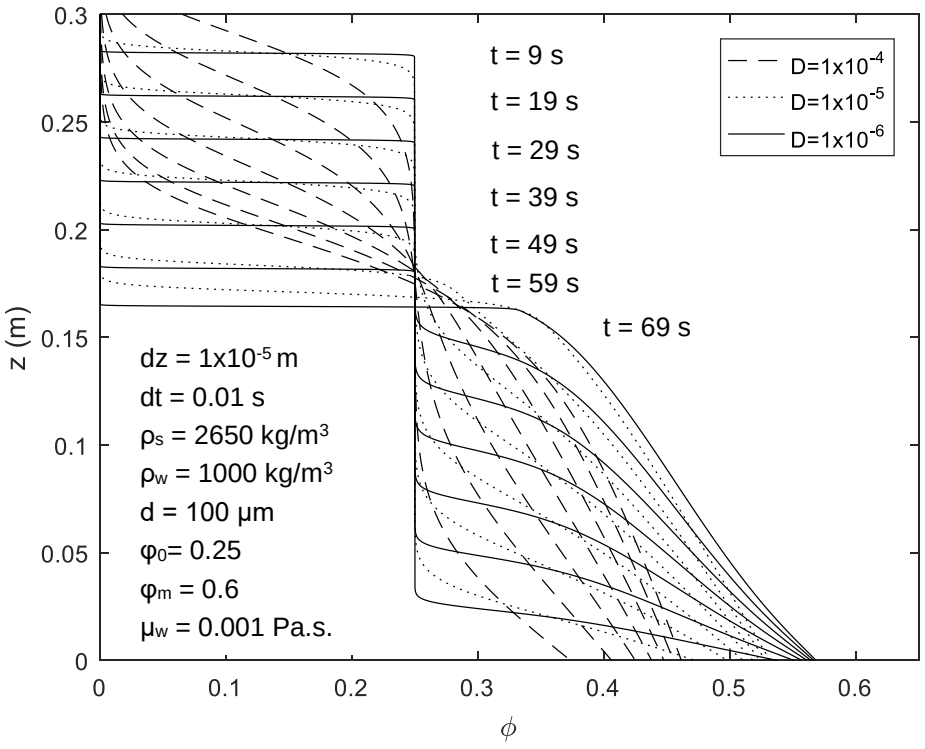

Figure 32: Evaluation of Diffusivity, D [m^2/s], on Hindered Settling of Coarse 100 μm Particles in Water

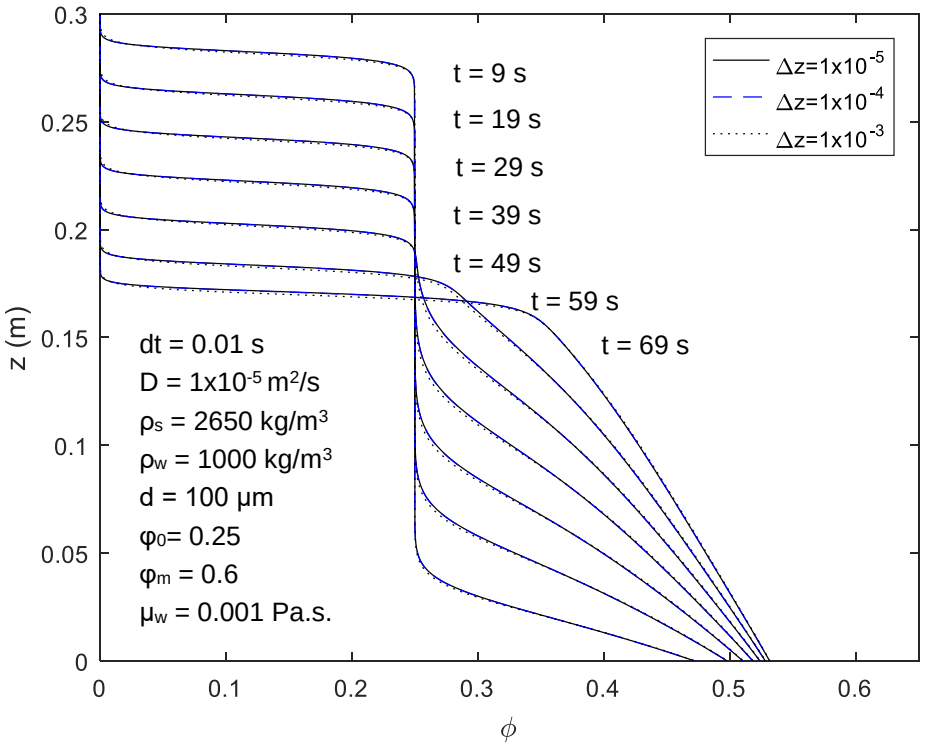

Figure 33: Evaluation of Element Size, Δz, on Hindered Settling of Coarse 100 μm Particles in Water

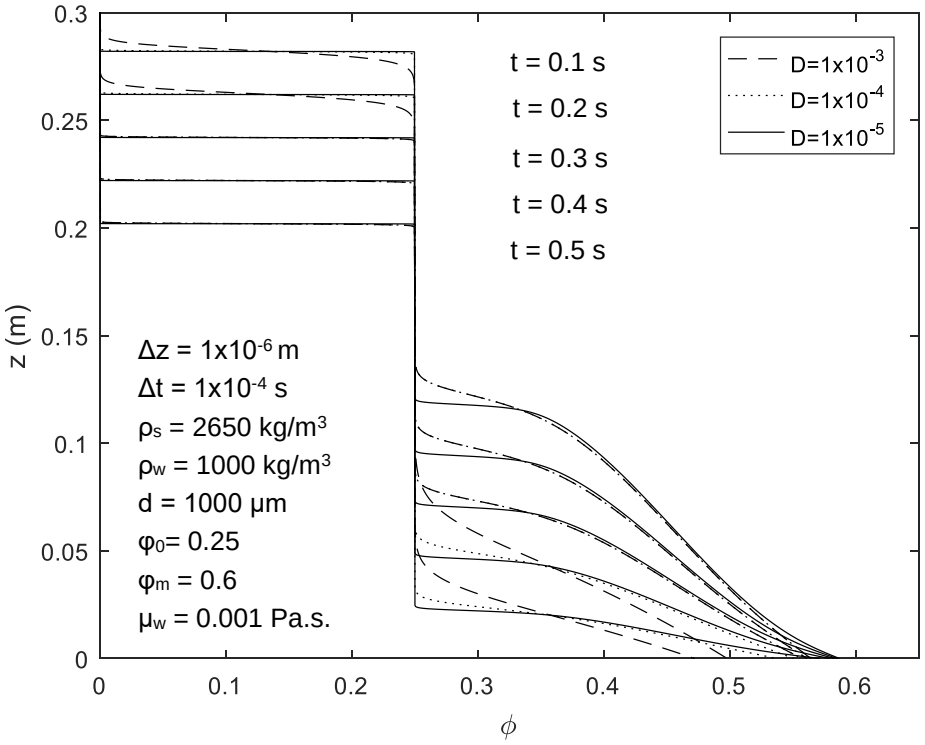

Figure 34: Evaluation of Diffusivity, D [m^2/s], on Hindered Settling of Coarse 1000 μm Particles in Water

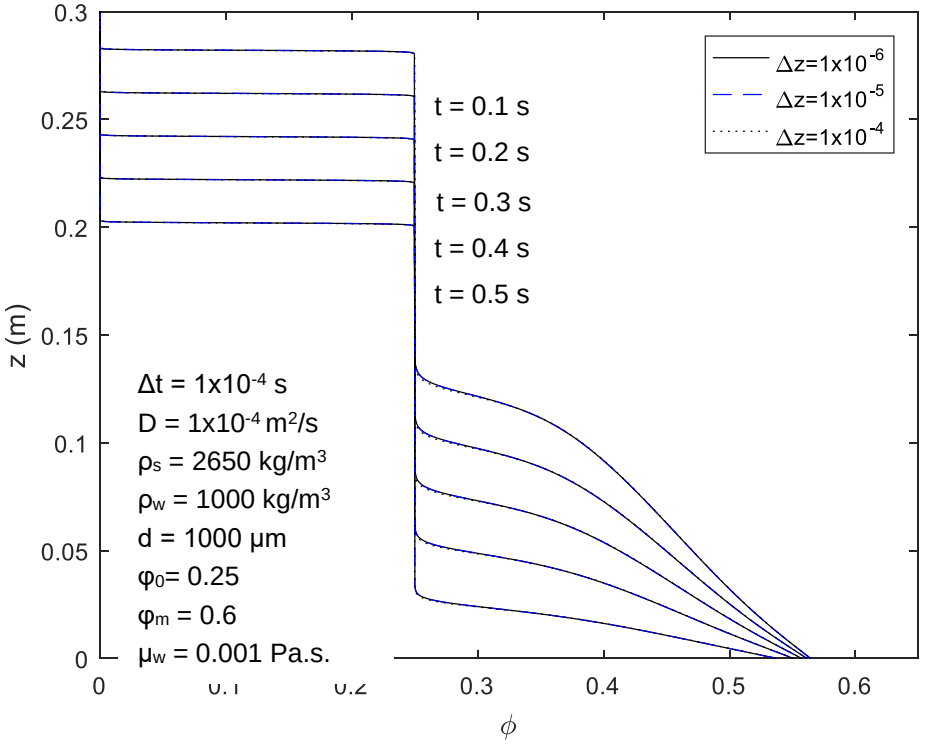

Figure 35: Evaluation of Element Size, Δz, on Hindered Settling of Coarse 1000 μm Particles in Water

5.4.6 Large Particle Size Consideration

For the cases investigated in remainder of this study, the Stokes flow assumption (Rep<1) generally holds and the settling predictions using those assumptions are appropriate. For cases with large particles and low viscosity, it is necessary to incorporate the particle drag into the settling formulation, as discussed in Section 2.5.1.

The key unknown for larger particle sizes is the most appropriate way to include the viscosity or rheology augmentation effect into the particle drag calculation. Two approaches are possible:

Method 1:

The drag coefficient is calculated assuming the carrier fluid viscosity, and the viscosity or rheology augmentation effect is incorporated only in the calculation of the hindered settling velocity from the terminal settling velocity:

$$C_D = \frac{432}{d^{*3}}\left(1 + 0.022d^{*3}\right)^{0.54} + 0.47\left[1 - exp\left(-0.15d^{*0.45}\right)\right], \quad (86)$$

where :

$$\mathrm{d}^* = \mathrm{d}\left[\frac{\rho_l g(\rho_p - \rho_l)}{\mu_l^2}\right]^{1/3},\ \mathrm{V_{ts}}^* = \mathrm{V_{ts}}\left[\frac{\mu_l g(\rho_p - \rho_l)}{{\rho_l}^2}\right]^{-1/3},\ \mathrm{V_{ts}^*} = \sqrt{\frac{4\mathrm{d}^*}{3\mathrm{C_D}}}, \quad (87)$$

and

$$v_{HS} = \frac{2\alpha}{9}\frac{g r_p^2\left(\rho_p - \rho_l\right)(1-\varphi)^2}{\mu_m}, \quad (88)$$

where the suspension viscosity is calculated using Brouwer's (2010) form:

$$\frac{\mu_m}{\mu_f} = \left(\frac{1-\varphi}{1-\varphi/\varphi_m}\right)^{B\varphi_m/1-\varphi_m}.$$

Method 2:

The suspension viscosity is included in the drag coefficient and terminal settling calculations, and only the concentration effect is incorporated into the hindered settling calculation:

$$C_D = \frac{432}{d^{*3}}\left(1 + 0.022d^{*3}\right)^{0.54} + 0.47\left[1 - exp\left(-0.15d^{*0.45}\right)\right], \quad (89)$$

where both the d* and Vts* terms:

$$d^* = d\left[\frac{\rho_l g(\rho_p-\rho_l)}{\mu_m^2}\right]^{1/3},\ V_{ts}{}^* = V_{ts}\left[\frac{\mu_m g(\rho_p-\rho_l)}{\rho_l{}^2}\right]^{-1/3}, \text{ and } V_{ts}^* = \sqrt{\frac{4d^*}{3C_D}}, \quad (90)$$

include the Brouwers (2010) suspension viscosity:

$$\frac{\mu_m}{\mu_f} = \left(\frac{1-\varphi}{1-\varphi/\varphi_m}\right)^{B\varphi_m/1-\varphi_m},$$

and only the concentration effect is included in the hindered settling velocity determination:

$$v_{HS} = V_{ts}(1-\varphi)^2. \quad (91)$$

Figure 36 presents the resulting concentration profiles predicted using Option 1 to the concentration profiles obtained from the CFD modelling of 100 um particles. Figure 37 presents the same comparison only considering the Option 2 method. The Richardson & Zaki (1954) and modified Richardson and Zaki methods using the Chen (2009) drag coefficient to determine the free terminal settling velocity are shown for reference in both figures.

As seen in the figures, utilizing Method 2 where the suspension viscosity is included in the drag coefficient determination, and only the particle concentration effect is included in the hindered settling calculation better replicates the CFD concentration profiles.

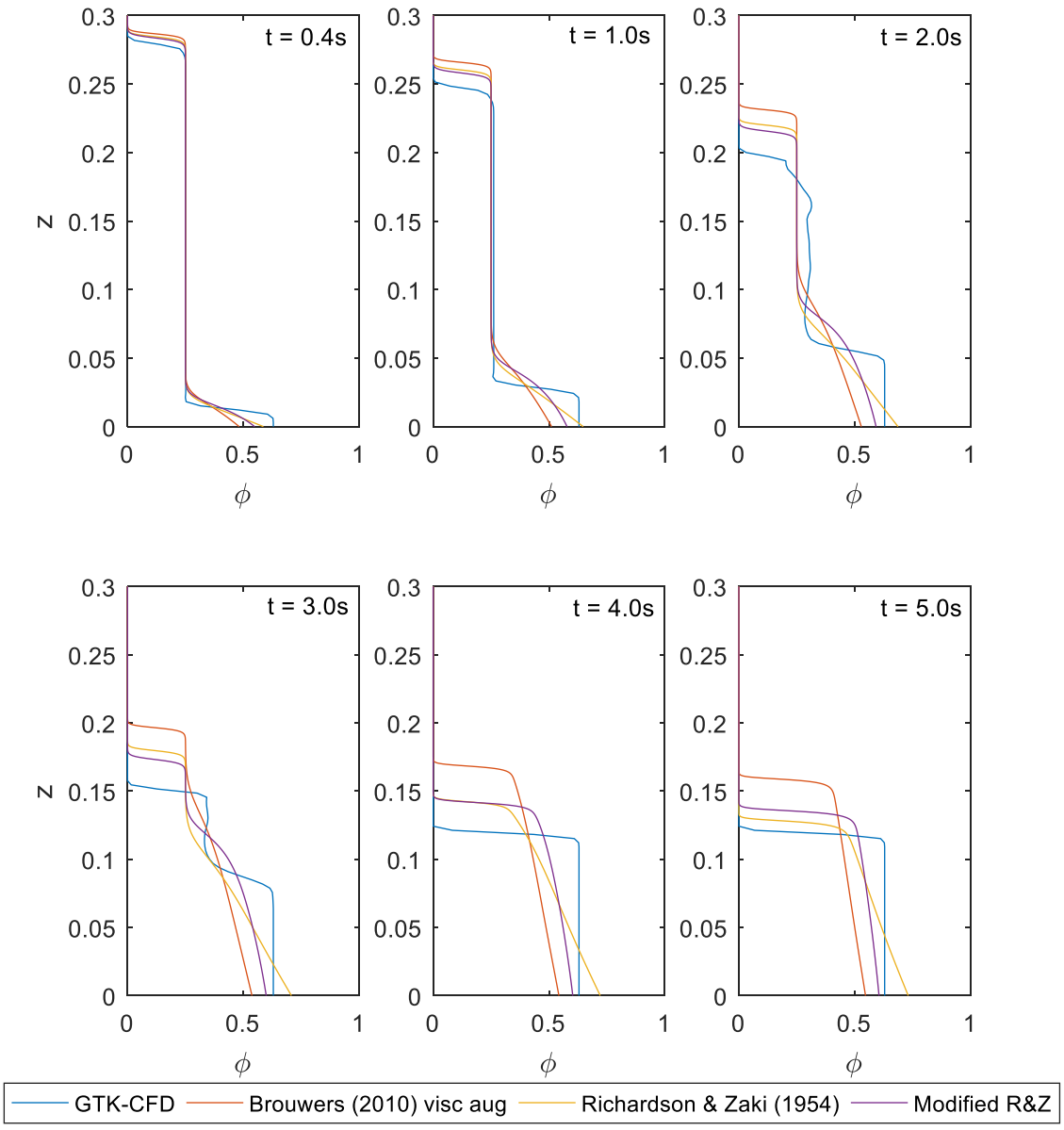

Figure 36: Comparison of 1000 μm Static Cylinder Settling Concentration Profiles with CFD Results (Large Particle Method 1)

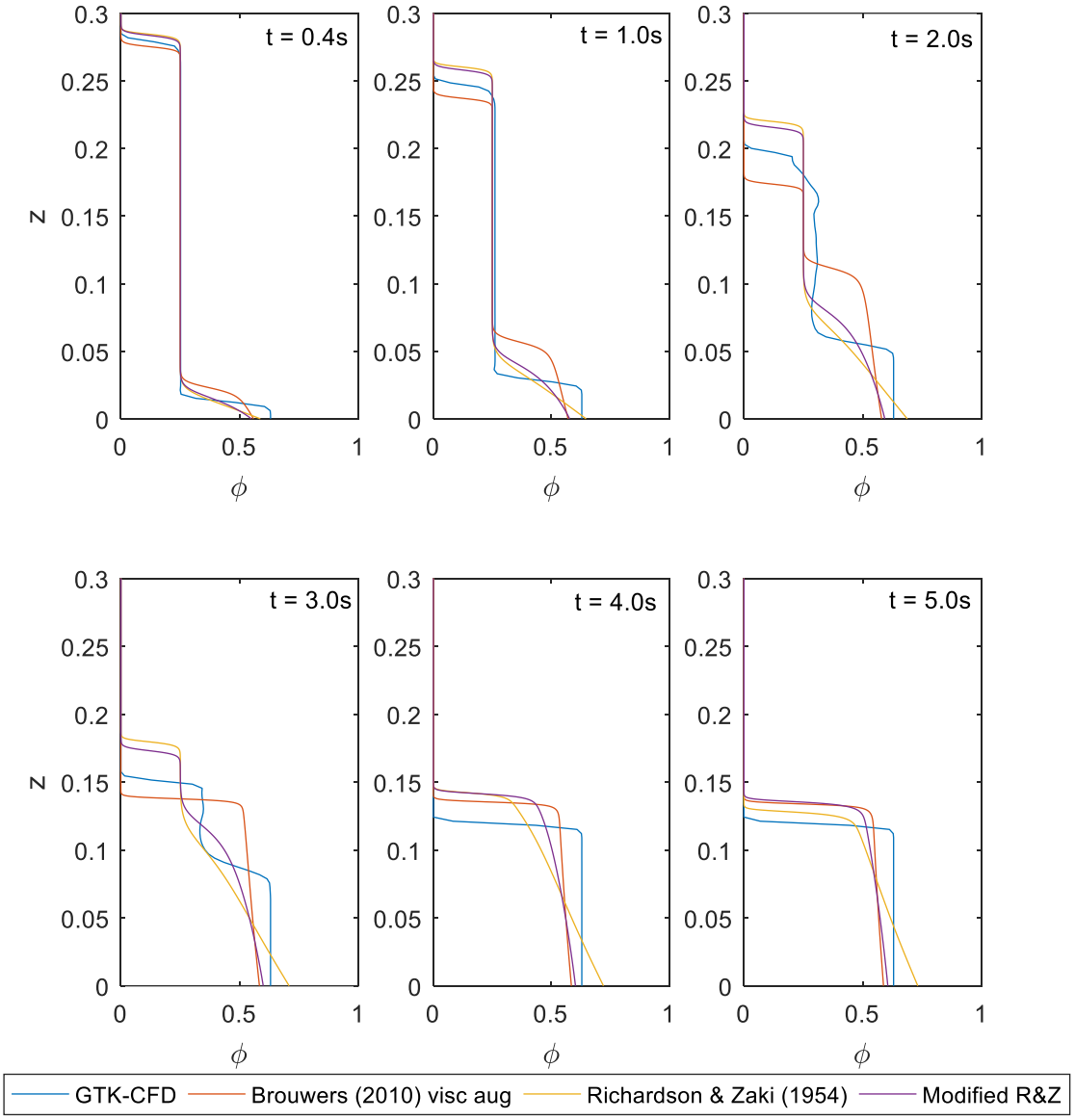

Figure 37: Comparison of 1000 µm Static Cylinder Settling Concentration Profiles with CFD Results (Large Particle Method 2)

5.5 Chapter Summary

The individual components of the 2D tailings flow model have been evaluated separately and calibrated to ensure they behave as expected prior to combining to form the complete beach flow model. In particular:

- The numerical integration Z-model for determining the flow velocity profile and discharge has been validated against homogeneous Newtonian and Bingham plastic analytical solutions. It

was also found to appropriately predict the velocity profiles for a Bingham plastic carrier fluid with varying coarse solid concentration.

- The shallow water flow model accurately predicted the stationary deposition of Bingham plastic fluid on an incline. It can also accommodate the accumulation of fluid on an essentially flat slope.
- The x-wise coarse particle advection model was found to be Courant number dependent. With the correct parameters, the advection agrees with the expected transport under constant velocity conditions. However, the overall beach flow model will require careful setup to ensure the x-wise particle transport follows the underlying fluid flow.
- Considering the relative magnitude of the vertical particle advection component, and the numerical instability at the flow front, it is excluded from the beach flow model.
- A model to couple the rheology augmentation effect to the hindered settling velocity was developed. The model agrees well with the predicted concentration profiles of Treinen and Jacobs (2015). The appropriate diffusivity and element sizes were determined for the upwind numerical settling model to ensure accurate results. Finally, an alternate model incorporating the particle drag coefficient for large particles outside of Stokes flow regime was presented to widen the suitability of the hindered settling model.

CHAPTER 6:
2D TAILINGS MODEL RESULTS AND DISCUSSION

6.1 Introduction

The final step in the 2D tailings model development is the combination of all of the individual model components, validated in Chapter 5, to form the complete tailings flow model. This chapter presents the results of this combined model, and compares the model prediction to Spelay's experimental test results investigating the coarse sand settling within free surface channel flow of Bingham plastic carrier fluid. Spelay's experimental data provides the most complete data with which to compare the 2D model predictions. Little additional complete experimental data exists for comparison of the 2D model.

6.2 Comparison to Spelay's (2007) 1D Model and Experimental Results

As discussed in Section 5.2.2, Spelay's (2007) varying concentration profiles with depth were input into the numerical integrated flow model as a means to validate the depth integrated velocity profile determination. The numerical model replicated the resulting velocity profiles reasonably well, ensuring that the computational scheme could correctly accommodate depth varying concentration profiles.

The next step in this comparison is to input only the material properties and flow rate into the numerical 2D beach flow model and compare the results to the predicted concentration profiles predicted by Spelay (2007). In this analysis the model is also compared to Spelay's experimental concentration profiles.

The discussion begins first by comparing Spelay's (2007) 1D model results to his experimental data. Figure 38 presents this comparison plotted as a function of normalized depth, $\zeta = z/H$. The general trends of the thickened tailings experimental concentration profiles and 1D numerical model profiles are in fairly good agreement. The CT-gypsum cases agree less well. Several sources that cause this disagreement:

- The experimental test work was conducted in a flume with circular segment cross section, whereas Spelay's (2007) 1D model considers infinite sheet flow. Spelay accounts for this

variation by using the hydraulic radius as the input to the 1D model rather than the measured flow depth.

- Spelay's 1D (2007) model does not allow for the increase in flow depth as solids are deposited on the beach. This is likely the primary source of discrepancy in the CT-gypsum cases. The sand solids concentration has increased significantly through the flow depth in these cases and is not captured by Spelay's model.

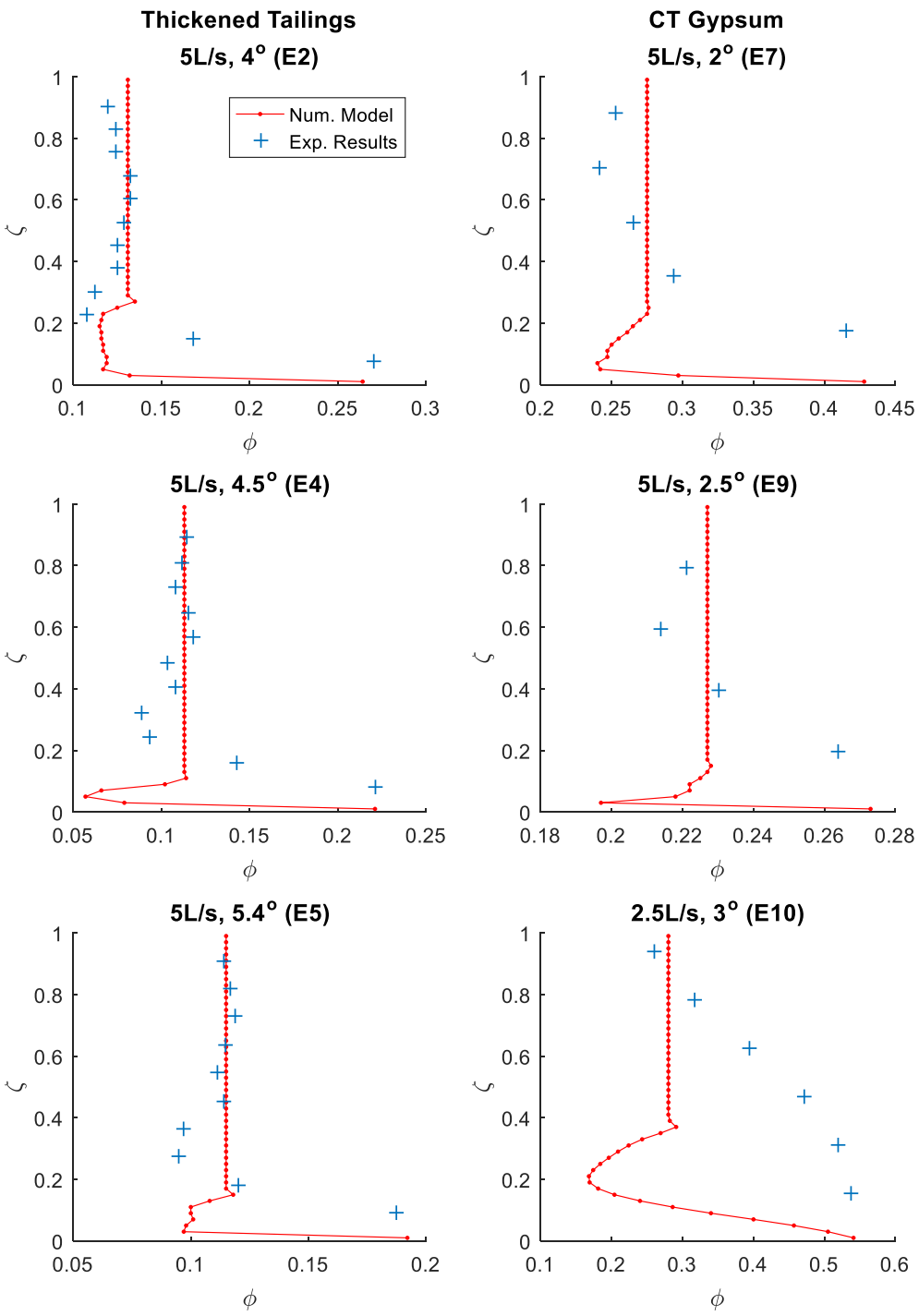

Figure 38: Comparison of Spelay's (2007) 1D Numerical Model to Experimental Results

The comparison of this work's 2D numerical beach flow model with Spelay's (2007) results utilizes the following approach:

- For each case, the input flow rate q_{in}, is adjusted until the flow velocity and flow depth at the inlet agreed with Spelay's model predictions. Table 9 presents the resulting flow rates depths, and velocities for the cases considered.
- The 2D model is then run until the concentration profile measured at x=14.75 m obtains a quasi-steady state. The concentrations are measured at this location to agree with the measurement location of Spelay's (2007) experimental test work (x= 14.8 m). The simulation duration varies due to the flow velocity down slope, but all of the simulations are run for at least 60 seconds to ensure the quasi-steady state has been reached.
- The predicted concentration plots for each of the simulations are plotted at two times:
    1. At a time approximately equivalent to the simulation time reported by Spelay (2007). He notes in his results that the simulations haven't necessarily reached steady state, so this first comparison aims to compare the two model predictions. Since the flow must first reach the x= 14.75 m measurement point in the 2D simulations[19], an initialization time is added to Spelay's simulation time so that the comparison between the two is approximately equal. Note that that the comparison isn't exact since the particles will have already settled within the 2D flow model prior to reaching the measurement location.
    2. At the final simulation time of the model run. The intent of this comparison is to provide a steady state concentration profile to compare to the experimental results. The slurry is recirculated for a relatively long duration during the experimental test work. Typically, 60 s was adequate to reach steady quasi-state conditions in the model. Some models were run longer as necessary to verify steady conditions.

[19] Note that this doesn't necessarily align with the time that it would take slurry to reach the measurement point considering the mean flow velocity (t = Uxz/x) since the particles near the bed slope travel slower than the mean flow velocity. The initialization time was found by the time at which the concentration at the bed reach approximately the initial concentration.

Model runs for four of Spelay's (2007) cases: E2, E5, E7 and E10 are reported in the following subsections. The E4 case is not compared since there wasn't good agreement between the velocity profiles; the flow case was just on the threshold of allowable flow considering the yield stress. Case E9 is not evaluated since it had fairly similar behavior to the other CT-gypsum cases.

Table 9: Comparison of Model Flow Parameters

Case	**Thickened Tailings**			**CT-Tailings with Gypsum**		
Spelay numerical model reference	E2	E4	E5	E7	E9	E10
Spelay test reference	15	16	17	12	13	14
Slope	4.0°	4.5°	5.4°	2.0°	2.5°	3°
Flow rate	5 L/s	5 L/s	5 L/s	5 L/s	5 L/s	2.5 L/s
H (Rh of exp.)	0.0455 m	0.0441 m	0.0415 m	0.0256 m	0.0231 m	0.0281 m
Uxz plug	1.63 m/s	0.18 m/s	0.67 m/s	1.34 m/s	0.076 m/s	4.37 m/s
2D Model Parameters						
Q 2D model	0.0678 m^2/s		0.027 m^2/s	0.03 m^2/s		0.105 m^2/s
H 2D model[1]	0.0456 m		0.0418 m	0.0256 m		0.0282 m
Uxz plug[1]	1.61 m/s		0.675 m/s	1.31 m/s		4.30 m/s
Δx	0.5 m		0.5 m	1.0 m		1.0 m
nZ	500		500	500		500
Dsettle	$1x10^{-7}$ m^2/s		$1x10^{-7}$ m^2/s	$1x10^{-6}$ m^2/s		$1x10^{-6}$ m^2/s
Δt main	0.2 s		0.2 s	0.2 s		0.1 s
Δt flow	0.005 s		0.005 s	0.005 s		0.005 s
Δt settle	0.00001 s		0.0001 s	0.00001 s		0.0001 s

[1]Resulting output value at model inlet node at start of simulation

6.2.1 TT Case E2 Comparison

Figure 39 presents the time progression of the 2D concentration contour plot down the slope for Spelay's (2007) E2 thickened tailings flow case. To accommodate the scale difference between length and height, the flow depth is a normalized so that the bed is at 0 m height along the beach length[20]. The flow

[20] This normalization results in an apparent flat underlying beach slope in the figures. The actual slope remains constant and is provided in Table 9.

depth remains relatively constant down the slope for this case but there is an increase in flow depth along the beach slope to account for the deposited coarse particles. The deposition is however fairly small since the majority of the coarse particles remain suspended within the large unsheared plug zone, as presented in the subsequent figures.

The region of zero concentration that expands under the flow front (dark blue region in Figure 39 along with the concentration profiles for the other cases presented in Figure 43, Figure 46, and Figure 53) is an artifact in the modelling due to the flow velocity profile, and resulting coarse particle x-wise advection, being much slower near the bed than at the top. The initial flow solver step creates a small concentration free layer at the flow front on the first flow solution iteration that is stretched down the incline. Particle settling is also not calculated until the flow depth reaches 0.02m in depth, which helps further propagates this artifact.

Indicated on the lowest plot in Figure 39 is the 14.75 m measurement location where the concentration profiles are evaluated. Figure 40 presents the resulting time-varied flow velocity, $U_{xz}(x,z)$, concentration, φ, coarse settling velocity, vs, and coarse solids flux, φvs, profiles at x = 14.75m. the profiles are plotted as a function of the normalized depth as in Figure 39. The upper plug portion of the flow velocity profile doesn't vary significantly with time since the flow must ultimately match the driving potential due to the inclined slope. But, the shape of the lower portion of the profile does change as solids settle to the bed and the augmented rheology causes stationary flow. The horizontal lines on top of the velocity profiles indicate the flow depth and how it increases as the coarse sand settles. The profiles at the measurement location (14.75m) reach a quasi-steady state at 75 s. The profiles change only slightly 70 and 75 seconds.

Spelay (2007) noted a zone within the fluid-shear region where the particles settle faster. This zone is clearly seen within the settling velocity and flux profiles. The zone shifts upwards as the coarse fraction settles on the bed.

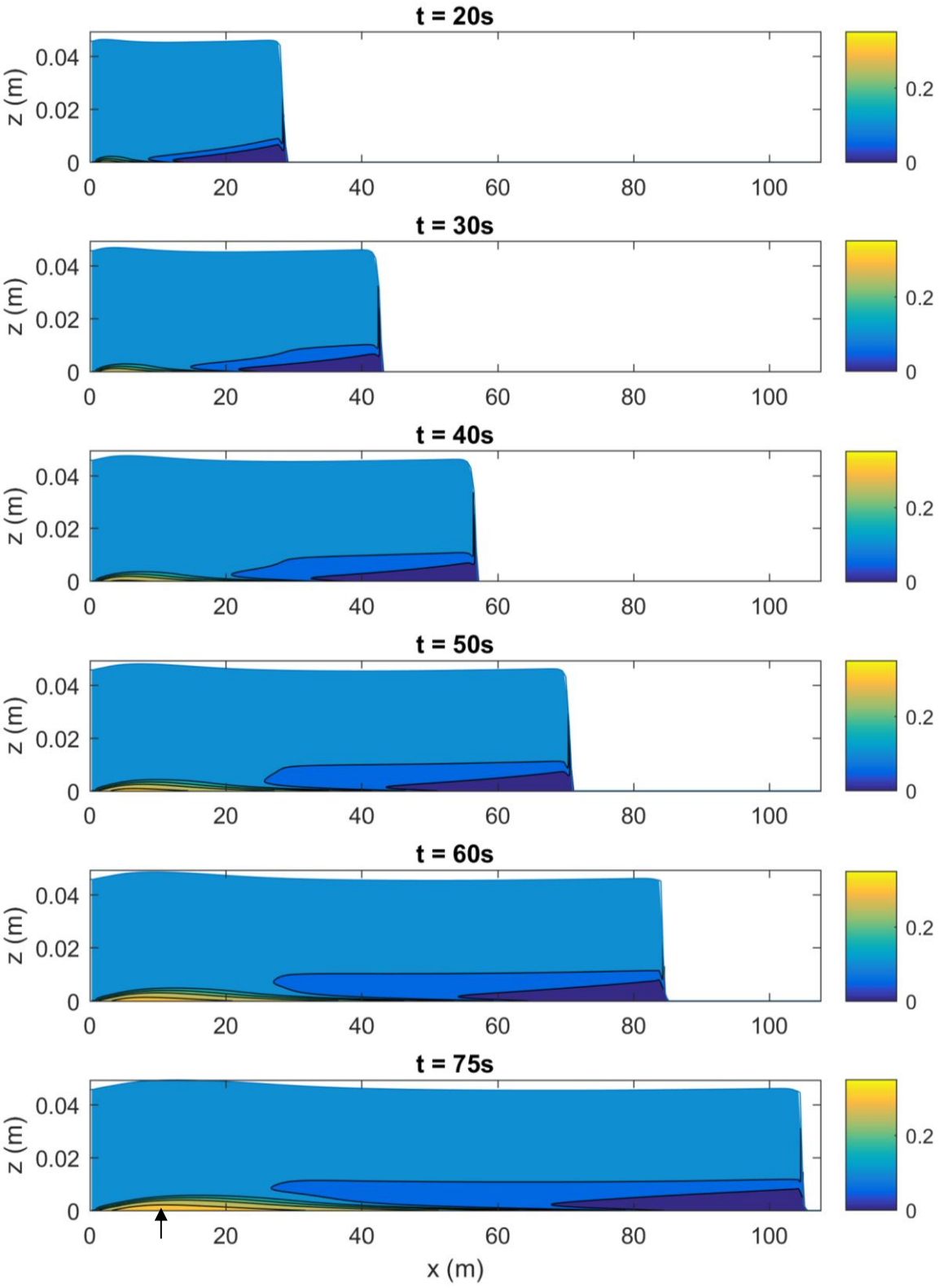

Figure 39: Case E2 Sand Concentration Contour Plot vs. Time (Variable Mixture Density)

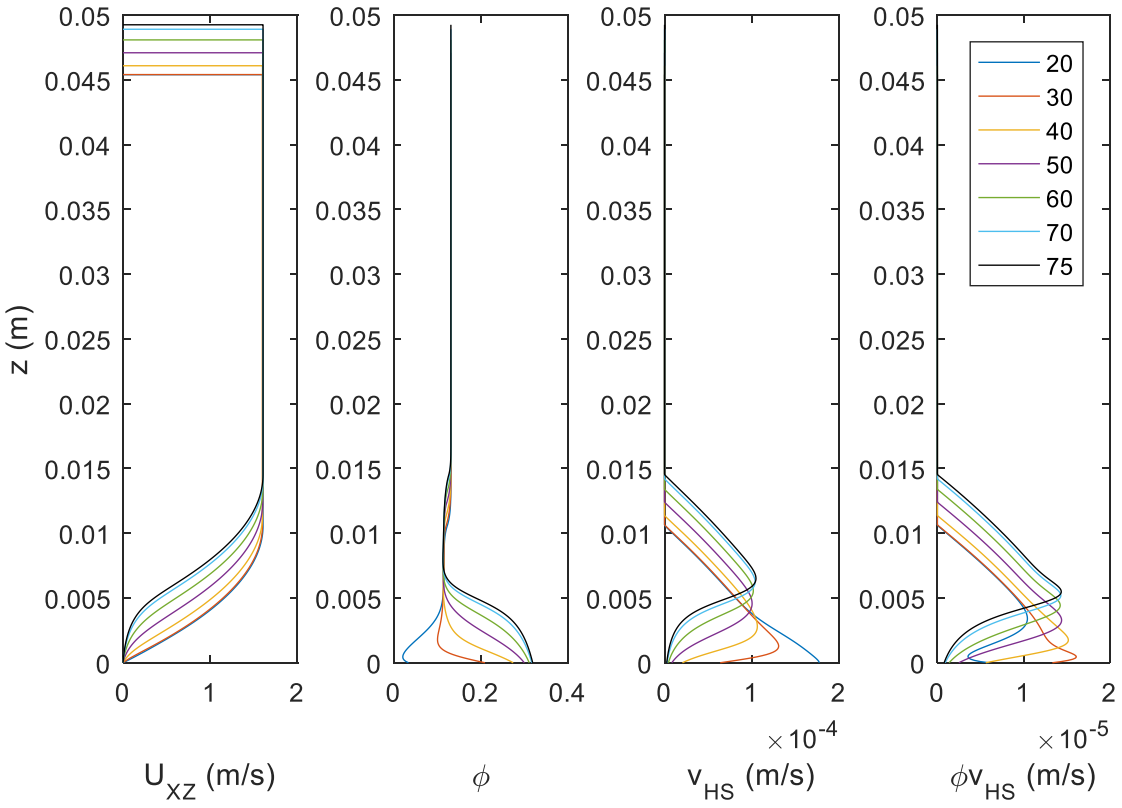

Figure 40: Case E2 Velocity, Concentration and Solids Flux Profiles vs Time at x = 14.75m (Variable Mixture Density)

Figure 41 compares the resulting concentration profile at x = 14.75 m to Spelay's (2007) 1D model and experimental profiles. The Gillies rheology augmentation model is used in the simulations. The profiles are plotted as a function of ζ to allow comparison with Spelay's predictions. As discussed above, the 2D model profiles are plotted at an approximately equivalent time scale (10 s initialization +10 s simulation time) to compare to Spelay's 9.5 s simulation time. Also plotted in the figure is the quasi-steady profile reached at 75s.

Two density scenarios are considered in the plot:

- The mixture density is allowed to vary with depth as the coarse particles settle. This scenario more accurately represents actual conditions and was incorporated into the model development discussed in Chapter 4.

- The mixture density is held constant in the shallow water flow model velocity profile determinations.

In most applications, the density is assumed constant with depth in developing the shallow water equations. This constant mixture density case enables the variable density formulation to be compared to the typical constant formulation to ensure the variable density approach doesn't vary significantly from the customary approach. The two density scenarios produce fairly similar profiles; but, the variable density model is able to predict higher settled concentrations at the bed.

There is some agreement between Spelay's (2007) numerical model predictions at 9.5 seconds and the 2D model predictions at 10 s+10 s. The 2D simulations vary considerably at that time step since coarse particles are beginning to accumulate on the bed. It is clear from the simulations that 10 s is not sufficient to reach the steady concentration profile conditions at the measurement location. The 2D model better agrees with the experimental results near the bed compared to Spelay's model prediction.

The particle depletion within the shear zone in the 2D model is not as pronounced as experimentally observed or predicted by Spelay (2007), but the absolute difference between the 2D prediction and experimental measurements is only approximately 1%.

It is important to recognize that Spelay's (2007) experimental measurements were conducted in a relatively small 156.7 mm inner diameter semi-circular cross section flume. The experimental concentration profiles are chord averaged concentrations acquired with a traversing gamma ray densitometer. Near the free surface, the densitometer will measure across both the sheared and unsheared region. Geometry effects will have some impact on the concentration profiles and exact agreement between the 2D model and Spelay's experimental measurements is not expected.

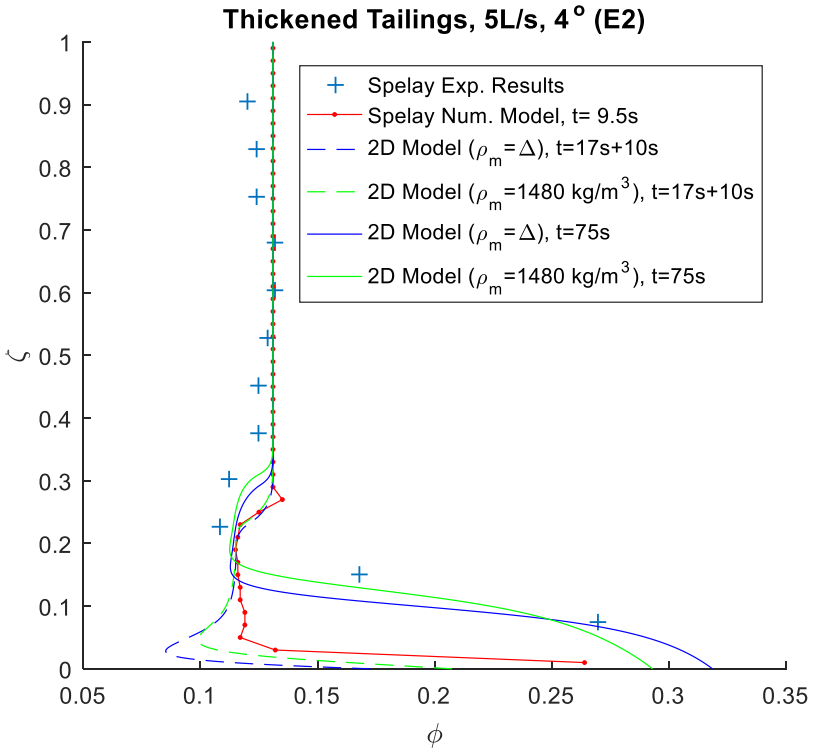

Figure 41: E2 Sand Concentration Profile Comparison to Spelay E2 Experimental and Numerical Results, (x=14.75 m, Gillies Rheology Augmentation Model)

Also of interest in this study is the impact the rheology augmentation model has on the predicted concentration profiles. Figure 42 presents a comparison of the Gillies model selected for this study, and the Rahman (2011) rheology augmentation model. For comparison, the Rahman and Gillies models are plotted in Figure 7 and Figure 8 above in Section 2.5.2. The Rahman model has a higher augmentation effect at low solids concentrations, but significantly lower augmentation impact than Gillies at high concentrations.

As seen in Figure 42 the Rahman (2011) model produces a shallower, but higher concentration accumulation of solid particles at the bed. At the initial 13.1%v solids concentration, the Rahman augmented yield stress is only approximately 20% higher than the Gillies augmented yield stress, so it is not surprising that the concentration profiles are similar for this case.

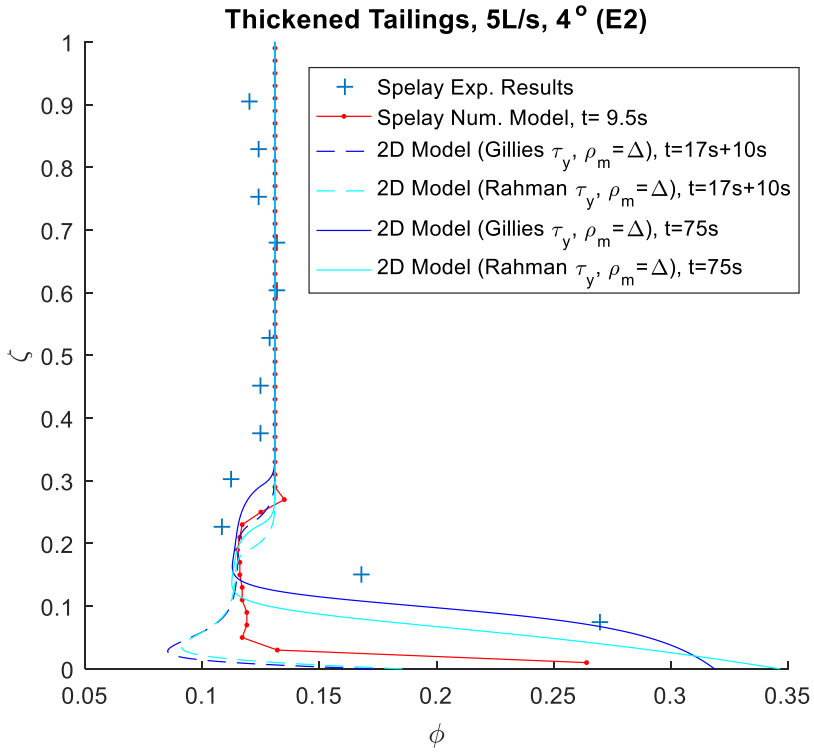

Figure 42: Comparison of Gillies and Rahman Models at 14.75 m for Spelay E2 Case. (Variable Mixture Density)

6.2.2 TT Case E5 Comparison

The next case evaluated using the 2D beach flow model is Spelay's (2007) E5 thickened tailings case. This case has higher channel slope and higher rheology than the E2 case above, but slightly lower 11.5%v coarse solids concentration than the 13.1% concentration in E2. Figure 43 presents the time evolution of the coarse sand concentration profile along the slope.

The unsheared plug dominates this flow cases so little solids deposition is seen along the beach length. Figure 44 presents the velocity, concentration, settling velocity, and solids flux profiles at the 14.75 m location. As seen in the figure, the top 85% of the flow is the unsheared plug where no coarse particle settling occurs. The flow depth only increases slightly (approximately 2 mm) during the simulation time.

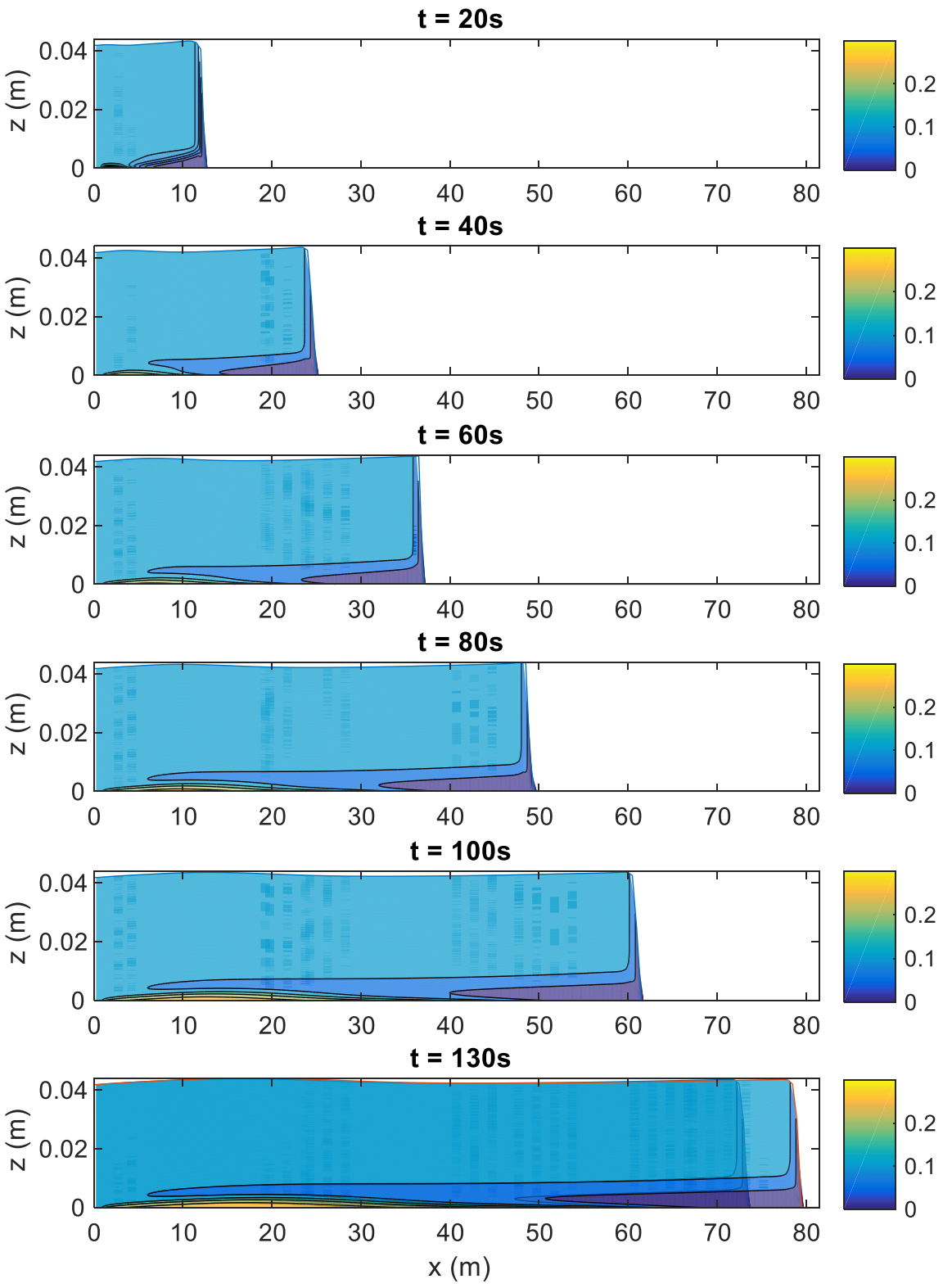

Figure 43: Case E5 Sand Concentration Contour Plot vs. Time (Variable Mixture Density)

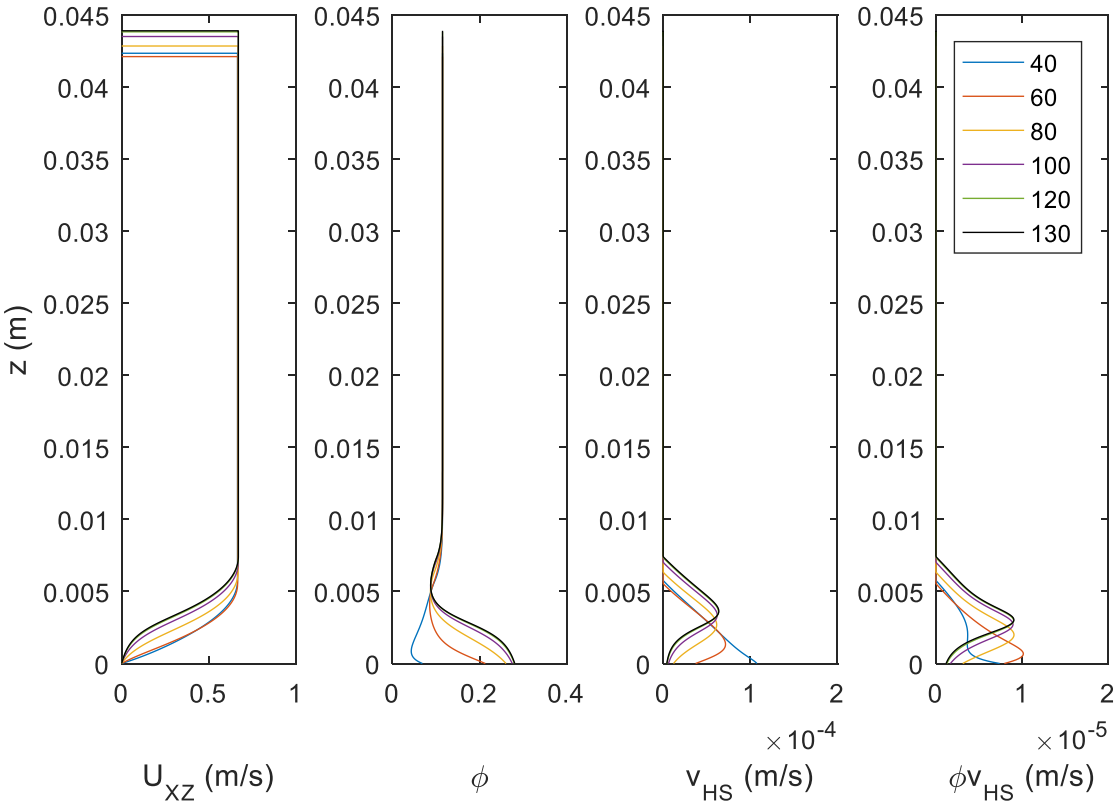

Figure 44: Case E5 Velocity, Concentration and Solids Flux Profiles vs. Time (x = 14.75m)

Figure 45 presents the comparison between the 2D model predicted profiles and Spelay's (2007) experimental and 1D model predictions. Only the variable mixture case is presented for this option since it is more representative and was in closer agreement than the results for constant mixture density case in the E2 case. The 2D model profiles are plotted at an approximately equivalent time scale (40.5 s initialization +8.5 s simulation time) to compare to Spelay's 8.5 s simulation time. Also plotted in the figure is the quasi-steady profile reached at 120s. Also included in the figure is the comparison between the Gillies (2006) and Rahman (2011) rheology augmentation models.

The 2D simulations at the 8.5 s time actually match fairly well with Spelay's 8.5 simulation predictions. However, as noted in Case E2, solids are depositing onto the bed quickly at this stage and the 2D simulation profiles change fairly rapidly at this stage in the simulation.

The quasi-steady concentration profiles at 120 s follow the same general trend as the experimental results, but the 2D model under predicts the depth of the accumulated coarse sand fraction for both the Gillies (2006) and Rahman (2011) cases.

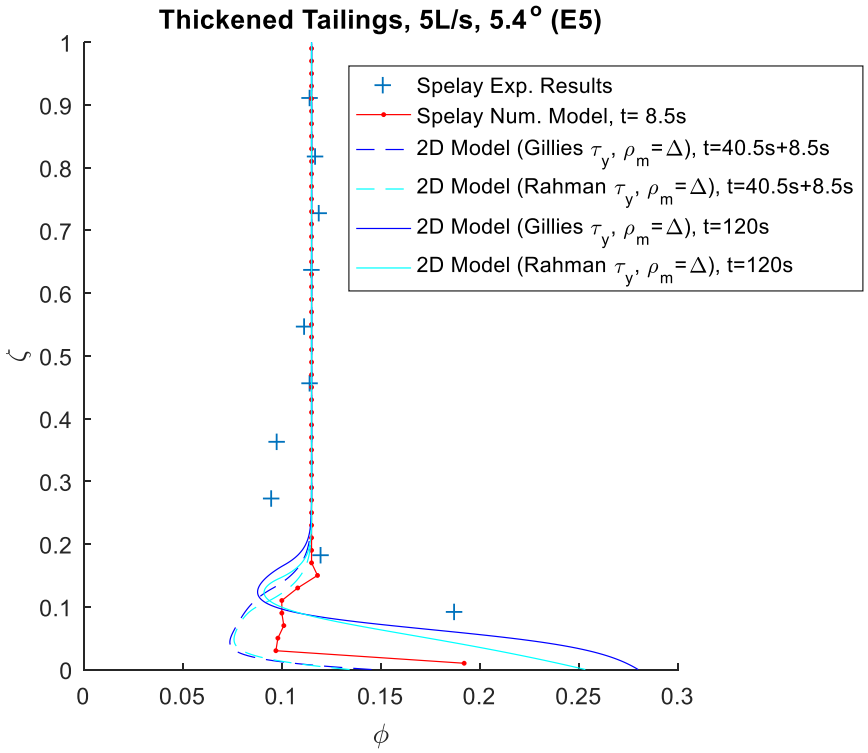

Figure 45: E5 Sand Concentration Profile Comparison to Spelay Experimental and Numerical Results, (x=14.75 m)

6.2.3 CT Case E10 Comparison

Based on Spelay's (2007) experimental data, the CT-gypsum models (E10 here and E7 in the next section) are expected to have significant coarse particle settling. Figure 46 presents the coarse particle concentration contour plot for the E10 CT case as the tailings flow downs the inclined slope. The coarse particles settle over a long down-beach distance, and to a relatively deep depth within the flow. As seen in the figure, the shear depleted particle zone (green zone above the high concentration bed) increases across the deposited bed, and the unsheared plug region agove it decreases in size.

Figure 47 presents the velocity, concentration, hindered settling velicity and settling flux profiles at 14.5 m[21] down the beach. The flow depth increases singificantly between 10 s and 30 s, but ultimately the profiles have reached a qusi-steady state at 60 s. The flow depth increases only slightly between 40 s and 60 s. Figure 48 presents the concentration profiles through the deepest coarse particle cross section, located at 44.5 m. the concentrations and velocity profiles. The overall flow velocity decreases down the beach. This velocity decrease is due to the flow depth increase down the beach, and the overal flattening of the bed slope as the stationary coarse particle bed depth increases.

It is interesting to note that the U_{XZ} and V_{HS} velocity profiles indicate an unsheared plug zone at 44.5 m, but the concentration is actually not constant within that plug any longer. This is due to the changing velocity down the slope. The flow velocity initially increases within the first 7 m of the slope as the flow encounters and flows overtop the deposited solids. It then gradually slows across the remainder of deposited bed. As the velocity slows the unsheared plug region grows, capturing coarse particles that have previously undergone settling. Figure 49 presents the contour plot of the flow velocity.

[21]In this simulation with 1 m x spacing the closest node to 14.8 is at the 14.5m half node.

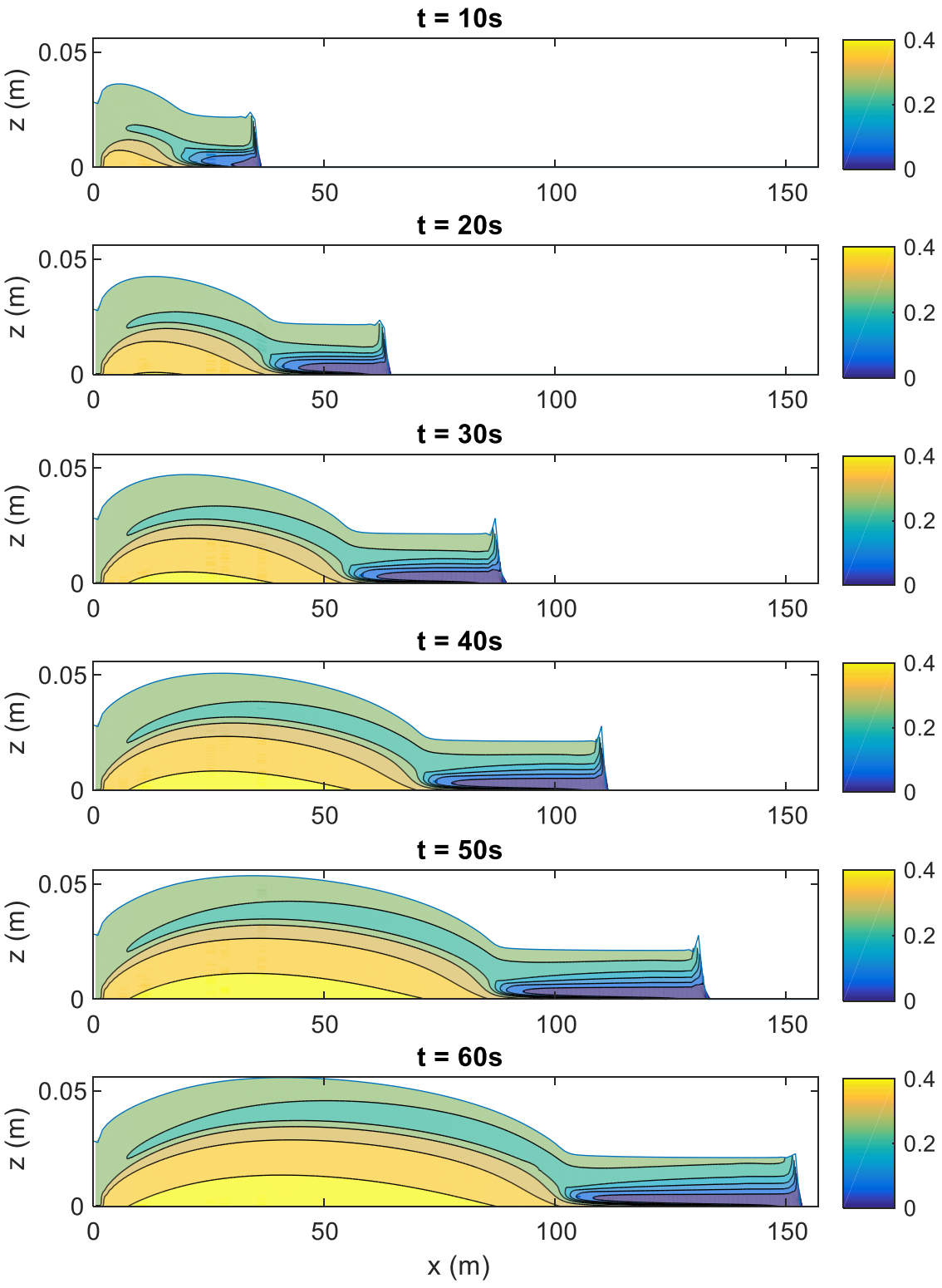

Figure 46: Case E10 Sand Concentration Contour Plot vs. Time (Variable Mixture Density)

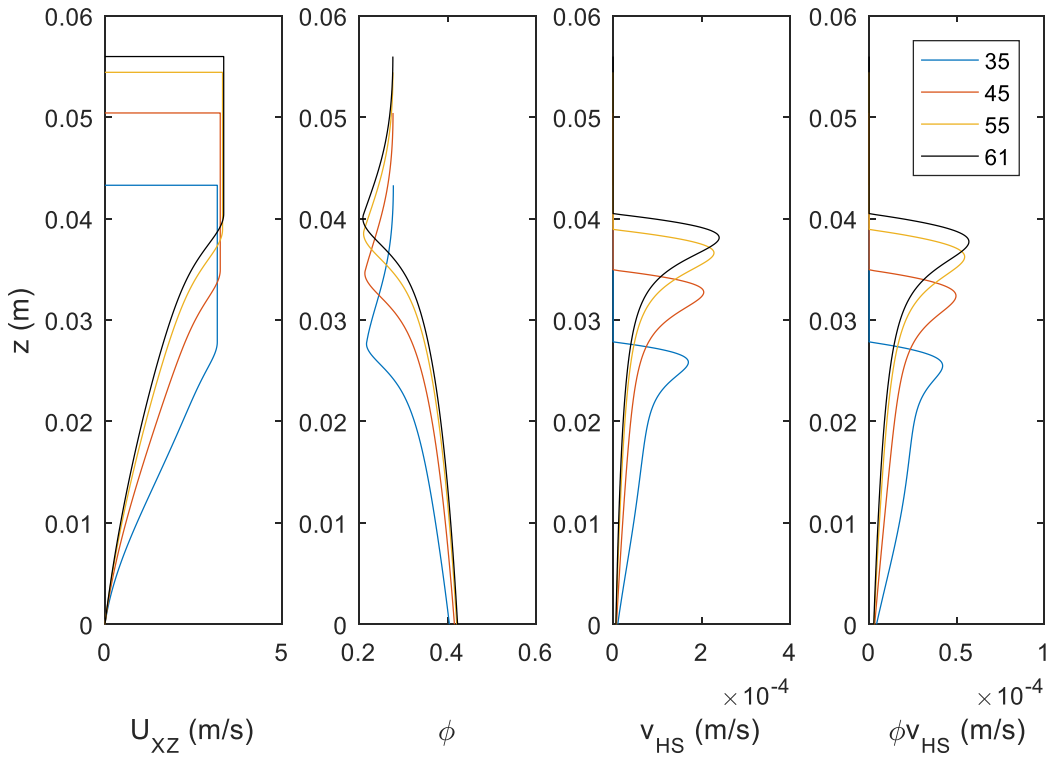

Figure 47: Case E10 Velocity, Concentration and Solids Flux Profiles vs. Time (x = 14.5m)

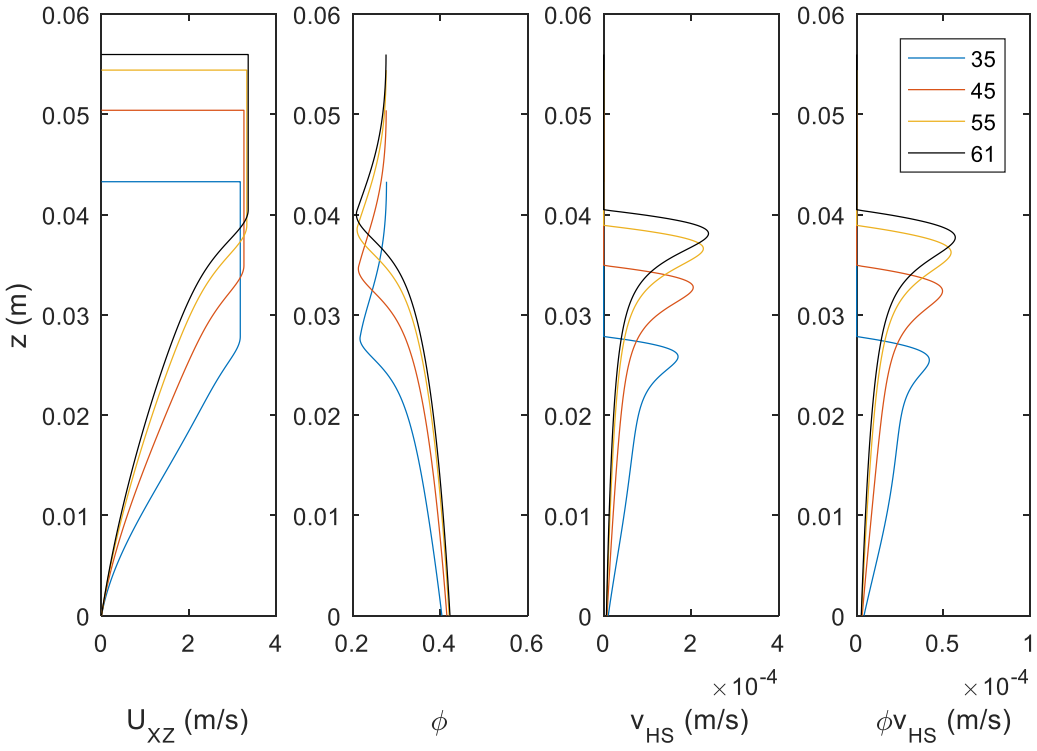

Figure 48: Case E10 Velocity, Concentration and Solids Flux Profiles vs. Time (x = 44.5m)

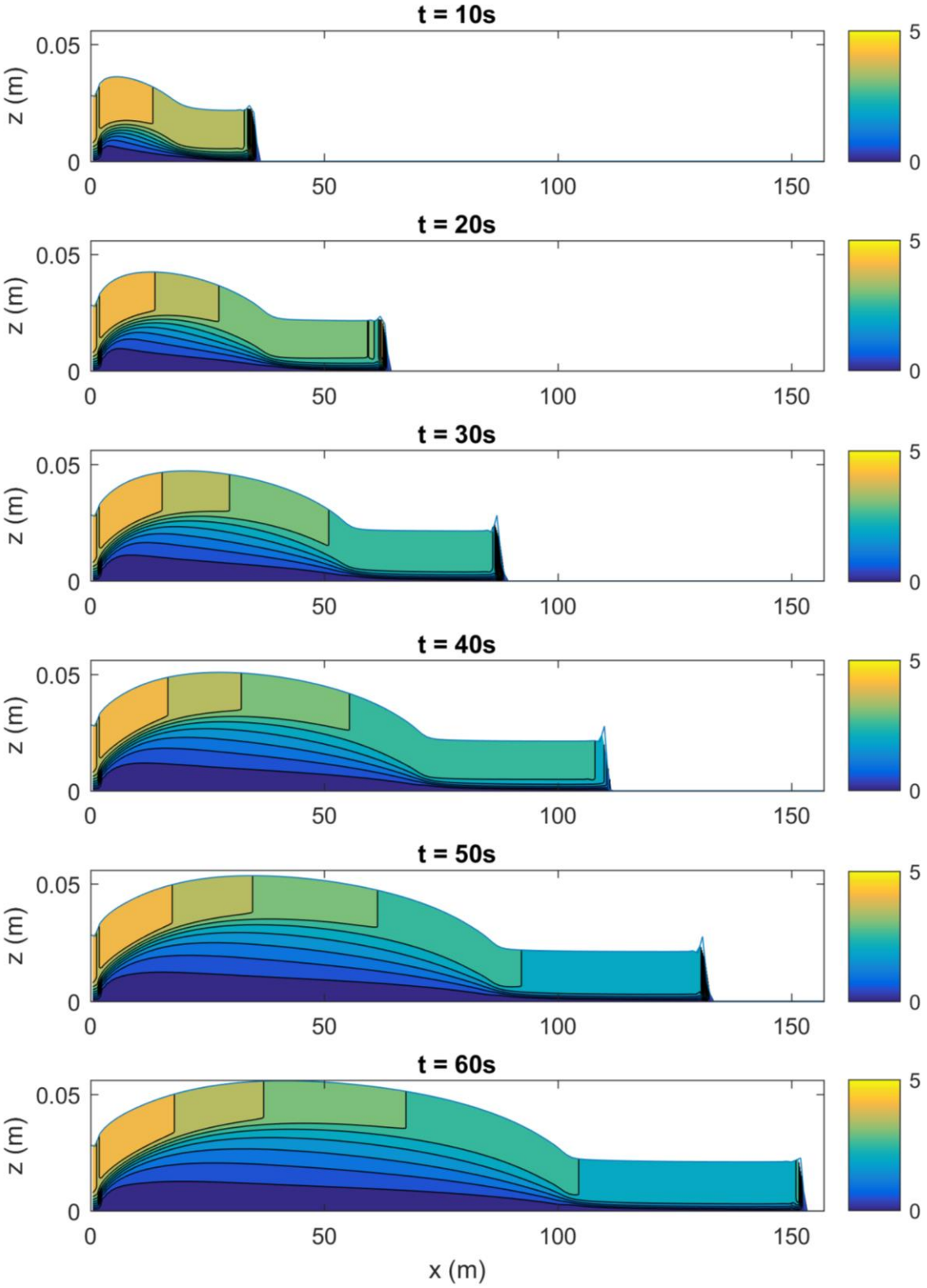

Figure 49: U_{XZ} Flow Velocity Contour Plot Profile vs. Time (Variable Mixture Density)

Figure 50 presents the comparison between the 2D model predictions and Spelay's (2007) experimental and 1D numerical results at 14.5 m. For comparison Figure 51 presents the concentration plots through the deepest-settled coarse particle cross section at 44.5 m. As with case E2, the profiles considering both variable mixture density and constant mixture density are presented. The two density approaches yield similar results for the higher coarse solid concentration CT cases.

The profiles indicate a deeper settled bed region at x = 44.5 m, which better corresponds with Spelay's experimental data. As with case E7, the 2D model simulations produce the same general profile shape as the experimental results. However, the 2D model under predicts the settled bed concentration using the Gillies rheology augmentation model. Also, the shear depleted zone is present in the simulation predictions, but it was not observed in the experimental data.

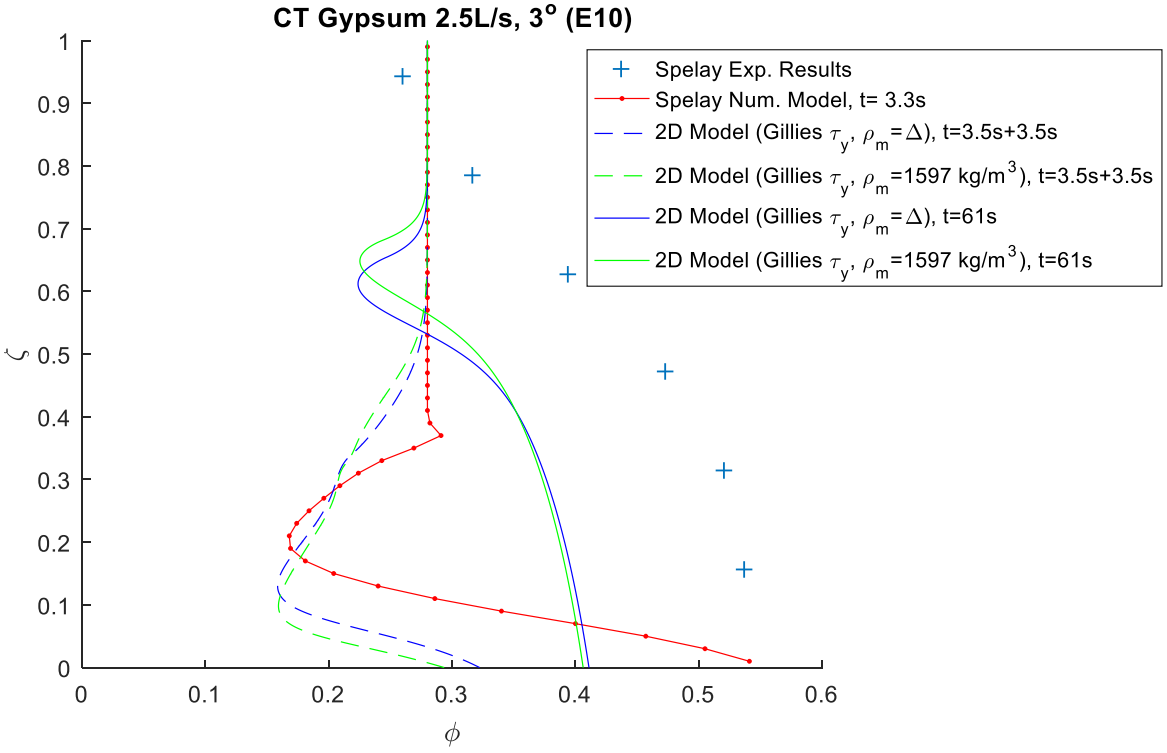

Figure 50: E10 Sand Concentration Profile Comparison to Spelay Experimental and Numerical Results, (x=14.75 m)

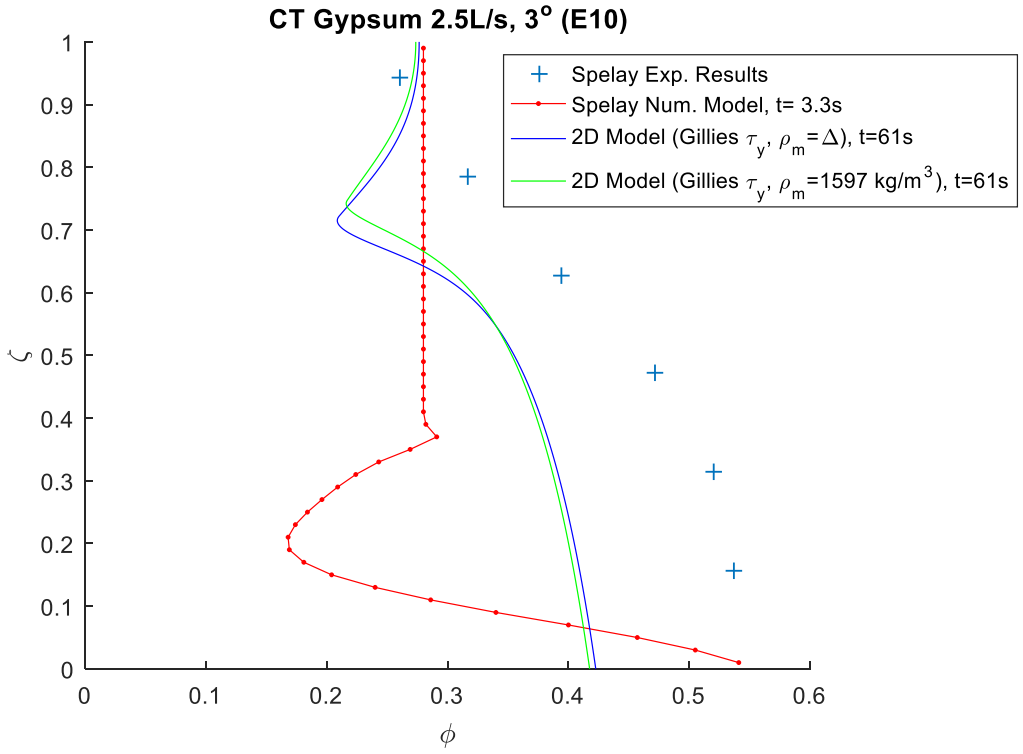

Figure 51: E10 Sand Concentration Profile Comparison to Spelay Experimental and Numerical Results, (x=44.5 m)

Figure 52 presents the comparison between the Gillies (2006) and the Rahman (2011) augmentation models. The Rahman model is better able to predict the settled bed concentration right at the bed, but the overall settled coarse solids bed is much shallower than the experimental concentration profile. The Gillies model better captures the overall shape through the flow, but the steep increase in rheology near the maximum packing concentration in the Gillies model limits the settled concentration within the deposit. As a result, the yield stress stops the flow and limits settling prior to reaching the maximum packing concentration. This yields a "gelled" bed type arrangement proposed by Talmon (2004) rather than closely packed particles with particle-particle contact.

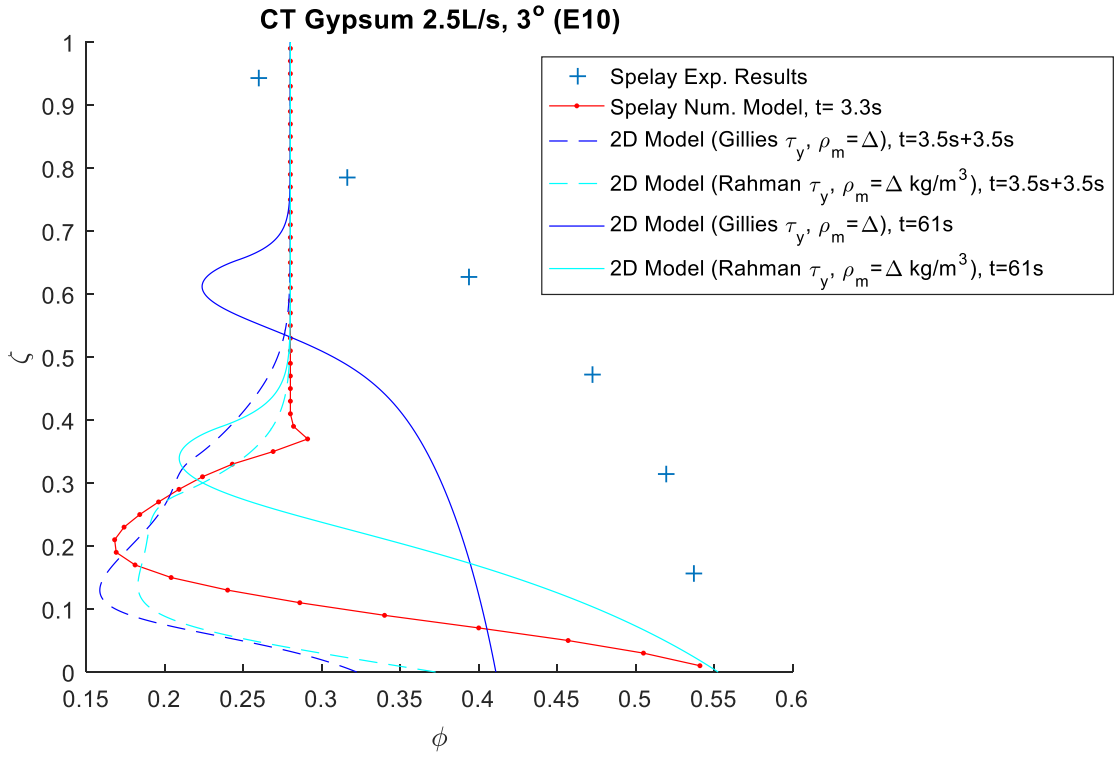

Figure 52: Comparison of Gillies and Rahman Models at 14.5 m for Spelay E10 Case. (Variable Mixture Density)

6.2.4 CT Case E7 Comparison

Figure 53 presents the E7 case contour plot of concentration as the flow moves down the inclined slope. As with the E10 case, coarse particles are deposited over a large area, and there is a very noticeable increase in the flow depth over the deposited coarse fraction. The deposited area also increases in length with time. The shear depleted zone is visible between the deposited solids and unsheared plug flow.

Figure 54 presents the time-varying velocity, concentration, solids settling velocity and solids flux profiles at the reference location. The flow depth increases significantly as the coarse sand settles to the bed. Of particular interest is the change in shape of the lower half of the velocity profile as coarse solids begin to accumulate on the bed slope. The lower 25% of the flow depth is nearly stationary at the end of the simulation time, although the settled mass is still moving slowly down the slope. The hindered settling velocity and corresponding settling flux also varies significantly with time as the coarse fraction settles to the bed.

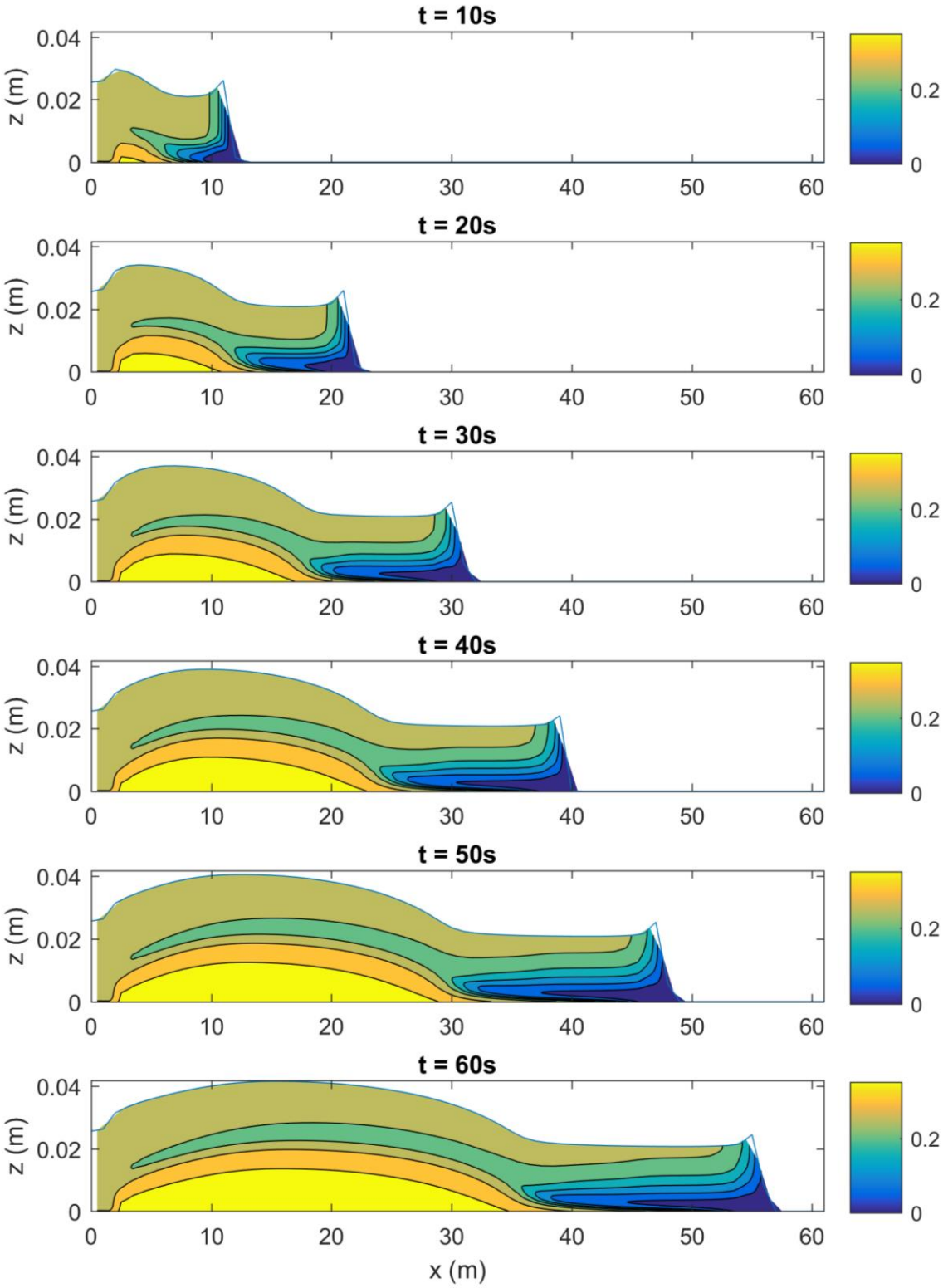

Figure 53: Case E7 Sand Concentration Contour Plot vs. Time (Variable Mixture Density)

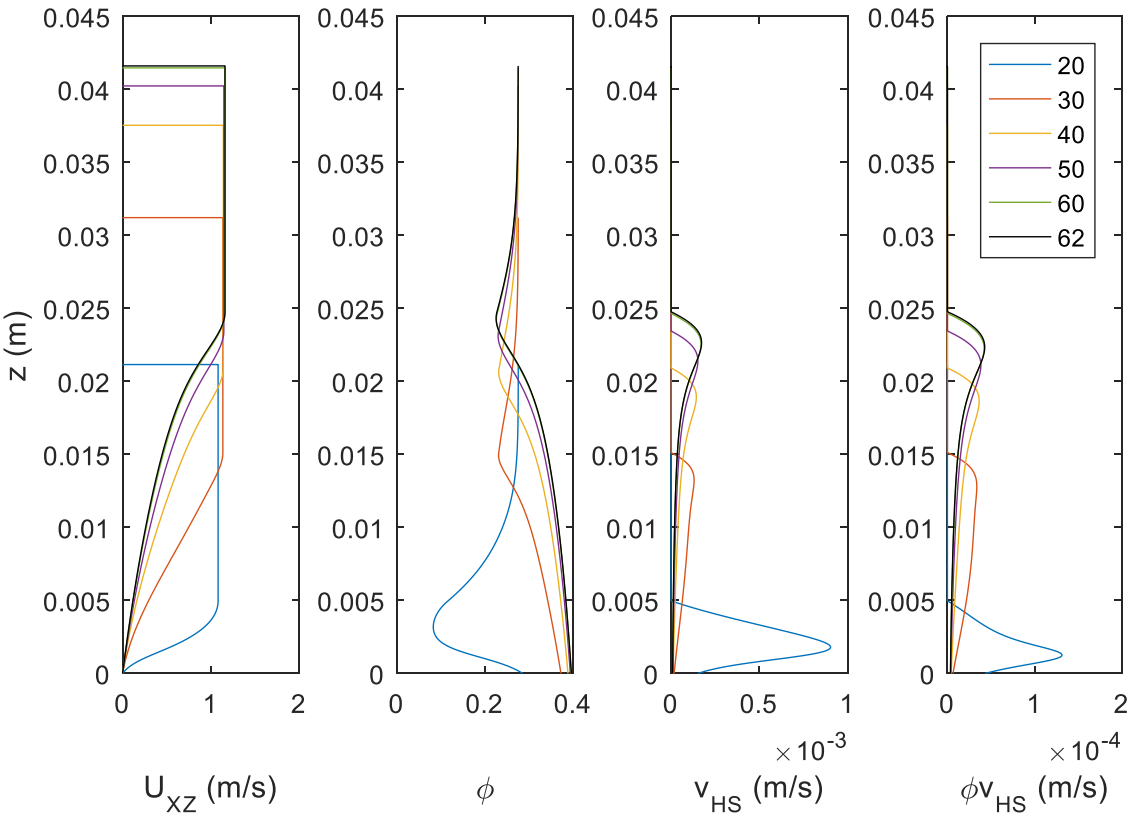

Figure 54: Case E7 Velocity, Concentration and Solids Flux Profiles vs Time (x = 14.75m)

Figure 55 presents the comparison between the 2D numerical model results at 14.5[22] m and Spelay's (2007) experimental concentration profiles and numerical prediction. As with the E5 case, only the variable mixture case is presented for this option. The 2D model profiles are plotted at an approximately equivalent time scale (23.5 s initialization +0.65 s simulation time) to compare to Spelay's 0.65 s simulation time. The figure also includes the quasi-steady profile reached at 62s.

The Gillies (2006) and Rahman (2011) rheology augmentation models yield fairly different results. At 27.%v initial concentration, Rahman yield stress augmentation is approximately 50% higher than the Gillies model. However, as the bed approaches the coarse packing concentration, the Gillies relationship increases exponentially. As with the E10 Gillies case, a "gelled" bed type arrangement is formed.

[22] As with case E10, the closest point in the 2D model to the reference location is at 14.5 m. Little difference is expected between the profiles at 14.5 and 14.8m

Conversely, the Rahman model predicts a more gradual rheology augmentation up to the maximum packing concentration[23]. As a result, the coarse fraction is able to settle to a higher concentration using the Rahman model.

In this E7 case, the lower portion of the experimental data better aligns with the Rahman (2011) prediction, while the particle depleted shear region is closer aligned to the Gillies model. Neither appears to appropriately capture the settled bed behavior. However, both predictions are improvements over Spelay's 1D model prediction.

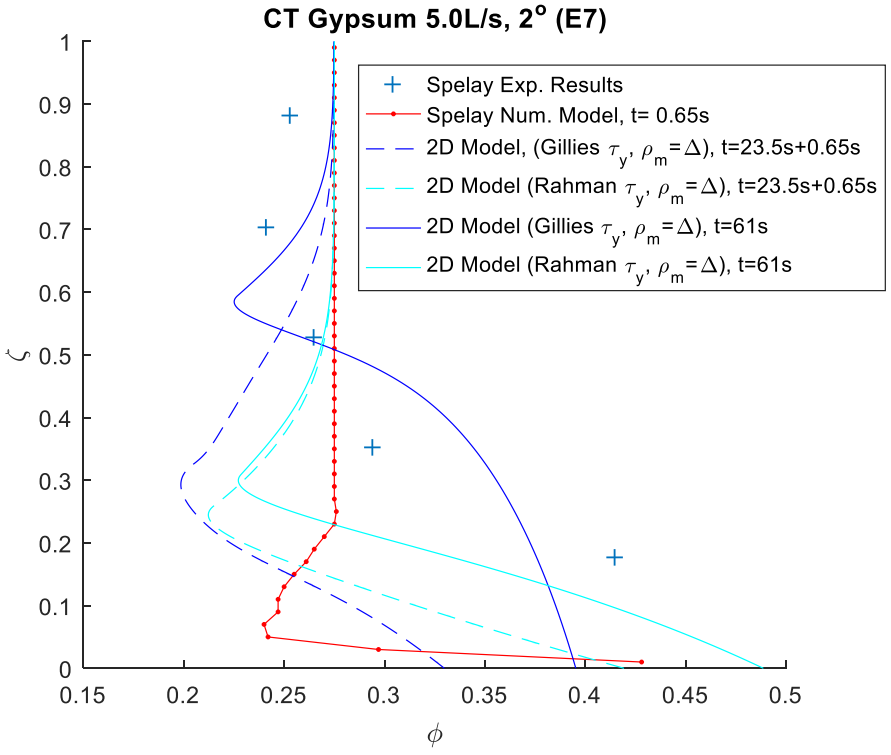

Figure 55: E7 Sand Concentration Profile Comparison to Spelay Experimental and Numerical Results, (x=14.5 m)

[23] Note that the Rahman model would still produce a gelled bed type coarse particle deposit.

6.3 Discussion of 2D Model Results

6.3.1 Shear Particle Depletion

Spelay (2007) argues that the flow of coarse particle laden slurries in laminar flow channels "never reaches a steady state as particles will continue to settle until the sheared region becomes completely depleted of particles" (p229). His simulations showing the long term evolution of the coarse sand concentration profile and resulting shear particle depletion for case E2 is presented in Figure 56 and in Figure 57 for case E7.

The 2D simulation results in this study indicate a quasi-steady state is reached eventually at a given point on the inclined slope, as indicated in the concentration profiles in Figure 40, Figure 44, Figure 54, and Figure 47. A quasi-steady state is reached because of the continual fresh material fed from upstream. Note that it is only a quasi-steady state because the coarse particles are still slowly settling through the viscoplastic fluid and the concentration profile will change slowly over a long duration of time. However, the majority of the settling appears to occur relatively quickly and the concentration profile reaches a quasi-steady state in the simulation times presented for each case. This is reinforced by the steady profiles measured in Spelay's (2007) experimental work. Because the upstream flow reaches a quasi-equilibrium, the coarse fraction is ultimately transported down the beach and the deposited bed of coarse solids grows along the slope.

From a Lagrangian viewpoint Spelay's (2007) model predictions are valid. If a snapshot of the flow profile is followed down the beach, the sheared-zone coarse solids concentration decreases as it moves down the beach due to the particle depletion within the sheared zone. This is seen in the contour plots in the sections above, particularly in Figure 53 and Figure 46 for the CT cases where only the coarse fraction in the unsheared plug remains at the end (toe) of the flow profile, and the sheared zone consists only of carrier fluid.

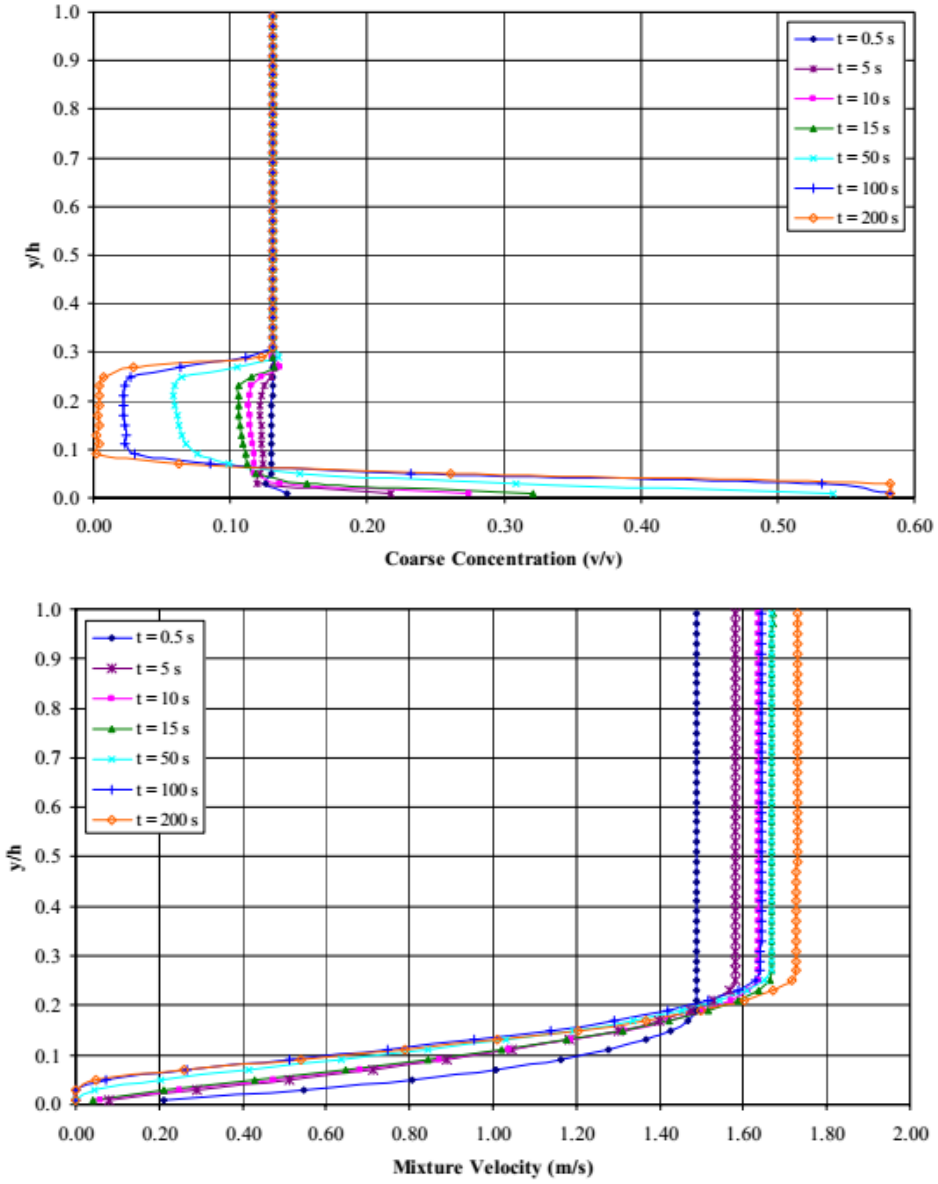

Figure 56: Spelay (2007)'s Figure 6.6 (p. 229) Indicating Long Term Depletion of particles in TT (E2) Flows

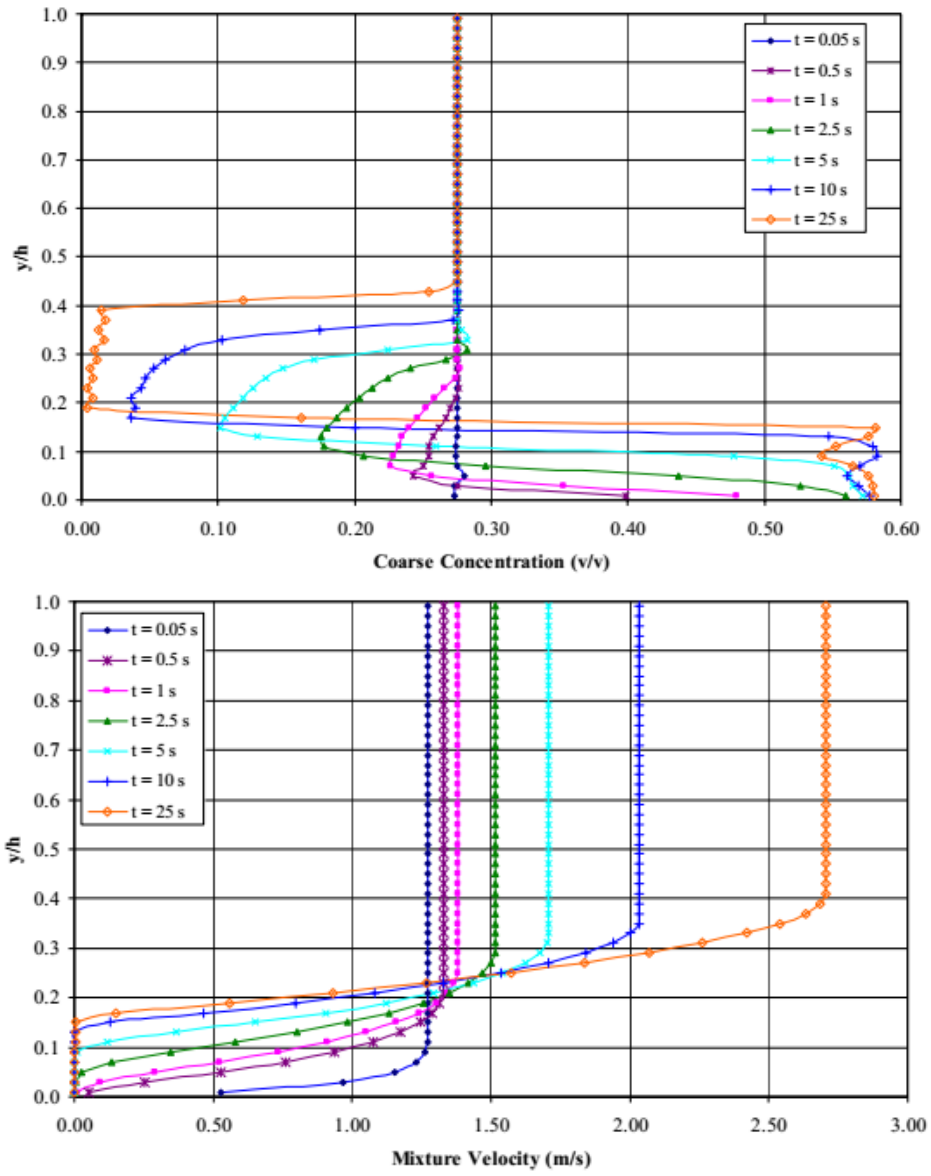

Figure 57: Spelay (2007)'s Figure 6.15 (p. 239) Indicating Long Term Depletion of particles in CT (E7) Flows

6.3.2 Unsheared Plug Transport

The phenomenon just described requires further evaluation. From a physical standpoint, it is not expected that an unsheared plug with a higher density will travel on top of the lower-density shear depleted layer for a long duration. The higher density layer would ultimately sink into the lower-density layer and likely destroy the unsheared plug. The 2D beach flow model developed in this study is not able to predict

this sinking behavior. The predicted concentration profiles in Section XX that are beyond the settled bed portion of the beach for the analysis cases may not be physically realistic.

Note however that Spelay (2007) did measure an usheared plug travelling overtop a shear depleted zone in his experimental test work. The test work was completed using a relatively short 18.5 m long flume with recirculating flow. Given the relatively small density difference between the unsheared plug and shear-depleted zone for the TT cases E2 and E5, the plug likely didn't have time to sink before reaching the end of the flume and being remixed and reintroduced into the start of the flume. The lack of a distinct unsheared plug in Case E7 and absence of a shear-depleted region in Case E10 may be the result of the plug sinking.

Along with the relative density difference between the unsheared plug and shear-depleted region, the cross sectional geometry of the channel or flume may play also a role in the transport of an unsheared plug. As with Spelay's (2007) semi-circular cross section flume, Pirouz et al. (2013) observed stable plug flow in naturally formed elliptical cross section tailings channels during large scale flume testing. The circular geometry and resulting sheared region along the bed perimeter may help confine the plug for a longer duration than would be expected in sheet flow.

An additional concept that requires future evaluation is whether the unsheared plug sinking causes overbanking along the flow channel. Charlebois et al. (2013) argued this is a key depositional mechanism for flocculated MFT slurries.

6.3.3 Potential Additional Comparison Cases

As noted in the chapter introduction little complete data is available to evaluate the 2D model against. The experimental data provided in Sanders et al. (2002) is a precursor to Spelay's (2007) work and would provide several additional experimental cases considering oil sand thickened tailings slurries at lower yield stresses[24]. Additional test campaigns with partial data are available in the literature that may also valuable to further evaluate the model in future studies.

[24] 12 Pa to 14 Pa yield stress, compared to Spelay's cases with 33 Pa to 47 Pa yield stress.

Pirouz et al. (2013) provides limited concentration profile data measured in laminar flow flume tests at the Chuquicamata mine in Chile. However, the polydisperse nature of the tailings makes predicting the settling of a single particle size, as in the case of the 2D model difficult to accomplish.

The large scale 5.5 m wide by 55 m long experimental flume investigation completed by van Kestern et al. (2015) using a homogeneous viscoplastic carrier fluid and mono-sized coarse particle provides key validation data for the 2D model measured under relatively steady laboratory conditions. However, most of the flume tests completed for that study resulted in channelized flow making it difficult to directly compare to the 2D sheet flow model results. The data is also still being analyzed and compiled at the time of writing this thesis.

Sittoni's (2015) 2D modelling of oil sand NST and Whole Tailings slurries provide settling concentration profiles utilizing a similar modelling approach. However, the results provide only a preliminary heuristic evaluation of the current Delft-3D tailings flow model. The 2D model in this study was not able to converge to a solution in trying to replicate Sittoni's (2015) results. Sittoni et al.'s more recent work (2016) provides a more complete comparison case. The Delft3D model predictions of 2D sheet flow behavior shows similar behavior to the shear settling in this study. The work was published just prior to this thesis and has therefore not been evaluated as part of this study. Future comparison of the two models is recommended.

In a different light, predicting the slump/dam break behavior of mixture with varying carrier fluid rheology and coarse solids content investigated by Dunn (2004) may be useful. Although the particles considered in that study are large (1.0 mm to 6.7 mm) and do not fall within the range considered for the rheology augmentation model development. Adaption of the 2D model boundary conditions would also be required to model the dam-break type behavior.

6.4 Engineering Implications

The results from the flow scenarios investigated in this chapter have several practical implications on tailings deposition planning and overall long term flow modelling:

6.4.1 Beach Slope Prediction

One of the key motivators for developing a tailings flow prediction model is to be able to better evaluate and improve the current tailings beach slope prediction models presented in Section 1.2.2. Beach slope prediction models that consider sheet flow have been shown to generally not be appropriate for predicting the overall deposited tailings profile (Charlebois et al. 2013; Simms et al. 2011). Consequently, no direct improvements or recommendations regarding beach slope prediction methods can be made from this currently study, outside of the potential impact the coarse particle settling has on the bulk flow velocity as discussed below. It is anticipated that developing a flow model that considers channelized flow will help validate the two widely used beach slope models (Fitton's and McPhail's models). Ultimately a full 3D tailings flow model will help investigate the interaction between flow fanning and channelization down the beach.

6.4.2 Flow Velocity Determination in Beach Slope Models

The beach slope prediction models discussed in Section 1.2.2 require the determination of the bulk flow velocity down the beach to predict the beach slope (Fitton and Slatter 2013) or overall beach profile (McPhail 2008). The bulk flow velocity down the beach is typically treated as constant in these models. Figure 58 plots the bulk flow velocity (Q/H for 2D flow) for the four cases considered[25] in this chapter. From this figure, particle settling within the flow either:

- Has little impact on the overall flow behavior (i.e. TT flow cases.) In these cases, assuming a constant bulk flow velocity is appropriate.
- Substantially alters the flow velocity profile as seen in Figure 47 and Figure 54, and ultimately causes a large decrease in bulk flow velocity across the deposited solids. In these cases, it is necessary to understand the settling behavior and its impact on the bulk flow velocity to

[25]The variable mixture density cases utilizing the Gillies (2006) rheology augmentation model at the final time step for each scenario are presented.

correctly predict the ultimate beach profile. Utilizing an approach similar to McPhail's initial (McPhail 1995) model that captures the down-beach settling is most appropriate.

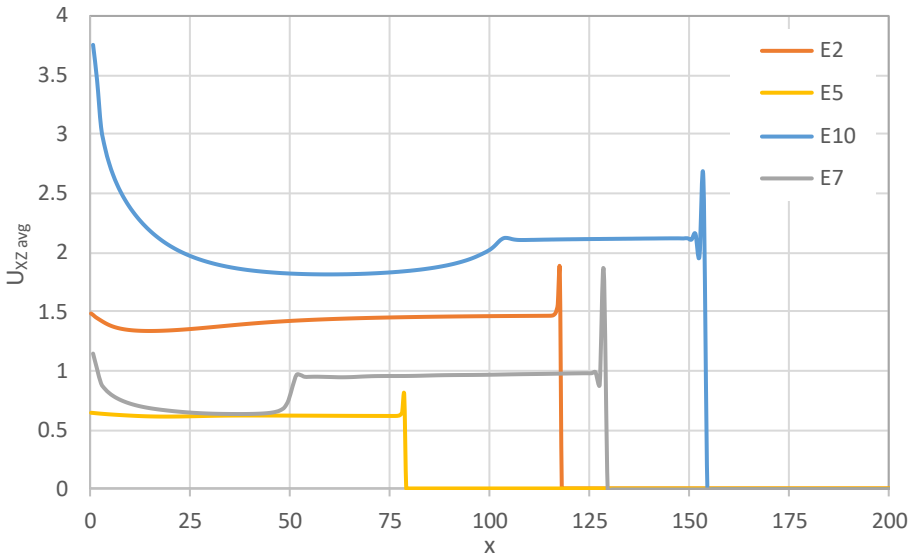

Figure 58: Bulk Flow Velocity (Q/H) Comparison

6.4.3 Design of Non-Segregating Tailings Deposition

Often one of the key objectives in tailings deposition planning, particularly in oil sand tailings operations (Talmon et al. 2014b), is to maintain a non-segregating mixture within the tailings containment facility. Utilizing the 2D model presented in this work would assist engineers evaluate the potential flow segregation and tailor the carrier fluid rheological properties, coarse sand concentration, discharge rate, and embankment slope to minimize (or maximize in some situations) the amount of segregation within the beach flow. Performing a numerical parametric study ahead of segregation testing helps optimize the test conditions ahead of final validation test work.

6.4.4 Predicting Long Duration Tailings Flows

Ultimately the 2D model provides a valuable tool for determining the particle settling behavior and resulting impact on the flow behavior within sheet flow down a tailings beach. The 2D model better predicts the coarse particle settling within the laminar Bingham plastic flows measured by Spelay (2007) than

Spelay's 1D depth only based model. The model also provides highly accurate velocity and concentration profiles through the flow depth.

However, the simulations presented in the above evaluation cases all have relatively short durations (25 to 120 seconds). The simulation required between several hours and several days to complete the iterative calculations. The majority of this calculation time was completing the settling calculations at each beach coordinate x location. The highly nonlinear and varying flux profiles presented in Figure 40, Figure 43, Figure 53 and Figure 47, require vary small element sizes (500 elements through the flow depth[26]), and small times steps ($1x10^{-4}$ to $1x10^{-5}$ s) to predict an appropriate solution using the upwind finite difference scheme. The large number of z elements in turn resulted in significantly larger calculation requirements for the x-wise advection and flow velocity profile determinations than necessary if settling is excluded.

Ultimately the E2 and E5 simulation cases approached the computation limits of a single Intel i7 quad core processor with 8 GB of RAM. In industrial applications tailings flows within a storage facility are continuously discharged to an area over days or months. To be able to model longer duration tailings flow simulations it would be necessary to:

- Improve the efficiency of the model subroutines and limit the number of iterations required at each x and z point. As an example, a method to solve a vectorized tri-diagonal system of equations in parallel along the beach is presented in Section 4.6.
- Develop averaging methods to reduce the z-wise computation requirements for the settling calculations. Averaging could potentially significantly reduce the computation requirements, but would result in a lower resolution model prediction. If accurately predicting the concentration profile evolution over time is critical in the modelling, this averaging may not be appropriate.

[26] Given the flow depths, this numerical requirement resulted in element sizes that were actually technically smaller than the particle diameter considered for the coarse sand fraction.

- Migrate the model to a more computationally efficient or compiled programming language. The 2D model utilizes Matlab version 9.0 (2016). Utilizing a lower level programming language would likely increase computation speed.
- Utilize high performance computing with parallel processors to increase both computation speed and system memory available for the calculations.

6.5 Chapter Summary

This chapter presents the results of the 2D model simulations considering two thickened tailings (TT) and two composite tailings (CT) slurry cases from Spelay's (2007) experimental work.

Considering the thickened tailings (TT) cases, the predicted concentration profile for the E2 case agrees quite well with the experimental data. The model under predicts the accumulated solids depth in the settled bed for the E5 case.

Utilizing a variable density with depth within the shallow water flow solver yields improved concentration profile predictions. However, the differences between the constant mixture density and variable density predictions are not significant. The Gillies (2006) and Rahman (2011) rheology augmentation models produced fairly similar results for the TT cases. The models don't differ significantly at the TT coarse solids concentration range (11 to 13%v). The Gillies model tended to better agree with the experimental data.

For the CT cases, the Gillies (2006) and Rahman (2011) rheology augmentation models predicted fairly different concentration profiles through the flow depth. This is due to the higher coarse sand volume concentration considered for the CT cases (E7 and E10). Neither model appropriately captured the experimental concentration profile. The steeper Gillies model resulted in a lower settled bed concentration similar to a "gelled bed" type deposit of Talmon (2004). The shallower Rahman rheology augmentation model predicted a higher concentration but much lower deposited bed. Additional particle-particle interactions may be occurring as the coarse particle fraction approaches the maximum bed packing

concentration. This inter-particle interaction is not solely accounted for in the rheology augmentation model.

The overall concentration predictions are in better agreement with the experimental data than Spelay's (2007) initial 1D model predictions. The 2D model is better able to predict the settling, accumulation of coarse solids, and resulting flow depth increase along the inclined slope than Spelay's 1D settling model, which requires a fixed flow height. The 2D model has the distinct advantage of predicting both the z-wise particle settling and the x-wise particle transport.

All of the simulations ultimately reached a quasi-steady state where the concentration and velocity profiles at a given location do not change significantly with time. This is in agreement with Spelay's (2007) measurement of steady experimental concentration profiles at the 14.8 m location within the test flume. However, steady conditions are not observed down the length of the slope. Coarse particles are continually accumulated along the bed slope due to the coarse particle depletion within the sheared zone.

Through this comparison with the experimental laminar settling tests work, the 2D model is shown to be a useful tool in predicting the coarse particle concentrations and flow velocity profiles along the slope. A deposit length of up to approximately 100 m, depending on flow velocity, and simulation times up to 120 s were obtained in this evaluation. However, the 2D model is not able to capture any unsheared plug sinking due to the density differential between the unsheared plug and shear depletion zone. To be able to model long term and larger scale 3D beach flows, it is expected that this phenomenon requires further investigation and likely incorporation into the model. Additionally, some averaging will likely be required to reduce the computational requirements for the model.

CHAPTER 7:
SUMMARY AND CONCLUSIONS

The primary focus of this study was to develop a two dimensional free surface beach flow model. This two dimensional model serves as a building block in ultimately advancing the model to a full three dimensional model. A 3D model is ultimately necessary to capture the complex interactions that occur within the tailings beach flows. The 2D model developed for this study is able to capture the free surface viscoplastic carrier fluid flow behavior along with coarse particle transport and settling behavior within the flow in two dimensional laminar sheet flow. By developing a standalone model, the implementation could focus on coupling the particle transport and flow interaction through rheology augmentation without having to adapt a less suitable, but existing model.

As part of the study, the individual flow, transport and settling model components have been validated to ensure proper behavior. Two key novel advancements were made through this development. The first is the coupling of the rheology augmentation and hindered settling behavior as discussed in Section 5.4.3. This coupling enables the coarse particle influence on both the flow behavior and settling behavior to be modelled together as a continuous process. The key development in this coupling was utilizing the suspension viscosity coupling into the hindered settling model discussed in Blazejewski (2012). Adapting this approach, the apparent viscosity, which included both the shear thinning effect from the shallow water flow model and the rheology augmentation effect, was incorporated into the hindered settling model.

A second novel development was the proposed method for expanding the rheology augmentation and hindered settling coupling to particle flows beyond the Stoke's flow regime. The second method proposed in Section 5.4.6, where the suspension viscosity is included in the drag coefficient, and the concentration effect is only included in the hindered settling calculation, appeared to work well for large particles in Newtonian flows. Further investigation into this proposed method is warranted.

One additional finding to note in the initial component development was the Courant number dependence of the cubic hermite interpolation scheme used for the x-wise particle advection. It is believed

that the numerical implementation of the interpolation scheme in the *pchip()* function in Matlab may be the source of this Courant number dependence. Developing a standalone interpolation function, or investigating alternate implementations, may help clarify the dependence.

Ultimately the model is able to fairly accurately predict the coarse particle settling within the laminar viscoplastic flow for the Thickened Tailings (TT) and Composite Tailings (CT) slurries investigated. The TT tailings had a fairly large unsheared plug flow with little settling within the sheared flow. The CT tailings have significant coarse sand settling within the sheared flow and accumulation on the bed slope.

Both the Gillies (2006) and Rahman (2011) rheology augmentation models predicted the concentration profile within the TT flows fairly well. This was due to the relatively initial low coarse particle concentration within the slurry. For the CT flows, the Gillies model unpredicted the coarse particle packing concentration, while the Rahman model under predicted the deposited bed depth, but better agreed with the maximum settled solids concentration. Additional particle-particle interactions are likely occurring in the CT flows that are not entirely predicted by the rheology augmentation phenomenon.

This work serves as a key development step in more accurately predicting free surface tailings beach flows. The individual model components have been validated to accurately predict the settling and particle advection behavior. They serve a building blocks for any future expansion of the model to accommodate long duration, 3D beach flows. The computational requirements for the currently-implemented numerical settling model will likely require adaptation to be able to efficiently predict the coarse particle settling within larger 3D and longer duration models.

The 2D model accurately predicts the coarse particle settling within 2D sheet flow conditions and serves as a useful tool to better understand the impact coarse particle rheology augmentation has on the settling of particles within viscoplastic sheet flows.

CHAPTER 8:
FUTURE WORK

Multiple areas within this study, and within understanding tailings beach flow behavior require further investigation. In direct relation to this study, and in order from most significant impact to least:

(i) Adapting the model to evaluate channelized flow behavior rather than sheet flow behavior. Tailings are primarily transported via channelized flow within the tailings deposit. The two most common beach slope prediction models assume the tailings beach slope is determined within this channelized flow region. Developing a model to predict the transport and settling within this regime would help verify the assumptions made in the development of these beach slope models.

(ii) Incorporating turbulent flow behavior and additional turbulent influences on particle migration into the model. In many cases, thickened tailings are discharged into the tailing storage facility at relatively low solids concentration with relatively low carrier fluid density and rheological behavior. While the carrier fluid is still viscoplastic, the flow down the beach is turbulent. The resulting turbulent eddy effects prevent particle settling and result in total tailings transport. Understanding the conditions under which no coarse particle settling is observed would help engineers develop deposition strategies to ensure relatively homogeneous tailings placement throughout the tailings storage facility.

(iii) Conducting experimental validation test work considering a range of viscoplastic carrier fluids and coarse particle fractions under laminar, wide channel flow to mimic the sheet flow conditions of the 2D model.

(iv) Incorporating and evaluating the non-Newtonian particle settling behavior. Particle settling within a viscoplastic fluid is complicated by development of unyielded regions around particles, as well as particle clustering. Better capturing this behavior may result in improved

particle settling behavior prediction. However, the influence this has on the overall tailings flow and deposition prediction is expected to be small.

The overall goal in tailings beach flow modelling is the development of a full 3D tailings beach flow model that can efficiently accommodate large spatial distances, but still capture the key particle transport and settling phenomena. The next development step for this modelling is to expand the model to include lateral flow and particle transport. Of particular interest to expand this study to 3D flows:

(i) Investigate the mechanisms that result in transition to channelized flow from initial sheet flow. As discussed in Section 2.6, it is believed that tailings deposition and accumulation within the tailings storage facility, and the ultimate beach slope profile is an interplay between flow fanning and channelization down the beach. The degree to which particle settling and rheology augmentation causes material build up on the lateral extents of the fan profile and the eventual channelization through the fan is not well understood.

(ii) Evaluating deposition strategies to optimize the tailings storage facility capacity by determining discharge spigot sizing and spacing that provides the most suitable beach profile within the deposit given the planned deposit geometry. There is currently very little understanding of the influence discharge rate and spacing between discharges has on the beach profile; parametric modelling would help optimize deposition planning.

REFERENCES

Acrivos, A., Mauri, R., and Fan, X. (1993). "Shear-induced resuspension in a couette device." *International Journal of Multiphase Flow*, 19(5), 797–802.

Ancey, C., and Jorrot, H. H. (2001). "Yield stress for particle suspensions within a clay dispersion." *Journal of Rheology*, 45(April), 297–319.

Bagnold, R. a. (1954). "Experiments on a gravity-free dispersion of large solid spheres in a newtonian fluid under shear." *Proceedings of the Royal Society A: Mathematical, Physical and Engineering Sciences*, 225(1160), 49–63.

Balmforth, N. J., Craster, R. V., Rust, A. C., and Sassi, R. (2006). "Viscoplastic flow over an inclined surface." *Journal of Non-Newtonian Fluid Mechanics*, 139, 103–127.

Balmforth, N. J., Craster, R. V., and Sassi, R. (2002). "Shallow viscoplastic flow on an inclined plane." *Journal of Fluid Mechanics*, 470, 1–29.

Barnes, H. A. (1999). "The yield stress — a review or ' panta roi '— everything flows?" *Journal of Non-Newtonian Fluid Mech*, 81(May 1998), 133–178.

Beaulne, M., and Mitsoulis, E. (1997). "Creeping motion of a sphere in tubes filled with Herschel – Bulkley fluids." *Journal of Non-Newtonian Fluid Mechanics*, 72, 55–71.

Beris, B. A. N., Tsamopoulos, J. A., Armstrong, R. C., and Brown, A. N. D. R. A. (1985). "Creeping motion of a sphere through a Bingham plastic." *Journal of Fluid Mechanics*, 158, 219–244.

Blackery, J., and Mitsoulis, E. (1997). "Creeping motion of a sphere in tubes filled with a Bingham plastic material." *Journal of Non-Newtonian Fluid Mechanics*, 70, 59–77.

Blazejewski, R. (2012). "Apparent viscosity and settling velocity of suspensions of rigid monosized spheres in Stokes flow." *International Journal of Multiphase Flow*, Elsevier Ltd, 39, 179–185.

Blight, G. (2009). *Geotechnical Engineering for Mine Waste Storage Facilities*. CRC Press.

Blight, G., Thomson, RR, and Vorster, K. (1985). "Profiles of hydraulic-fill tailings beaches, and seepage through hydraulically sorted tailings." *Journal of the South African Institute of Mining and Metallurgy*, 85(5), 157–161.

Boger, Hart, B. C. (2008). "Making and unsustainable industry more sustainable." *Proceeings of the 11th International Seminar on Paste and Thickened Tailings*, A. Fourie, A; Jewell, R; Slatter, P; Paterson, ed., Australian Center for Geomechanics, Perth, 3–13.

Brouwers, H. J. H. (2010). "Viscosity of a concentrated suspension of rigid monosized particles." *Physical Review E - Statistical, Nonlinear, and Soft Matter Physics*, 81(5), 1–11.

Bürger, R., Diehl, S., Faras, S., Nopens, I., and Torfs, E. (2013). "A consistent modelling method for secondary settling tanks: A reliable numerical method." *Water Science and Technology2*, 68(1), 192–208.

Chanson, H. (2004). *The Hydraulics of Open Channel Flow: An Introduction*. Elsevier.

Chapra, S., and Canale, R. (2002). *Numerical Methods for Engineers*. McGraw-Hill, New York City.

Charlebois, L. E., Mcphail, G. I., Revington, A., and van Zyl, D. (2013). "Observations of tailings flow and application of the McPhail beach profile model to oil sands and metal mine tailings." *Proceedings of the Seventeenth International Conference on Tailings and Mine Waste*, University of Alberta Geotechnical Center, Edmonton, Canada, 169–180.

Chen, H. X., and Zhang, L. M. (2015). "EDDA 1.0: Integrated simulation of debris flow erosion, deposition and property changes." *Geoscientific Model Development*, 8(3), 829–844.

Chen, S.-C., Peng, S.-H., and Capart, H. (2007). "Two-layer shallow water computation of mud flow intrusions into quiescent water." *Journal of Hydraulic Research*, 45(1), 13–25.

Cheng, N. S. (2009). "Comparison of formulas for drag coefficient and settling velocity of spherical particles." *Powder Technology*, Elsevier B.V., 189(3), 395–398.

Chhabra, R. P. (2006). *Bubbles, Drops, and Particles in Non-Newtonian Fluids*. CRC Press.

Corp. of Engineers, U. A. (2016). "HEC-RAS." <http://www.hec.usace.army.mil/software/hec-ras/> (Jan. 3, 2017).

Coussot, P., and Proust, S. (1996). “Slow, unconfined spreading of a mudflow.” *Journal of Geophysical Research*, 101(B11), 25217–25229.
Deltares. (2016). “Delft-3D.” <https://oss.deltares.nl/web/delft3d> (Jan. 3, 2017).
DHI. (2016). “Mike.” <http://www.mikepoweredbydhi.com/> (Jan. 3, 2017).
Diehl, S., Farås, S., and Mauritsson, G. (2015). “Fast reliable simulations of secondary settling tanks in wastewater treatment with semi-implicit time discretization.” *Computers and Mathematics with Applications*, Elsevier Ltd, 70(4), 459–477.
Dunn, F. (2004). “A study of the relationship between various slurry material characteristics and the flow behavior of co-deposited kimerlite tailings upon deposition.” University of Witwaterstrand.
Einstein, A. (1906). “Eine neue bestimmung der molekul-dimensionen.” *Annalen dr Physik*, 19, 289–306.
Fitton, T. G. (2007). “Tailings Beach Slope Prediction.” RMIT.
Fitton, T. G., Bhattacharya, S. N., and Chryss, A. G. (2007). “Three-dimensional modeling of tailings beach shape.” *Computer-Aided Civil and Infrastructure Engineering*, 23(1), 31–44.
Fitton, T. G., Chryss, A. G., and Bhattacharya, S. N. (2006). “Tailings beach slope prediction: A new rheological method.” *International Journal of Mining, Reclamation and Environment*, 20(3), 181–202.
Fitton, T. G., and Slatter, P. (2013). “A tailings beach slope model featuring plug flow.” *Proceedings of the 16th International Seminar on Paste and Thickened Tailings*, R. J. Jewell, A. Fourie, J. Caldwell, and J. Pimenta, eds., Australian Center for Geomechanics, Perth, Australia, 493–503.
“Flo-2D Pro.” (2016). Flo-2D Software Inc, Nutrioso, AZ.
Fourie, A. (2012). “Paste and thickened tailings: has the promise been fulfilled?” *GeoCongress 2012: State of the Art and Practice in Geotechnical Engineering*, R. D. Hryciw, A. Athanasopoulos-Zekkos, and N. Yesiller, eds., ASCE, Oakland, California, 4126–4135.
Fritsch, F. N., and Carlson, R. E. (1980). “Monotone picewise cubic interpolation.” *Journal on Numerical Analysis*, 17(2), 238–246.
Garside, J., and Al-Dibouni, M. R. (1977). “Velocity-voidage relationships for fluidization and sedimentation in solid-liquid systems.” *Industrial & Engineering Chemistry Process Design and Development*, 16(2), 206–214.
Gillies, R. G., and Shook, C. A. (2000). “Modelling high concentration settling slurries.” *The Canadian Journal of Chemical Engineering*, 78, 709–716.
Gumulya, M. (2009). “The Settling of Spheres in Viscoplastic Fluids.” Curtin University of Technology.
Gumulya, M. M., Horsley, R. R., and Wilson, K. C. (2007). “The settling of consecutive spheres in viscoplastic fluids.” *International Journal of Mineral Processing*, 82(2), 106–115.
Hanssen, J. L. J. (2016). “Towards improving predictions of non-Newtonian settling slurries with Delft3D : theoretical development and validation in 1DV towards improving predictions of non-Newtonian settling slurries with Delft3D : theoretical development and validation in 1DV.” Delft University of Technology.
Henriquez, J., and Simms, P. (2009). “Dynamic imaging and modelling of multilayer deposition of gold paste tailings.” *Minerals Engineering*, Elsevier Ltd, 22(2), 128–139.
Hernando, L., Omari, A., and Reungoat, D. (2014). “Experimental study of sedimentation of concentrated mono-disperse suspensions : Determination of sedimentation modes.” *Powder Technology*, Elsevier B.V., 258, 265–271.
Highgate, D. J., and Whorlow, R. W. (1970). “Rheological properties of suspensions of spheres in non-Newtonian media.” *Rheologica Acta*, 9(4), 569–576.
Holly, F. M., and Preissmann, A. (1977). “Accurate calculation of transport in two dimensions.” *Journal of the Hydraulics Division*, 103(HY11), 1259–1277.
Holly, F. M., and Usseglio-Polatera, J. (1984). “Dispersion simulation in two-dimensional tidal flow.” *Journal of Hydraulic Engineering*, 110(7), 905–926.
Hooke, R. (2005). *Principles of Glacier Mechanics*. Cambridge University Press, Cambridge.
Imran, J., Harff, P., and Parker, G. (2001). “A numerical model of submarine debris flow with graphical user interface.” *Computers and Geosciences*, 27, 717–729.

Johnson, A. M. (1970). *Phyiscal Processes in Geology: A Method for Interpretation of Natural Phenomena; Intrusions in Igneous Rocks, Fractures, and Folds, Flow of Debris and Ice*. Freeman, Cooper & Company, San Francisco.

Julien, P. Y., and Lan, Y. (1991). "Rheology of hyperconcentrations." *Journal of Hydraulic Engineering*, 117(3), 346–353.

Julien, P. Y., and León, C. S. (2000). "Mud floods, mudflows and debris flows classification, rheology and structural design." *Proceedings of International Workshop on the Debris Flow Disaster*, Caracas, Venezuela.

Kesteren, W. Van, Ree, T. Van De, Talmon, A., De, M., Pardo, L., Luger, D., and Sittoni, L. (2015). "A large-scale experimental study of high density slurries depositon on beaches." *Proceedings of the 17th International Conference on Transport and Sedimentation of Solid Particles*, J. Sobota and C. van Rhee, eds., Wroclaw University of Environmental and Life Sciences, Wroclaw, Poland, 147–154.

Kranenburg, C. (1992). *Hindered Settling and Consolidation of Mud - Analytical Results*. Delft, Netherlands.

Krieger, I. M. (1972). "Rheology of monodisperse latices." *Advances in Colloid and Interface Science*, 3(2), 111–136.

Krieger, I. M., and Dougherty, T. J. (1959). "A mechanism for non-Newtonian flow in suspensions of rigid spheres." *Transactions of the Society of Rheology*, 3(1), 137–152.

Kupper, A. (1991). "Design of Hydraulic Fill." University of Albera.

Kynch, G. J. (1952). "A theory of sedimentation." *Transactions of the Faraday Society*, 48, 166–176.

Kynch, G. J. (1959). "Sedimentation and effective viscosity." *Nature*, 184(4695), 1311.

Landel, R. F., Moser, B. G., and Bauman, A. J. (1963). "Rheology of concentrated suspensions - effect of a surfactant." *Proceedings of the 4th International Congress on Rheology II*, Brown University, 663–692.

Leighton, D., and Acrivos, A. (1985). "The lift on a small sphere touching a plane in the presence of a simple shear flow." *Journal of Applied Mathematics and Physics*, 36(1), 174–178.

Leighton, D., and Acrivos, A. (1986). "Viscous resuspension." *Chemical Engineering Science*, 41(6), 1377–1384.

Leighton, D., and Acrivos, A. (1987a). "The shear-induced migration of particles in concentrated suspensions." *Journal of Fluid Mechanics*, 181, 415–439.

Leighton, D., and Acrivos, A. (1987b). "Measurement of shear-induced self-diffusion in concentrated suspensions of spheres." *Journal of Fluid Mechanics*, 177, 109–191.

Li, A. (2011). "Prediction of tailings beach slopes and tailings flow profiles." *Proceedings of the 14th International Seminar on Paste and Thickened Tailings*, R. Jewell and A. Fourie, eds., Australian Center for Geomechanics, Perth, Australia, 307–322.

Liu, K. F., and Mei, C. C. (1990). "Approximate equations for the slow spreading of a thin sheet of Bingham plastic fluid." *Physics of Fluids A: Fluid Dynamics*, 2(1), 30–36.

McPhail, G. (1995). "Prediction of the Beaching Characteristics of Hydraulically Placed Tailings." University of the Witwatersrand , Johannesburg.

McPhail, G. (2008). "Prediction of the beach profile of high-density thickened tailings from rheological and small-scale trial deposition data." *Proceedings of the 11th International Seminar on Paste and Thickened Talings*, A. Fourie, R. J. Jewell, P. A, and P. Slatter, eds., Austrailian Center for Geomechanics, Perth, Australia, 179–188.

Mizani, S., Simms, P., and He, L. (2010). "'Out of pipe' dewatering of thickened tailings during deposition." *Proceedings of the 13th International Seminar on Paste and Thickened Tailings*, R. J. Jewell and A. Fourie, eds., Australian Center for Geomechanics, Perth, Australia, 393–402.

Morris, P. H., and Williams, D. J. (1997). "Hydraulic conditions leading to exponential mine tailings delta profiles." *Transactions of the Institution of Mining and Metallurgy, Section A - Mining Industry*, 107, A34–A37.

O'Brien, J. (1986). "Physical Processes, Rheology and Modeling of Mud Flows." Colorado State University.

O'Brien, J., and Julien, P. Y. (1988). "Laboratory analysis of mudflow properties." *Journal of Hydraulic Engineering*, 114(9), 877–887.

O'Brien, J., Julien, P. Y., and Fullerton, W. (1993). "Two dimensional water flood and mudflow simulation." *Journal of Hydraulic Engineering*, 119(2), 224–261.

Oliver, D. (1960). "Sedimentation and effective viscosity." *Nature*, 185(4714), 912–913.

Ovarlez, G., Bertrand, F., Coussot, P., and Chateau, X. (2012). "Shear-induced sedimentation in yield stress fluids." *Journal of Non-Newtonian Fluid Mechanics*, Elsevier B.V., 177–178, 19–28.

Pane, V. (1985). "Sedimentation and Consolidation of Clays." University of Colorado.

Paulsen, E. (2007). "Investigating the Effect of Coarse Particle Addition on the Rheology of Fine Clay Slurries." University of Stellenbosch.

Phillips, R. J., Armstrong, R. C., Brown, R. a., Graham, A. L., and Abbott, J. R. (1992). "A constitutive equation for concentrated suspensions that accounts for shear-induced particle migration." *Physics of Fluids A: Fluid Dynamics*, 4(1), 30–40.

Pierson, T. . (2005). "Hyperconcentrated flow - transitional process between water flow and debris flow." *Debris-flow Hazards and Related Phenomena*, J. M and H. O, eds., Springer-Verlag Berlin Heidelberg, 159–202.

Pinheiro, M., Sobkowicz, J., Boswell, J., and Wells, S. (2012). "Modelling of the deposition profile of in-line flocculated mature fine tailings in beach cells." *Geo-Manitoba 2012*, Winnipeg, Canada.

Pirouz, B., Javadi, S., Seddon, K., and Williams, M. P. A. (2014). "Modified beach slope prediction model for non-segregating thickened tailings." *Proceedings of the 17th International Seminar on Paste and Thickened Tailings*, R. J. Jewell, A. Fourie, P. S. Wells, and D. van Zyl, eds., Australian Center for Geomechanics, Perth, Australia, 31–45.

Pirouz, B., Seddon, K., Pavissich, C., Williams, P., and Echevarria, J. (2013). "Flow through tile flume testing for beach flope evaluation at Chuquicamata Mine Codelco, Chile." *Proceedings of the 16th International Seminar on Paste and Thickened Tailings*, R. J. Jewell, J. Caldwell, A. Fourie, and J. Pimenta, eds., Australian Center for Geomechanics, Perth, Australia, 457–472.

Pirouz, B., and Williams, M. P. A. (2007). "Prediction of non-segregating thickened tailings beach slope – a new method." *Proceedings of the 10th International Seminar on Paste and Thickened Tailings*, A. Fourie and R. J. Jewell, eds., Australian Center for Geomechanics, Perth, Australia, 315–327.

Rahman, H. (2011). "Yield Stresses of Mixtures with Bimodal Size Distributions." University of Alberta.

Rajaram, H. (2015). "CVEN 5537 Numerical methods in civil engineering." University of Colorado.

Richardson, J. F., and Zaki, W. N. (1954a). "Sedimentation and fluidisation: Part I." *Transaction of the Institute of Chemical Engineers*, Institution of Chemical Engineers, 32, 35–53.

Richardson, J. F., and Zaki, W. N. (1954b). "The sedimentation of a suspension of uniform spheres under conditions of viscous flow." *Chemical Engineering Science*, 3(2), 65–73.

Robinsky, E. I. (1975). "Thickened discharge - A new approach to tailings disposal." *Canadian Institute of Mining and Metallurgy Bulletin*, 75–92.

Robinson, C. D. (1926). "Some factors influencing sedimentation." *Industrial & Engineering Chemistry*, 18(8), 869–871.

Rudman, M., Blackburn, H. M., Graham, L. J. W., and Pullum, L. (2004). "Turbulent pipe flow of shear-thinning fluids." *Journal of Non-Newtonian Fluid Mechanics*, 118(1), 33–48.

Sanders, R. S., Schaan, J., Gillies, R. G., and Schook, C. A. (2002). "Solids transport in laminar, open-channel flow of non-Newtonian slurries." *Proceedings of the 15th International Conference on Hydrotransport*, N. Heywood, ed., BHR Group, Cranfield, UK, 597–611.

Sanders, R. S., Schaan, J., Hughes, R., and Shook, C. A. (2004). "Performance of sand slurry pipelines in the oil sands industry." *The Canadian Journal of Chemical Engineering*, 82, 850–857.

Schaan, J., Sumner, R., Gillies, R. G., and Shook, C. (2000). "The effect of particle shape on pipeline friction for newtonian slurries of fine particles." *Canadian Journal of Chemical Engineering*, 78, 717–725.

Schaflinger, U., Acrivos, A., and Zhang, K. (1990). "Viscous resuspension of a sediment within a laminar and stratified flow." *International Journal of Multiphase Flow*, 16(4), 567–578.

Sheets, B., Wagner, T., Swenson, J., Horton, J., Langseth, J., and Sittoni, L. (2014). "Muddy river deltas as analogues for oil sand tailings beaches: Improving fines capture and operational efficiency with tailings beach modeling." *Proceedings of the 4th International Oil Sands Tailings ConferenceInternational*, D. Sego, W. Wilson, and N. Beier, eds., University of Alberta Dept. of Civil & Envionmental Engineering, Edmonton, Canada, 397–405.

Simms, P. (2007). "On the relation between laboratory flume tests and deposition angles of high density tailings." *Proceedings of the 10th International Seminar on Paste and Thickened Tailings*, A. Fourie and R. J. Jewell, eds., Australian Center for Geomechanics, Perth, Australia, 329–335.

Simms, P., Williams, M. P. A., Fitton, T. G., and Mcphail, G. (2011). "Beaching angles and evolution of stack geometry for thickened tailings — a review." *Proceedings of the 14th International Seminar on Paste and Thickened Tailings*, R. J. Jewell and A. Fourie, eds., Australian Center for Geomechanics, Perth, Australia, 323–338.

Singh, A., Nir, A., and Semiat, R. (2006). "Free-surface flow of concentrated suspensions." *International Journal of Multiphase Flow*, 32(7), 775–790.

Sisson, R., Lacoste-bouchet, P., Vera, M., Costello, M., Hedblom, E., Sheets, B., Nesler, D., Solseng, P., Fandrey, A., van Kesteren, W. G. M., Talmon, A. M., and Sittoni, L. (2012). "An analytical model for tailings deposition developed from pilot scale testing." *Proceedings of the Third International Oil Sands Tailings Conference*, D. Sego, W. Wilson, and B. N, eds., University of Alberta Dept of Civil & Envionmental Engineering, Edmonton, Canada, 53–63.

Sittoni, L., Talmon, A., Kester, J. Van, and Uittenbogaard, R. (2015). "Latest numerical developments for the prediction of beaching flow and segregation behavior of thick non-Newtonian mixtures." *Proceedings of the 17th International Conference on Transport and Sedimentation of Solid Particles*, J. Sobota and C. van Rhee, eds., Wroclaw University of Environmental and Life Sciences, Wroclaw, Poland, 309–316.

Sittoni, L., Talmon, A. M., JLJ, H., van Es, H., van Kester, J. A., Uittenbogaard, R. E., Winterwerp, J. C., and C., van R. (2016). "Optimizing tailings deposition to maximize fines capture: Latest advance in predive modeling tools." *Proceedings of the 5th International Oil Sands Tailings Conference*, D. Sego, G. W. Wilson, and N. A. Beier, eds., University of Alberta Dept. of Civil & Envionmental Engineering, Edmonton, Canada, 32–39.

Spelay, R. B. (2007). "Solids Transport in Laminar, Open Channel Flow of Non-Newtonian Slurries." University of Saskatchewan.

Spelay, R. B., Gillies, R. G., and Sanders, R. S. (2014). *An SRC multi-client project: Evolution of the SRC pipeflow model and a new approach to modelling laminar, non-Newtonian flows (Confidential Report #12849-1C14)*. Saskatoon.

Steinour, H. H. (1944). "Rate of sedimentation, nonflocculated suspensions of uniform spheres." *Industrial & Engineering Chemistry*, 36(7), 618–624.

Stowe, J., Farrell, I., Treinen, J., and Cooke, R. (2014). "Method for measuring rheology at low shear rates." *Proceedings of the 19th International Conference on Hydrotransport*, S. Sanders and S. Sumner, eds., BHR Group, Cranfield, UK, 69–77.

Swenson, J. B., Sheets, B., Kolstad, D., and Kesteren, W. Van. (2014). "Semi-analytical modeling of thickened tailings flows." *Proceedings of the 4th International Oil Sands Tailings Conference*, D. Sego, W. Wilson, and N. Beier, eds., University of Alberta Dept. of Civil & Envionmental Engineering, Edmonton, Canada, 415–423.

Tabuteau, H., Coussot, P., and de Bruyn, J. R. (2007). "Drag force on a sphere in steady motion through a yield-stress fluid." *Journal of Rheology*, 51(1), 125.

Takahashi, T. (2007). *Debris Flow*. Taylor & Francis, London.

Talmon, A., Hanssen, J. L. J., Winterwerp, J., Sittoni, L., and Van, C. (2016). "Implementation of tailings rheology in a predictive open-channel beaching model." *Proceedings of the 19th International Seminar on Paste and Thickened Tailings*, S. Barrera and R. J. Jewell, eds., Australian Center for Geomechanics, Perth, Australia.

Talmon, A. M., and Huisman, M. (2005). "Fall velocity of particles in shear flow of drilling fluids."

Tunnelling and Underground Space Technology, 20(2), 193–201.

Talmon, A. M., van Kesteren, W. G. M., Mastbergen, D. R., Pennekamp, J. G. S., and Sheets, B. (2014a). "Calculation methodology for segregation of solids in non-Newtonian carrier fluids." *Proceedings of the 17th International Seminar on Paste and Thickened Tailings2*, R. J. Jewell, A. Fourie, P. S. Wells, and D. van Zyl, eds., Australian Center for Geomechanics, Perth, Australia, 139–154.

Talmon, A. M., Kesteren, W. G. M. Van, Sittoni, L., and Hedblom, E. P. (2014b). "Shear cell tests for quantification of tailings segregation." *The Canadian Journal of Chemical Engineering*, 92(2), 362–373.

Talmon, A. M., and Mastbergen, D. R. (2004). "Solids transport by drilling fluids: concentrated bentonite-sand-slurries." *Proceedings of the 12th International Conference on Tansport and Sedimentation of Solid Particles*, Prague, Czech Republic, 641–649.

Thomas, A. D. (1999). "The influence of coarse particles on the rheology of fine particle slurries." *Proceedings of Rheology in the Mineral Industry II*, Engineering Foundation Conferences, Kahuku, Hawaii.

Thomas, A., and Fitton, T. G. (2011). "Analysis of tailings beach slopes based on slurry pipeline experience." *Proceedings of the 14th International Seminar on Paste and Thickened Tailings*, R. J. Jewell and A. Fourie, eds., Australian Center for Geomechanics, Perth, Australia, 295–306.

Thomas, D. G. (1965). "Transport characteristics of suspension: VIII. A note on the viscosity of Newtonian suspensions of uniform spherical particles." *Journal of Colloid Science*, 20(3), 267–277.

Treinen, J., Cooke, R., and Znidarčić, D. (2014). "A discussion of the critical drivers for tailings beach flows." *Proceedings of the 17th International Seminar on Paste and Thickened Tailings*, R. J. Jewell, A. Fourie, P. S. Wells, and D. van Zyl, eds., Australian Center for Geomechanics, Perth, Australia, 19–30.

Treinen, J., and Jacobs, J. (2015). "The applicability of the Eulerian-Eulerian CFD approach using granular kinetic theory to predict particle settling and migration in viscoplastic fluids." *Proceedings of the 17th International Conference on Transport and Sedimentation of Solid Particles*, J. Sobota and C. van Rhee, eds., Wroclaw University of Environmental and Life Sciences, Wroclaw, Poland, 345–354.

Treinen, J., and Jewell, R. J. (2015). "Beach Slope Prediction Approaches." *Paste and Thickened Tailings - A Guide*, R. J. Jewell and A. Fourie, eds., Australian Center for Geomechanics, Perth, Australia, 219–227.

Tsai, T. L., Chiang, S. W., and Yang, J. C. (2004). "Characteristics method with cubic-spline interpolation for open channel flow computation." *International Journal for Numerical Methods in Fluids*, 46(6), 663–683.

Urroz, B. G. E. (2004). "Method of Characteristics for Pure Advection." Utah State University.

Vreugdenhil, C. (1994). *Numerical Methods for Shallow Water Flow*. Springer Science+Business Media, Dordrecht.

Wildemuth, C. R., and Williams, M. C. (1985). "A new interpretation of viscosity and yield stress in dense slurries: Coal and other irregular particles." *Rheologica Acta*, 24(1), 75–91.

Winterwerp, J. C., and van Kesteren, W. G. M. (2004). *Introduction to the physics of cohesive sediment in the marine environment*. *Developments in Sedimentology*, (T. van Loon, ed.), Elsevier, Amsterdam.

Xu, J., Gillies, R. G., Small, M., and Shook, C. A. (1993). "Laminar and turbulent flow of kaolin slurries." *Proceedings of the 12th Internatonal Conference on Hydrotransport*, C. Shook, ed., BHR Group, Cranfield, UK, 595–613.

Yang, J. (2009). "Computational fluid dynamics modeling of deposition of oil sand slurry into mature fine tailings." University of Alberta.

Yuhi, M., and Mei, C. C. (2004). "Slow spreading of fluid mud over a conical surface." *Journal of Fluid Mechanics*, 519, 337–358.

Zhang, K., and Acrivos, A. (1994). "Viscous resuspension in fully developed laminar pipe flows." *International Journal of Multiphase Flow*, 20(3), 579–591.

Zhou, Z., Solomon, M. J., Scales, P. J., and Boger, D. V. (1999). "The yield stress of concentrated flocculated suspensions of size distributed particles." *Journal of Rheology*, 43(3), 651–671.

APPENDIX A –INCLUSION OF ADDITIONAL SHEAR STRESS COMPONENTS

For this model, only viscous shear stress and yield stress, defined by the rheological model are included in the formulation. However, for future work additional shear stress components could be incorporated into the model. O'Brien et al. (1993) note that the total shear stress within a "hyperconcentrated sediment flows, including those described as debris flows, mud flows, and mud floods" can be written as:

$$\tau = \tau_c + \tau_{mc} + \tau_v + \tau_t + \tau_d, \tag{92}$$

where:

τ_c = cohesive yield stress parameter

τ_{mc} = Mohr-Coulomb shear stress

τ_v = viscous shear stress

τ_t = turbulent shear stress

τ_d = dispersive stress.

These components are combined into functions of only the shear rate and square of the shear rate:

$$\tau = \tau_y + \eta\left(\frac{du}{dz}\right) + C\left(\frac{du}{dz}\right)^2. \tag{93}$$

where τ_y includes both the cohesive and Mohr-Coulomb shear stresses, η is a viscosity parameter and C is a coefficient combing the remaining terms and is a function of the mixture density, volumetric concentration, and dispersive stress parameter, d_s:

$$C = \rho_m l^2 + f(\rho_m, \phi) d_s. \tag{94}$$

One example of this function is the well-known Bagnold dispersive stress (1954) definition as provided in (O'Brien et al. 1993):

$$f(\rho_m, \phi) = a_i \rho_m \left[\left(\frac{\phi_*}{\phi}\right) - 1\right]. \tag{95}$$

Note that Takahashi (2007) questions the approach of including a $(du/dz)^2$ component as being physically suspicious. A more rigorous method for including the influence of turbulence on the flow

behavior is the inclusion of the eddy viscosity and utilizing a “quasi-laminar” modelling approach (Vreugdenhil 1994).

APPENDIX B - THE PARTICLE SHEAR MIGRATION COMPONENT

Understanding the shear migration effect magnitude relative to the particle settling effect is important in understanding the particle motion within non-Newtonian fluids. The influence of the shear migration can be evaluated by comparing the shear diffusion flux to the magnitude of the particle sedimentation flux due to gravity.

The Péclet number is commonly used in studying diffusion and transport in both heat and mass transfer problems to evaluate the relative importance of different flux components.

B.1 Derivation of Péclet Number

Considering the two[27] particle fluxes of importance in this study, the Péclet number can be defined as the ratio of the sedimentation flux and shear diffusion flux:

$$P_e = \frac{J_g}{J_d}. \tag{96}$$

The sedimentation flux, $J_{g'}$ is defined as the product of the settling velocity and volumetric solids concentration:

$$J_g = v_s\varphi = \frac{2\Delta\rho a^2 g\varphi}{9\mu(\varphi)}, \tag{97}$$

where the dependency of the kinematic viscosity on particle volume fraction accounts for the hindered settling effect[28]. In this evaluation the Krieger-Dougherty relationship for $\mu(\varphi)$ is used to represent the hindered settling contribution.

---

[27] Particles motion may be caused by other phenomenon such as Brownian motion and thermal gradients. These are not considered in this study.

[28] The settling flux could equally be written as $v_s \cdot \phi \cdot f(\phi)$ where $f(\phi)$ is the hindrance function. Using the Kriger-Dougherty viscosity is an appropriate assumption in this evaluation since the hindrance function $f(\phi)$ varies from 1 (freely settled) to 0 (no settling) and the inverse of the Krieger-Dougherty relationship varies from 1 (fluid viscosity) to 0 (infinite viscosity at maximum solids packing). In fact using the Krieger Dougherty relationship to simulate the hindered settling is advantageous in that incorporates the cessation of settling at the maximum particle packing, whereas a typical Richardson and Zaki type hindrance function makes no consideration for maximum particle packing.

A typical shear diffusion flux definition:

$$J_d = -D\frac{d\varphi}{dz}, \tag{98}$$

can be transformed to the non-dimensional form for shear particle migration following the methods of Leighton and Acrivos (1986)

$$J_d = -\dot{\gamma}a^2\widehat{D}\frac{d\varphi}{dz}, \tag{99}$$

where $\widehat{D}$ is now the non-dimensional shear migration diffusion coefficient. Leighton and Acrivos *roughly approximate* the shear diffusion coefficient from their experimental work as:

$$\widehat{D} = \frac{1}{3}\left(1 + \frac{1}{2}e^{8.8\varphi}\right). \tag{100}$$

Combining equations (96), (97) and (98) and simplifying yields the following form of the Péclet number:

$$Pe = \frac{2\Delta\rho a^2 g\varphi}{9\mu(\varphi)\dot{\gamma}a^2\widehat{D}\frac{d\varphi}{dz}} = \frac{2\Delta\rho gZ}{9\mu(\varphi)\dot{\gamma}\widehat{D}}. \tag{101}$$

Note equation (101) is developed by assuming the concentration gradient is linear through the characteristic flow depth (i.e $d\phi/dZ \sim \phi/Z$). This assumption is appropriate as the intent of this study is to determine the magnitude of the Pe numbers. Interestingly the final Péclet number definition is independent of particle size, a.

Also note that when the two fluxes are equal, or Pe = 1, the fluid shear balances the sedimentation, and the particles remain suspended (Acrivos et al, 1993) with no particle motion, relative to the fluid, due to either flux component.

B.2 Parametric Péclet Number Evaluation

To evaluate the relative magnitude between the hindered settling and shear migration effects, the Péclet number is plotted considering a range of input conditions. Péclet numbers greater than one indicate settling dominates.

The baseline parameters listed in Table 10 are used in evaluating the influence of each parameter. These parameters are selected as they are typical of many mine tailings. Other than the variable being evaluated, the remaining parameters remain constant for each case.

Table 10: Baseline Parameters

Parameter	**Value**
ρ_w	1000 kg/m^3
ρ_{solids}	2650 kg/m^3
Z	0.25 m
ϕ	30%
ϕ_c	63%
μ_0	0.00105 Pa.s
$\mu_{suspension}$	Krieger-Dougherty $\mu(\varphi) = \mu_0\left(1 - \frac{\varphi}{\varphi_c}\right)^{-2.5\varphi_c}$
D	$\widehat{D} = \frac{1}{3}\left(1 + \frac{1}{2}e^{8.8\varphi}\right)$

Characteristic Channel Depth

The first evaluation considers the effect the flow depth, Z has on the Péclet number. As can be seen in Figure 59, the settling flux dominates over a wide range of flow depths (1 mm to 1 m).

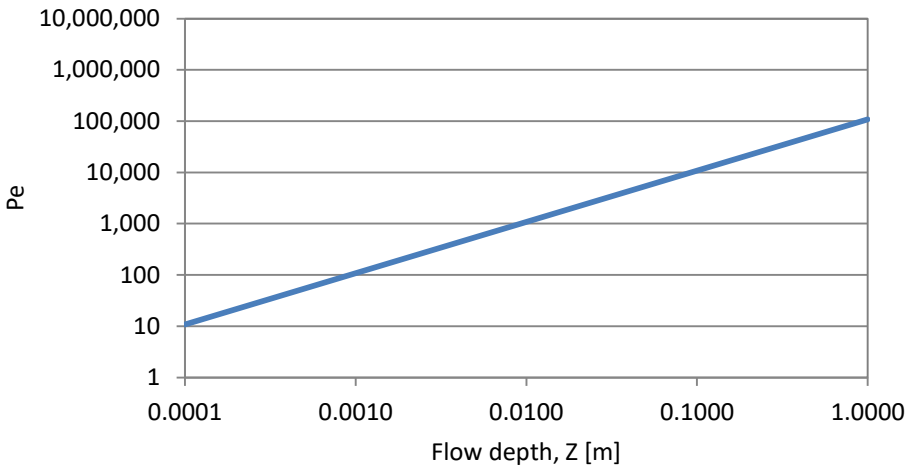

Figure 59: Pe vs. Characteristic Flow Depth

Shear rate

The next evaluation considers a range of bulk shear (strain) rates. Shear rates up to 5000 1/s are plotted in Figure 60 to show the general dominance of the settling effect over the shear migration effect. At higher bulk shear rates the flow will become turbulent, particle suspension due to turbulence will overcome the hindered settling effect and this Péclet number evaluation will not be appropriate. It is likely with the given baseline parameters in Table 10 that the flow would transition to turbulent at some point within the plotted range.

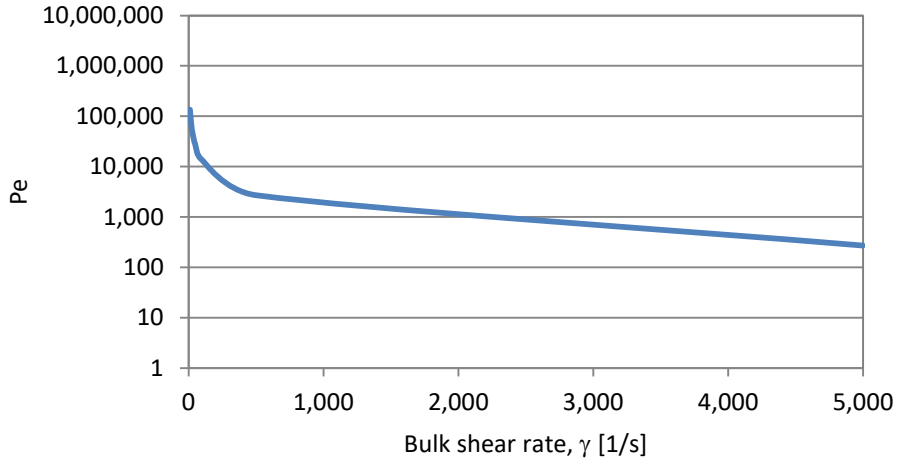

Figure 60: Pe vs. Bulk Shear Rate

Volume Concentration

Figure 61 presents the effect varying solids concentration has on the Péclet number. It is only when the volumetric concentration nears the maximum solids packing concentration (63%$_v$), does the Péclet number decrease drastically. Ultimately the Péclet number must necessarily become unity at 63%v since no settling can occur at the maximum packing concentration.

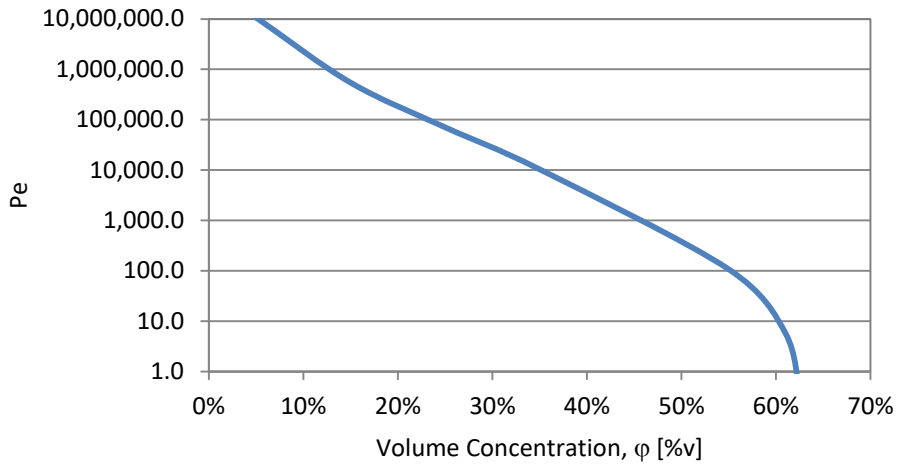

Figure 61: Pe vs solids volume fraction, ϕ

Density Differential

Figure 62 presents the effect the differential density between solids and liquid has on the Péclet number. As expected, as the density differential decreases, the hindered settling effect diminishes and the shear migration component increases. Note, however that even at a small density differential (~50 kg/m^3) the hindered settling still significantly dominates.

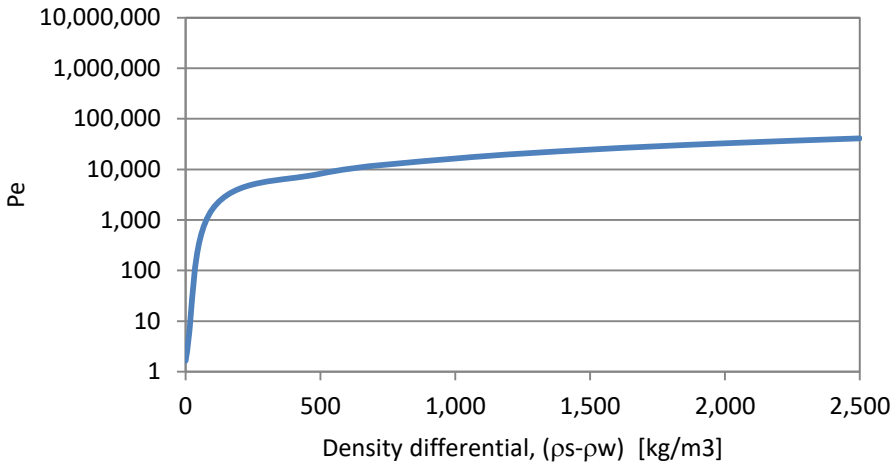

Figure 62: Pe vs. Density Differential

Suspension Viscosity

Presented in Figure 63 is the influence suspension viscosity[29] has on the Péclet number. As can be seen in the figure, a relatively small increase in the suspension viscosity has a significant effect on the Péclet number. This is because the hindered settling velocity decreases significantly with increased viscosity. A relatively high suspension viscosity of approximately 150 Pa.s is required to achieve a Péclet number of unity.

[29] In this case μ_0 is varied, but the reported viscosities in the figure account for the particle impact on viscosity.

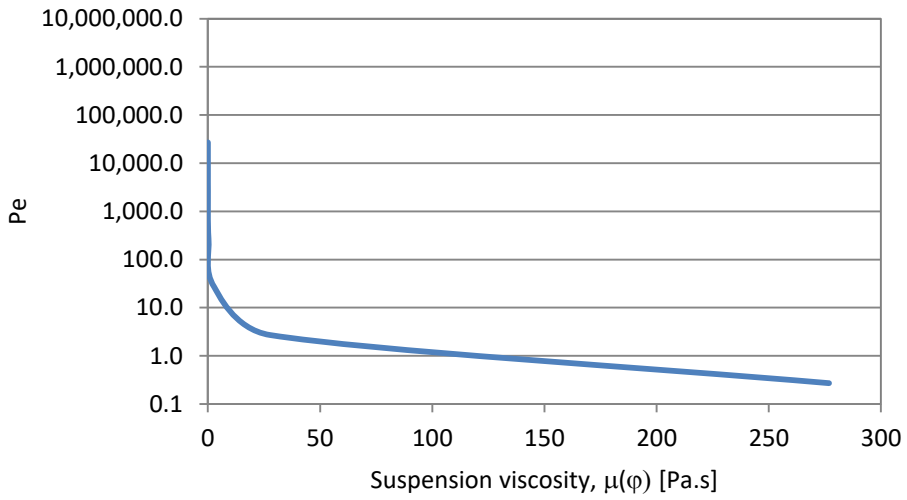

Figure 63: Pe vs. Suspension Viscosity, μ

Bingham Plastic Fluids

As discussed above, the Péclet number decreases with both increasing bulk shear rate and suspension viscosity. However, for shear thinning fluids such as Bingham plastics, the focus of this study, the apparent viscosity decreases with increasing shear rate.

This final Péclet number assessment evaluates these counter-acting behaviors for a Bingham plastic fluid. For reference, the resulting apparent fluid viscosity due to the variation in yield stress is presented for two shear rates: 10 1/s and 100 1/s in Figure 64.

The evaluation considers the same particle properties in Table 10, but the fluid viscosity is determined based on the Bingham plastic rheology model:

$$\mu_0(\dot{\gamma}) = \frac{\tau_y}{\dot{\gamma}} + K_{BP}. \tag{102}$$

Figure 65 presents the Péclet number as a function of Bingham yield stress considering the yield stress values and resulting apparent viscosities in Figure 64. The Bingham plastic viscosity is constant at 0.01 Pa.s for the evaluation. As seen in Figure 65 increasing yield stress has a more significant impact on the Péclet number than variations in shear rate. Note also that the settling flux still dominates the shear migration flux by at least an order of magnitude, even at high yield stress values where the hindered settling velocity will be extremely low.

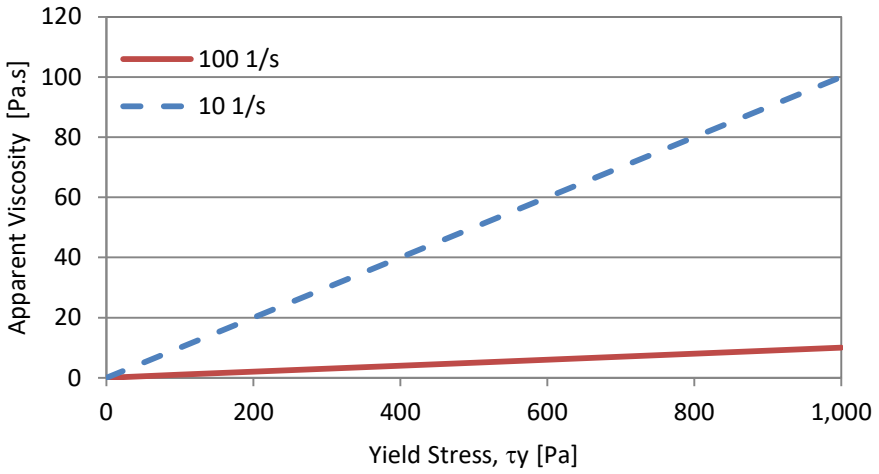

Figure 64 Resulting Apparent Viscosity vs Yield Stress for the Figure 65 Evaluation Case.

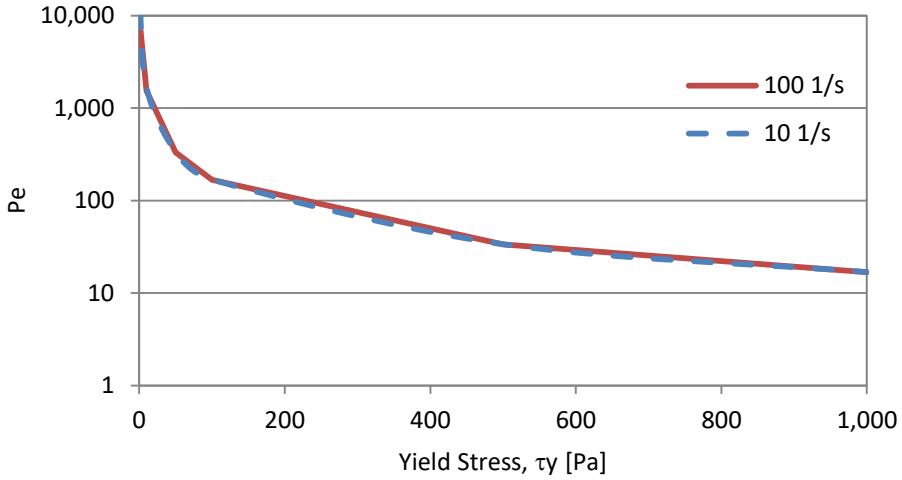

Figure 65: Pe vs. Yield stress for Non-Newtonian Fluid Rheology Presented in Figure 64

The evaluation becomes more interesting when the yield stress is held constant, and the solids concentration approaches the maximum packing concentration. Figure 66 presents this case, where two Bingham plastic yield stresses (10 Pa and 100 Pa) are considered and the volume concentration is varied from 25%v to 62%v.

In this case, it is actually possible to achieve a Péclet number less than 1 indicating the shear migration is more dominant than the settling component. This occurs near at approximately 55%v for the low yield stress fluid and at a lower concentration of 45%v for the high yield stress case.

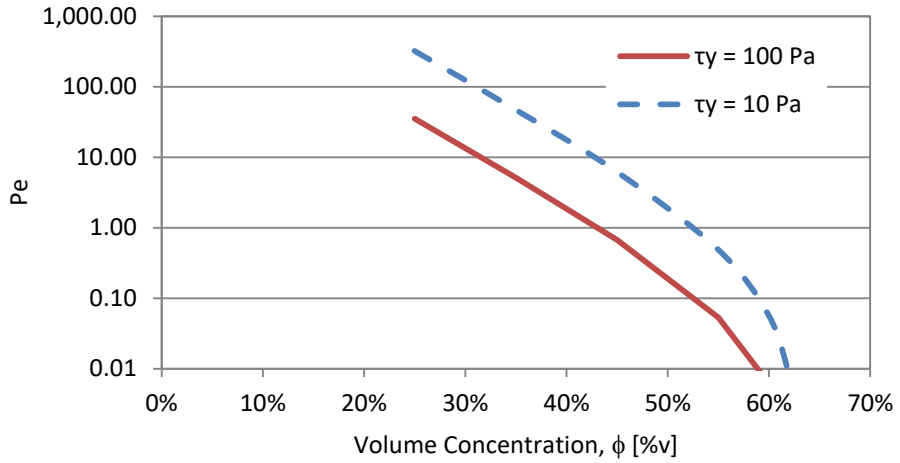

Figure 66: Pe vs. Volume Concentration in Bingham Plastic Fluid

B.3 Summary

This parametric evaluation indicates that hindered settling dominates the particle shear migration contribution in most flow scenarios of interest to this study. The shear migration component only comes into play in Newtonian fluids when:

- The density of the particles is nearly identical to the density of the fluid, which will typically not be the case in tailings beach flows, or
- When the particle volume concentration nears the maximum packing limit and the hindered settling contribution tends to zero.

The shear migration contribution has a larger impact, resulting in significantly lower Péclet numbers, when considering particles in Bingham plastic fluid. However, as with Newtonian fluids, the shear migration flux magnitude only nears the hindered settling magnitude when the solids volume concentration approaches the maximum solids volumetric concentration.

Overall this evaluation indicates that in general the particle shear migration can be dismissed when evaluating bulk tailings beach flows. However, the shear migration may become important when

considering particle settling and deposition near the channel bed. As the particle settle, the volumetric concentration will increase. As the maximum bed packing concentration is neared, the shear migration component may very likely result in the phenomenon discussed by Acrivos et al. (1993) where the shear migration and hindered settling components balance (Pe=1) and the particles remain in suspension rather than settle fully and stagnate within the flow channel.

Since the primary driver of this phenomenon is actually the substantial increase in fluid viscosity as the particles approach the maximum packing concentration, it may be possible to simply model this viscosity augmentation with settling and realize the same effect.

APPENDIX C – COORDINATE TRANSFORMATION

The partial derivatives in ζ become:

$\partial/\partial t$:

$$\frac{\partial}{\partial t} = \frac{\partial}{\partial t}\Big|_{x,\zeta,t} + \frac{\partial}{\partial x}\Big|_{x,\zeta,t}\frac{\partial x}{\partial t} + \frac{\partial}{\partial \xi}\Big|_{x,\zeta,t}\frac{\partial \zeta}{\partial t} \tag{103}$$

Since only H depends on t, $\frac{\partial \zeta}{\partial t} = \frac{-(z\text{-}z_b)}{H^2}\frac{\partial H}{\partial t}$ and the derivative becomes:

$$\frac{\partial}{\partial t} = \frac{\partial}{\partial t} + \frac{\partial}{\partial x}(0) + \frac{\partial}{\partial \zeta}\left(-\frac{z\text{-}z_b}{H^2}\frac{\partial H}{\partial t}\right)$$
$$\frac{\partial}{\partial t} = \frac{\partial}{\partial t} + \frac{\partial}{\partial \zeta}\left(-\frac{\zeta}{H}\frac{\partial H}{\partial t}\right) \tag{104}$$

$\partial/\partial x$:

$$\frac{\partial}{\partial x} = \frac{\partial}{\partial t}\Big|_{x,\zeta,t}\frac{\partial t}{\partial x} + \frac{\partial}{\partial x}\Big|_{x,\zeta,t} + \frac{\partial}{\partial \zeta}\Big|_{x,\zeta,t}\frac{\partial \zeta}{\partial x} \tag{105}$$

Similar to above, the derivative becomes:

$$\frac{\partial}{\partial x} = \frac{\partial}{\partial t}0 + \frac{\partial}{\partial x} + \frac{\partial}{\partial \zeta}\left(-\frac{z\text{-}z_b}{H^2}\frac{\partial H}{\partial x} - \frac{1}{H}\frac{\partial z_b}{\partial x}\right)$$
$$\frac{\partial}{\partial x} = \frac{\partial}{\partial x} + \frac{\partial}{\partial \zeta}\left(-\frac{\zeta}{H}\frac{\partial H}{\partial x} - \frac{1}{H}\frac{\partial z_b}{\partial x}\right) \tag{106}$$

and $\partial/\partial z$:

$$\frac{\partial}{\partial z} = \frac{\partial}{\partial t}\Big|_{x,\zeta,t}\frac{\partial t}{\partial x} + \frac{\partial}{\partial x}\Big|_{x,\zeta,t}\frac{\partial x}{\partial z} + \frac{\partial}{\partial \zeta}\Big|_{x,\zeta,t}\frac{\partial \zeta}{\partial z} \tag{107}$$

which becomes:

$$\frac{\partial}{\partial z} = \frac{\partial}{\partial t}(0) + \frac{\partial}{\partial x}(0) + \frac{\partial}{\partial \zeta}\frac{\partial z}{\partial \zeta}$$
$$\frac{\partial}{\partial z} = \frac{\partial}{\partial \zeta}\frac{1}{H} \tag{108}$$

Finally, the second order differential $\partial^2/\partial z^2$ in the diffusion term becomes:

$$\frac{\partial^2}{\partial z^2} = \frac{\partial}{\partial z}\frac{\partial}{\partial z} = \frac{\partial}{\partial z}\left(\frac{\partial}{\partial \zeta}\frac{1}{H}\right)$$
$$\frac{\partial}{\partial z} = \frac{\partial}{\partial \zeta}\frac{\partial z}{\partial \zeta}\left(\frac{\partial}{\partial \zeta}\frac{1}{H}\right) = \frac{1}{H^2}\frac{\partial^2}{\partial \zeta^2} \tag{109}$$

Substitution of the derivatives back into the particle transport model, and combining like terms yields the (x, ζ) scalar transport model in Section 4.4.2